

Chemical Compositions of Kinematically Selected Outer Halo Stars *

Lan Zhang^{1,2}, Miho Ishigaki³, Wako Aoki^{4,5}, Gang Zhao¹, and Masashi Chiba³

ABSTRACT

Chemical abundances of 26 metal-poor dwarfs and giants are determined from high-resolution and high signal-to-noise ratio spectra obtained with Subaru/HDS. The sample is selected so that most of the objects have outer-halo kinematics. Self-consistent atmospheric parameters were determined by an iterative procedure based on spectroscopic analysis. Abundances of 13 elements, including α -elements (Mg, Si, Ca, Ti), odd-Z light elements (Na, Sc), iron-peak elements (Cr, Mn, Fe, Ni, Zn) and neutron-capture elements (Y, Ba), are determined by two independent data reduction and LTE analysis procedures, confirming the consistency of the stellar parameters and abundances results. We find a decreasing trend of $[\alpha/\text{Fe}]$ with increasing $[\text{Fe}/\text{H}]$ for the range of $-3.5 < [\text{Fe}/\text{H}] < -1$, as found by Stephens and Boesgaard (2002). $[\text{Zn}/\text{Fe}]$ values of most objects in our sample are slightly lower than the bulk of halo stars previously studied. These results are discussed as possible chemical properties of the outer halo in the Galaxy.

Subject headings: Galaxy: abundances - Galaxy:halo - Galaxy: evolution - stars: abundances

*Based on data collected at the Subaru Telescope, which is operated by the National Astronomical Observatory of Japan

¹National Astronomical Observatories, CAS, 20A Datun Road, Chaoyang District, 100012, Beijing, China; gzhao@bao.ac.cn, zhanglan@bao.ac.cn

²Graduate University of the Chinese Academy of Sciences, 19A Yuquan Road, Shijingshan District, 100049, Beijing, China

³Astronomical Institute, Tohoku University, Sendai, 980-8578, Japan; miho@astr.tohoku.ac.jp, chiba@astr.tohoku.ac.jp

⁴National Astronomical Observatory of Japan, 2-21-1 Osawa, Mitaka, Tokyo 181-8588, Japan; aoki.wako@nao.ac.jp

⁵Department of Astronomical Science, School of Physical Sciences, The Graduate University of Advanced Studies (SOKENDAI), 2-21-1 Osawa, Mitaka, Tokyo 181-8588, Japan

1. Introduction

In recent years, comprehensive studies of stars in the Galactic old components, such as the halo and the thick disk, have been carried out to understand the origin of our Galaxy and its early evolution. A mainstream approach is to get such information through studying the detailed elemental abundances of metal deficient stars, because many of these objects have formed from primordial gas clouds during the early chemo-dynamical evolution of the Galaxy (e.g., Beers & Christlieb 2005 and references therein). Indeed, in the course of Galactic chemical evolution, heavy elements synthesized during the massive star evolution and the supernova explosion are mixed into interstellar matter, from which subsequent generations of stars are formed (e.g., Shigeyama & Tsujimoto 1998). Extremely metal-poor stars that we are currently observing are candidate low-mass stars among those formed in this early stage of the Galaxy. Chemical abundance studies for such metal-poor stars in the past few decades (e.g., Zhao & Magain 1990, 1991; McWilliam et al. 1995; Gratton et al. 1997; McWilliam 1998; Carretta et al. 2002; Cayrel et al. 2004; Barklem et al. 2005) and modeling of massive stars and supernova explosions (e.g., Heger & Woosley 2002; Umeda & Nomoto 2005) provide useful constraints on the nucleosynthesis processes in the early Galaxy.

These old stellar populations often show high space motions relative to the stars in the thin-disk component, which reflects the early dynamical motion of the Galaxy, such as an overall collapse and/or merging process. Thus, studies on kinematics of metal-poor stars provide unique information on Galactic structure and formation. For instance, Chiba & Beers (2000) studied the space motions of about 1200 metal-poor stars with $[\text{Fe}/\text{H}] < -0.6$, utilizing the accurate measurements of their proper motions by the Hipparcos mission. Their results have revealed characteristic kinematics of stars, such as a discontinuous change of mean rotational motion ($\langle V_\phi \rangle$) at $[\text{Fe}/\text{H}] \sim -1.7^1$, suggesting a discontinuous evolution of the Galaxy’s collapse between the formation stage of the halo and disk components, and some kinematical substructures as indicative of merging debris. Indeed, more evidence of merging of smaller galaxies in the formation of the Galaxy has been found (Ibata et al. 1994; Preston et al. 1994; Bullock & Johnston 2005). It has also been made clear that the halo is divided into two separate components, the flattened inner halo and spherical outer halo (e.g., Sommer-Larsen & Zhen 1990; Norris 1994). More recently, Carollo et al. (2007) showed, based on the large sample provided by Sloan Digital Sky Survey (SDSS), that the outer halo exhibits a net retrograde motion in contrast to a small prograde rotation of the inner halo, indicating that the Galaxy collapse was not monolithic unless otherwise its spin motion would have been unidirectional.

¹ $[\text{A}/\text{B}] = \log(N_{\text{A}}/N_{\text{B}}) - \log(N_{\text{A}}/N_{\text{B}})_{\odot}$

Further constraints on the scenario of Galaxy formation can be obtained from the detailed chemical abundances of individual stars in the nearby dwarf galaxies, which are possible remnants of building blocks of the Galactic halo. A key is the abundance ratio between the α elements and the iron-peak elements. For instance, while the bulk of halo stars have over-abundances of α elements, a significant fraction of stars in Galactic dwarf galaxies have comparatively low $[\alpha/\text{Fe}]$ ratios (e.g., Shetrone et al. 2001, 2003; Aoki et al. 2009b). However, the halo component itself holds a dual nature as mentioned above, so further studies of the relationship between chemical abundance such as α -elements and kinematical properties of individual halo stars will provide new insight into the formation of the Galaxy.

Analysis of chemical abundances and kinematics of a large sample of galactic halo stars have been carried out by e.g., Fulbright (2000, 2002) and Stephens & Boesgaard (2002) (hereafter SB02), who discussed a possible correlation between $[\alpha/\text{Fe}]$ and kinematical properties in particular for the halo stars having extreme orbital motions. While weak correlations between the abundances with some orbital parameters were suggested, their samples of field halo stars, including stars having extreme motions, show distinct chemical abundances from those seen in the nearby dwarf galaxies. From these results, it was concluded that the accretion of dwarf galaxies similar to those currently orbiting our Galaxy did not play a key role in the formation of the Galaxy. However, neither of them covered adequate number of stars that have large Z_{max} , the maximum distance of the orbit above and below the Galactic plane, which is one useful indicator to select outer halo stars, thereby allowing us to investigate any systematic trends in abundances as a function of orbital parameters. Moreover, no star with $[\text{Fe}/\text{H}] < -2.0$ was considered for the analysis of the abundance-kinematics correlation in the study of Fulbright (2002). Further studies of candidate outer halo stars covering a wider metallicity range are needed.

The aim of this work is thus to obtain detailed chemical abundances of metal-poor halo stars selected based on their orbital motions, so that the correlation between the abundance ratios and kinematics properties (i.e., if the star belongs to the inner or outer halo) is explored. We determine the abundances of elements including Na, α -elements (Mg, Si, Ca, Ti), Sc, iron peak elements (Cr, Mn, Ni, Zn) and heavy elements (Y, Ba) for 26 metal-poor halo stars. This work is based on high resolution and high signal-to-noise (S/N) ratio spectra from the Subaru Telescope as described in Section 2. The determination of atmospheric parameters and the procedures of abundance analysis are described in Section 3 and Section 4, respectively. In addition, the results for the derived elemental abundances and related discussion are given in Section 5 and Section 6. The summary is given in the last section.

2. Observations and data reduction

2.1. Selection of stars

In order to study the chemical abundances of outer halo stars, we selected candidate metal-poor stars for which large values of Z_{\max} have been obtained from catalogues of Beers et al. (2000), Carney et al. (1994) and Ryan & Norris (1991). Orbital parameters, R_{apo} (the maximum radial distances from the Galactic center) and Z_{\max} , were calculated from radial velocities, proper motions and distance in the method described in Chiba & Beers (2000). Although SB02 have studied candidates of outer halo stars, their sample includes only a few stars having large Z_{\max} . In order to study the high Z_{\max} range, we include red giant stars in our sample. Our sample also includes three stars that were studied by SB02 for comparison purposes.

Based on this selection, high resolution spectra were obtained for 32 stars (see § 2.2 for details). However, the S/N ratios are insufficient for six stars among them for the present purpose. Hence, the sample of the present work contains 26 stars, among which 16 stars are red giants and the others are main-sequence stars.

Among our sample, BD+04°2466 is reported as a binary member (Jorissen et al. 2005). Carney et al. (2003) reported that BD+01°3070 might be a binary because of its radial velocity variation. G 112–43 also possibly belongs to a binary system (Latham et al. 2002). There is no evidence of binarity for the other stars.

2.2. High resolution spectroscopy and data reduction

We obtained high-resolution spectra of our targets using the Subaru Telescope High Dispersion Spectrograph (HDS; Noguchi et al. 2002) in February 2003. Table 1 lists the objects and details of the observations. The spectra cover the wavelength range from 4100 to 6800 Å with a resolving power of 50,000. The CCD on-chip binning was not applied. Therefore, the resolution element is sampled by about six CCD pixels.

The standard MIDAS routines were used for data reduction, including order identification, wavelength calibration, flat-field correction, background subtraction, and 1D spectra extraction. The Doppler shift was corrected by measurements for at least 34 moderately strong and unblended lines before continuum rectification. The S/N ratios (per 0.9 km s⁻¹ pixel) of the reduced spectra at 5800 Å are presented in Table 1. Examples of a portion of spectra are shown in Fig. 1.

2.3. Equivalent widths

Three different methods were used to measure the equivalent widths: fitting of a Gaussian profile, fitting of a Voigt profile and a direct integration. The Gaussian fitting was adopted for weak lines with apparently no or little blending. The Voigt profile fitting is applied to strong lines. The direct integration is applied to moderately strong lines which can be distinguished clearly from others. The results are presented in Table 2 (electronic version)

The equivalent widths measured by the present work are compared with the results of SB02 for the three common stars (Fig. 2). Their spectra were taken with Keck/HIRES, and the spectral quality is similar to ours (mean S/N \sim 200, R = 30,000 \sim 60,000). We found that the agreement between the two measurements is fairly good. The correlations of the two measurements are presented as follows (dashed lines in Fig. 2):

$$\text{E.W.s(SB02)}_{\text{G } 15-13} = -0.02(\pm 0.31) + 1.029(\pm 0.008) \times \text{E.W.s(TW)} \text{ (m}\mathring{\text{A}})$$

$$\text{E.W.s(SB02)}_{\text{G } 166-37} = 0.14(\pm 0.77) + 1.002(\pm 0.017) \times \text{E.W.s(TW)} \text{ (m}\mathring{\text{A}})$$

$$\text{E.W.s(SB02)}_{\text{G } 238-30} = -0.11(\pm 0.44) + 0.979(\pm 0.022) \times \text{E.W.s(TW)} \text{ (m}\mathring{\text{A}})$$

The standard deviations of these three relations are 3.0 m $\mathring{\text{A}}$, 4.0 m $\mathring{\text{A}}$ and 1.6 m $\mathring{\text{A}}$, respectively.

The uncertainty of equivalent width measurement is estimated by using the formula of Cayrel (1988):

$$\sigma_w = \frac{1.5\sqrt{\text{FWHM}\delta_x}}{\text{S/N}} \quad (1)$$

where FWHM (in m $\mathring{\text{A}}$) is the full width at the half maximum of a line; δ_x is the pixel scale (m $\mathring{\text{A}}$ /pixel), and S/N is the signal-to-noise ratio estimated for the spectral order which contains the absorption lines. For instance, the lowest and highest S/N ratios are 80 and 520 among these spectra, which lead to the errors of 0.6 m $\mathring{\text{A}}$ and 0.07 m $\mathring{\text{A}}$, respectively. Taking the uncertainty of the continuum rectification into consideration, $3\sigma_w$ is adopted as the detection limit of absorption lines. We estimated that the errors of equivalent width measurements are 0.2 \sim 1.8 m $\mathring{\text{A}}$, depending on the S/N ratio and the strength of lines.

3. Stellar atmospheric parameters

3.1. Determination of effective temperature

The effective temperature (T_{eff}) is determined by making the abundances of Fe be independent of the excitation potential of Fe I lines used in the analysis (see § 4 for details of the abundance analysis). An initial value is set in the code to calculate the iron abundances from neutral species, and then a slope between $\log \epsilon(\text{Fe I})$ and the excitation potential is determined by least-square fit. This process is iterated until the slope is minimized (Fig. 3). **The perturbation of T_{eff} is added to change the slope, making the slope of the change within 1σ . Finally, the perturbations are taken as the uncertainties of T_{eff} , and they are around 100 K.**

We prefer the spectroscopic method to determine the effective temperature in the present work, because this can be applied to all objects in the sample, and many clean Fe I lines are available in our high S/N spectra.

The estimate of T_{eff} by profile fitting for Balmer lines is not adopted. This technique is sensitive to the continuum determination for the echelle order containing broad absorption features of Balmer lines. Moreover, for giant stars, the Balmer line profiles are not very sensitive to the effective temperature.

The estimate of T_{eff} from color indices (e.g. $V - K$) is not adopted to derive the final results in the present work, because photometry data for our sample are incomplete, and the T_{eff} estimate is sensitive to the interstellar reddening. The error of T_{eff} determined from $V - K$ due to the uncertainty of reddening is estimated to be as large as 100 K. Although such uncertainty exists in the method, we estimate T_{eff} from color indices for stars for which photometry data are available for comparison purposes. The T_{eff} scale for dwarfs from Alonso et al. (1996) and for giants from Alonso et al. (1999) are adopted, and the colors of the stars were taken from the 2MASS catalogue for near-infrared photometry and the Hipparcos catalogue (Perryman et al. 1997) for optical one. The dust maps of Schlegel et al. (1998) are employed to estimate the reddening values. The $E(B - V)$ values are corrected taking into account the finite distance to a star, by using the method described in Beers et al. (2000).

Since the Johnson system and the Telescope Carlo Sánchez system (TCS) were adopted in the work of Alonso et al. (1996, 1999), the JHK indices from 2MASS are transformed through the relations of Ramirez & Meléndez (2004):

$$J_{\text{TCS}} = J_{2\text{MASS}} + 0.001 - 0.049(J - K)_{2\text{MASS}} \quad (2)$$

$$H_{\text{TCS}} = H_{2\text{MASS}} - 0.018 + 0.003(J - K)_{2\text{MASS}} \quad (3)$$

$$K_{\text{TCS}} = K_{2\text{MASS}} - 0.014 + 0.034(J - K)_{2\text{MASS}} \quad (4)$$

Comparisons of T_{eff} derived from the color indices (hereafter CI, the average value derived from T_{eff}^{V-K} , T_{eff}^{J-H} and T_{eff}^{J-K}) with those from the spectroscopic analysis (hereafter SA) are listed in Table 3, and are shown in Fig. 4. The average and standard deviation of the difference is: $\langle T_{\text{eff}}^{\text{CI}} - T_{\text{eff}}^{\text{SA}} \rangle = 54$ and $\sigma = 99$. The difference is also given by linear least-square fit: $T_{\text{eff}}^{\text{CI}} = 20 + 1.01 \times T_{\text{eff}}^{\text{SA}}$

These comparisons indicate that the effective temperatures estimated from color indices for our sample are in fairly good agreement with those determined by the spectroscopic method in general.

3.2. Determination of other parameters

Surface gravity. $\log g$ is determined by forcing Fe I and Fe II to give the same iron abundance. In addition, Ti ionization equilibrium is also used to check the final results. Although this method is affected by non-LTE effects and uncertainties of atomic data, no other method provides reliable gravity for the whole sample. The uncertainties of Hipparcos parallaxes are larger than 40% for a half of our sample stars. The gravity is not well determined from Y2 isochrone for giants (Cohen et al. 2002). Therefore, ionization equilibrium of iron is used in the present analysis. **In order to estimate the uncertainty of the $\log g$ determination, we calculate the $\log g$ value that results in 0.1 dex discrepancy in Fe abundances from Fe I and Fe II. The typical error in $\log g$ derived by this calculation is 0.32 dex. We note that the typical Fe abundance error (random error) is 0.05 dex (§4.2), so the above estimate of the $\log g$ error is rather conservative.**

Metallicity. The solar abundance of $\log \varepsilon(\text{Fe})_{\odot} = 7.51$ (Anders & Grevesse 1989) is adopted to get the $[\text{Fe}/\text{H}]$ and $[\text{X}/\text{Fe}]$ values.

Micro-turbulent velocity. ξ_t is also determined from the abundance analysis. The abundances are derived from individual Fe I lines whose equivalent widths are in the range of 10 ~ 100 mÅ by changing the ξ_t value until these abundances are independent of their equivalent widths (Fig. 3). **With same method described in §3.1, the error of ξ_t is estimated. Typically, the error is 0.3 dex.** The determination of stellar parameters including T_{eff} is iterated until a consistent parameter set is obtained. The parameters of our sample determined by the above method are listed in Table 4. As an example, the Fe abundances derived

from individual Fe I lines are plotted as functions of excitation potential, equivalent width, and wavelength for HD 108577 in Fig. 3.

4. Elemental abundance analysis

The grid of the flux constant, homogeneous, LTE model atmospheres by Kurucz (1993) in which convection of overshoot approximation (Castelli et al. 1997) is considered is used in our abundance analysis. Abundance is calculated with the program ABONTEST8, developed by Dr. Pierre Magain at Liège, Belgium, by requiring the calculated equivalent width to agree with the observed value. Natural broadening, thermal broadening, van der Waals damping, and macro-turbulent velocity are all included in the calculation. The mean abundance of each element is derived from all available lines by giving equal weight to each line. The solar compositions of Anders & Grevesse (1989) were adopted to derive relative abundances.

4.1. Atomic data

The atomic line data for Na, Mg, Si, Ca, Ti, Cr, Fe, Ni, Y and Ba are adopted from Stephens (1999) and SB02. The references for individual lines are given in their papers. The $\log gf$ values of Sc, Mn and Zn are taken from Lawler & Dakin (1989), Booth et al. (1984) and Biémont & Godefroid (1980), respectively.

Absorption lines of Sc, Mn and Ba are known to be influenced by the hyperfine splitting (HFS). The splitting effect of these elements on abundance determination is largest for strong lines in which individual components are partially saturated. The HFS effect is smaller in weak lines and fully saturated lines. Our analysis includes the HFS effects using the line data of Sc II and Mn I from McWilliam et al. (1995), and references therein. The HFS data of Ba II are taken from McWilliam (1998) assuming the solar system isotopic mix given by Sneden et al. (1996).

4.2. Estimation of uncertainties

We estimate the uncertainties in the abundance determination for the two sources. One is the uncertainties in the analysis of individual lines, including random errors of equivalent widths, oscillator strengths, and damping constants; the other is the error due to the uncertainties of atmospheric parameters.

4.2.1. Errors from internal uncertainties

The typical uncertainty in the equivalent width measurement is about $0.6 \text{ m}\text{\AA}$ as mentioned in §2.3. This results in an error of about 0.04 dex in the elemental abundance calculation from an unblended, moderately strong line. The scatter of the abundance results from individual lines gives another estimate of the uncertainty from equivalent widths and other factors. The error is estimated by dividing the standard deviation of the derived abundances from individual lines by a square root of the number of lines used ($N^{\frac{1}{2}}$). The error is negligible when the number of lines used in the analysis is large. For instance, the standard deviation (σ) of the abundance results from 95 Fe I lines of G 112–43 is 0.06 dex, which is comparable with the estimate from equivalent width errors, and the random error ($\sigma \cdot N^{-\frac{1}{2}}$) is 0.006 dex. For elements for which only a small number of lines are available (e.g. Mg, Si), the σ of Fe I (typically 0.05 dex) is adopted in stead of the σ of those species.

4.2.2. Errors from the uncertainties of atmospheric parameters

From the discussion of §3.1, the error of T_{eff} is estimated to be on the order of 100 K. Considering uncertainties in Fe line analysis, the uncertainties of $\log g$ and micro-turbulent velocity are estimated to be 0.3 dex and $0.3 \text{ km}\cdot\text{s}^{-1}$, respectively. **These values are equivalent to the average error of the parameters.** The abundance changes by the changes of atmospheric parameters are listed in Table 5 for two stars in our sample: G 166–37 (main sequence) and HD 175305 (giant). We note that the abundance ratios of most elements ($[X/\text{Fe}]$ values) are relatively insensitive to variations of stellar parameters.

Finally, the abundance uncertainties is estimated by summing the atmospheric and internal uncertainties in quadrature.

4.3. Comparisons with an independent analysis

For our dataset, an independent abundance analysis is made by one of the authors (M.I.) using a different model atmospheres and an abundance analysis code, in order to demonstrate the reliability of the final results. Comparisons of the atmospheric parameters and chemical abundances between the two analyses are presented in Table 6, Table 7 and Fig. 5.

For the independent analysis (SA II), the data reduction is made using the standard IRAF routines. Equivalent widths are measured fitting Gaussian profiles to clean absorption

lines. The agreement of the equivalent widths between the two measurements is excellent; the root mean square (RMS) of the differences is 2.3 ± 0.1 mÅ on average. Stellar atmospheric parameters and abundance analysis were independently performed with an LTE abundance analysis code described in Aoki et al. (2009a) using the model atmosphere grid of Kurucz (1993) calculated with NEWODF assuming no convective overshooting (Castelli & Kurucz 2003). The HFS effects are taken into account in the estimate of Ba abundances. Effective temperatures, surface gravities, micro-turbulent velocities, and [Fe/H] are calculated with iterative process, as described in § 3. The resulting values of the atmospheric parameters reasonably agree each other:

$$T_{\text{eff}}^{\text{SAII}} = 53 + 0.99 \times T_{\text{eff}}^{\text{SA}}$$

$$\log g^{\text{SAII}} = -0.19 + 1.02 \times \log g^{\text{SA}}$$

$$[\text{Fe}/\text{H}]^{\text{SAII}} = 0.01 + 1.02 \times [\text{Fe}/\text{H}]^{\text{SA}}$$

$$\xi^{\text{SAII}} = -0.02 + 1.07 \times \xi^{\text{SA}}$$

The chemical abundance ratios determined by the two independent analysis agree within ~ 0.1 dex. We note that the [Fe/H] values derived by the second analysis are systematically lower by about 0.05 dex. This small difference can be explained by the difference of the model atmosphere grid. The Kurucz’s models assuming no overshooting are systematically cooler than those assuming overshooting, resulting in lower Fe abundances.

4.4. Comparison with previous work

The three common stars G 15–13, G 166–37 and G 238–30 in SB02, whose parameters were derived by the same analysis method as ours, are used for comparisons. Comparisons of atmospheric parameters are given in Table 8.

Comparisons of the abundance results derived by our analysis with those of SB02 are presented in Table 9 (the first three lines) for the three stars in common. The agreement between the two studies is fairly good in general. The [Fe/H] of G 238–30 derived in the present work is 0.16 dex higher than that of SB02. This is partially because we adopt 100 K higher T_{eff} in the analysis. It can result in a 0.08 dex difference. G 238–30 is most metal-deficient in our sample, and the number of iron lines used in the parameter determination is the smallest. It causes a error of 0.02 dex. **Besides, because of the relatively low S/N ratio and the weak iron lines of this star, the uncertainty of equivalent width is ~ 2 mÅ, which can lead to the error of ~ 0.05 dex.** These could be the main reasons for the comparatively large discrepancy in T_{eff} and [Fe/H] between the two studies.

The $[\text{Na}/\text{Fe}]$ of G 15–13 and G 166–37 derived by our analysis is higher than those of SB02. The primary reason for this discrepancy might be the difference of equivalent widths. Our calculation shows that the derived Na abundance increases by 0.07 dex for the increase of equivalent widths by 1 mÅ. For G 15–13, our equivalent widths of Na I $\lambda\lambda 5682$ and 5688 are $0.5 \sim 2.6$ mÅ higher than those in SB02, while, for G 116–37, the value of Na I 5682 is 2.4 mÅ larger and that of 5688 is 0.7 mÅ smaller than those in SB02. Such differences at least partially explain the differences of the Na abundances between the two studies for the two stars. The effects of equivalent width errors are significant, because of the weakness of the Na lines, compared with the lines of other elements. **The situation is similar for $[\text{Ti}/\text{Fe}]$ of G 238–30.**

In order to confirm the consistency of the abundance analysis technique with model atmospheres, we determined stellar parameters and abundances using the equivalent widths presented in the paper of SB02 for three stars having intermediate metallicity (G 5–19, G 9–36 and G 215–47). The comparisons of the results are given in Table 9 (the middle three lines). Our re-analysis well reproduces the results of SB02, confirming the consistency between the two analyses. A small systematic difference in $[\text{Mg}/\text{Fe}]$ between the two works is found, that is, our results are systematically lower by $0.04 \sim 0.11$ dex than those in SB02.

Finally, the analysis for the same stellar parameters adopting the equivalent widths of SB02 are attempted, and the results are compared with those of SB02 in Table 9 (the bottom three lines). The agreement is excellent, confirming the consistency of the abundance analysis code between the two studies.

5. Chemical abundance results

The derived abundances by the present analysis are summarized in Table 10 - 14. We show the abundance ratios of elements with respect to Fe as a function of metallicity in Fig. 6.

5.1. α -elements

In our analysis, abundances of α -elements are measured from 3 lines of magnesium, 3 lines of silicon, 23 lines of calcium, and 33 lines of titanium for most stars.

The average value and standard deviation of abundance ratios for each element are as follows: $[\text{Mg}/\text{Fe}] = +0.31 \pm 0.15$ dex (25 stars), $[\text{Si}/\text{Fe}] = +0.36 \pm 0.17$ dex (20 stars), $[\text{Ca}/\text{Fe}] = +0.29 \pm 0.15$ dex (26 stars) and $[\text{Ti}/\text{Fe}] = +0.27 \pm 0.13$ dex (26 stars). The average of these

abundance ratios for the four elements ($\langle[\alpha/\text{Fe}]\rangle$) derived from our sample is $+0.30\pm 0.08$ for giants and $+0.29\pm 0.13$ for dwarfs. The behaviors of magnesium, silicon and calcium are similar: an increasing trend of their relative abundance with decreasing metallicity can be seen in Fig. 6, while the average abundance ratio of Ti is lower than those of other three elements (see bottom panel of Fig. 7). A possible interpretation is that Ti is formed during complete and incomplete silicon burning while Si and Ca are produced by incomplete explosive silicon and oxygen burning (Cayrel et al. 2004).

In Fig. 7, we show our results for the four α -elements along with previous abundance studies (SB02; Gratton et al. 2003). Most of the previous studies for metal-poor stars that are mainly belonging to the inner halo concluded that $[\alpha/\text{Fe}]$ is constant for $[\text{Fe}/\text{H}] < -1$. McWilliam et al. (1995) and Ryan et al. (1996) showed that $[\alpha/\text{Fe}] \sim +0.4$ dex for $[\text{Fe}/\text{H}] < -2$, while Gratton et al. (1997) gave a mean $[\alpha/\text{Fe}]$ ($+0.26\pm 0.08$) for most halo stars through self-consistent analysis of 100 metal-poor ($[\text{Fe}/\text{H}] < -0.5$) dwarfs. On the other hand, our results of $[\alpha/\text{Fe}]$ values show a slope for $[\text{Fe}/\text{H}] < -1$, as found by SB02. The slope of $[\alpha/\text{Fe}]$ versus $[\text{Fe}/\text{H}]$ found in our analysis is -0.14 , which is similar to the value found by SB02 (-0.15) for 55 metal-poor halo stars. The dependence of chemical abundance trend on the kinematics properties is discussed in § 6.

5.2. Light odd-Z elements

5.2.1. Sodium

For stars with metallicities of $[\text{Fe}/\text{H}] > -2.5$, four lines at $\lambda\lambda 5682, 5688, 6154$ and 6160 were used for sodium abundance determination. The deviations from LTE formation for these lines are less than 0.1 dex (Baumüller et al. 1998), which is smaller than the typical errors in our analysis (0.1 dex). Hence, the non-LTE effects on these lines can be neglected. However, for some extremely metal-poor stars in our sample, these lines are too weak to be detected. Therefore, resonance lines at $\lambda\lambda 5890$ and 5896 were included to compute the sodium abundances for stars with $[\text{Fe}/\text{H}] < -2.5$. Non-LTE effects of these two lines in metal-poor dwarfs cannot be ignored (Baumüller et al. 1998). The abundance values derived by resonance lines are corrected by the estimate of non-LTE effects by Gehren et al. (2004, 2006).

Gehren et al. (2006) analyzed sodium abundances with non-LTE correction for 55 metal-poor dwarf stars. In the upper panel of Fig. 8, our results are compared with those in their study. For dwarfs the two sets of results agree well, while the $[\text{Na}/\text{Fe}]_{\text{NLTE}}$ values of giants in our sample are ~ 0.35 dex larger than in dwarfs in $-2.7 \lesssim [\text{Fe}/\text{H}] \lesssim -1.7$. In several

giants, the initial sodium abundance may be changed because of the products of the Ne-Na cycle from deeper layers being dredged to the surfaces (Andrievsky et al. 2007); The $[\text{Na}/\text{Fe}]$ in some giants might be explained by this effect, although a small systematic errors in the $[\text{Na}/\text{Fe}]$ ratios for giants and dwarfs are not excluded.

5.2.2. Scandium

In Fig. 6, the average of $[\text{Sc}/\text{Fe}]$ ratios of dwarfs is greater than the solar abundance ratio, while for giants there is a slowly decreasing trend with decreasing metallicity with a scatter of 0.14 dex. In the bottom panel of Fig. 8, our results are compared with those in Zhao & Magain (1990). They studied 20 metal-poor dwarfs, and found the overabundance of scandium relative to iron. A weak decreasing trend with decreasing metallicity for $[\text{Sc}/\text{Fe}]$ of giants is noticed. The $[\text{Sc}/\text{Fe}]$ of dwarfs are statistically 0.15 dex larger than that of giants in the similar metallicity range, mostly because of the high $[\text{Sc}/\text{Fe}]$ values derived by Zhao & Magain (1990). Similar conclusion was also reported very recently by Bonifacio et al. (2009).

5.3. Iron peak elements

Abundances of four iron-peak elements, Cr, Mn, Ni and Zn, were determined in our present paper.

The results of $[\text{Cr}/\text{Fe}]$ derived from neutral lines in our analysis show a decreasing trend with decreasing metallicity for giants. This confirms the results of previous studies for low-metallicity stars (McWilliam et al. 1995; Gratton et al. 2003; Cayrel et al. 2004; Barklem et al. 2005). Our results are shown with the previous work in the upper panel of Fig. 9. In Fig. 10, Cr abundances from Cr II lines and logarithmic abundance difference of Cr from Cr II and Cr I lines ($[\text{Cr}_{\text{II}}/\text{Cr}_{\text{I}}]$) are plotted as functions of $[\text{Fe}/\text{H}]$. The decreasing abundance ratio of Cr with decreasing $[\text{Fe}/\text{H}]$ is not found in $[\text{Cr}/\text{Fe}]_{\text{II}}$. The average $[\text{Cr}_{\text{II}}/\text{Cr}_{\text{I}}]$ is 0.32 dex for giants and 0.28 dex for dwarfs. Similar offset between neutral and ionize Cr was also reported in Lai et al. (2008). Sobek et al. (2007) suggested that this discrepancy may be due to NLTE effects. Besides, the decreasing trend found for Cr in giants is not seen in dwarfs studied by SB02 and Gratton et al. (2003). Such a result is also found by Lai et al. (2008) and Bonifacio et al. (2009). Possible explanations for this discrepancy were discussed by Lai et al. (2008), and is not repeated here.

Our $[\text{Mn}/\text{Fe}]$ presents a plateau at -0.44 dex in $-2.5 < [\text{Fe}/\text{H}] < -1$. In the second

panel of Fig. 9, combining with the halo dwarf samples of Gratton et al. (2003), a ~ 0.16 dex systematic difference of $[\text{Mn}/\text{Fe}]$ between dwarfs and giants in the metallicity range of $-2 < [\text{Fe}/\text{H}] < -1$ is noticed. Although we lack of enough data for lower metallicity range ($[\text{Fe}/\text{H}] < -3$), Bonifacio et al. (2009) presented that such phenomena are also found in extreme metal-poor stars. They also suggested that the discrepancy of these two elements between giants and dwarfs may be reduced if 3D models are adopted.

The Ni abundance ratios shown in Fig. 6 are approximately constant around the solar value. $\langle [\text{Ni}/\text{Fe}] \rangle = -0.06 \pm 0.08$ dex. This result agrees well with the study of Stephens (1999) ($\langle [\text{Ni}/\text{Fe}] \rangle = -0.09 \pm 0.07$) and SB02 ($\langle [\text{Ni}/\text{Fe}] \rangle = -0.06 \pm 0.20$). Tsujimoto et al. (1995) mentioned that $[\text{Ni}/\text{Fe}]$ yields in the mass-averaged SNe II are roughly consistent with solar abundance ratios.

Several previous works conclude that $[\text{Zn}/\text{Fe}] \sim 0$ for $-2.5 \lesssim [\text{Fe}/\text{H}] < 0$, while at a lower metallicity, the ratio increases with declining of $[\text{Fe}/\text{H}]$ (Cayrel et al. 2004; Barklem et al. 2005; Umeda & Nomoto 2005). In the comparison with Barklem et al. (2005) in the bottom panel of Fig. 9, we found that these features are not clear in our sample because of the existence of low $[\text{Zn}/\text{Fe}]$ stars in $[\text{Fe}/\text{H}] < -2.5$. Moreover, the $[\text{Zn}/\text{Fe}]$ of our sample is lower than other stars studied by previous work in general. This suggests the low Zn abundance in outer halo stars. This possibility is discussed in §6 in more detail.

5.4. Neutron capture elements

The last two panels of Fig. 6 show the abundance ratios $[\text{Y}/\text{Fe}]$ and $[\text{Ba}/\text{Fe}]$ as a function of $[\text{Fe}/\text{H}]$. Comparisons with previous works are presented in Fig. 11. Ba is also chosen as the reference element to investigate the $[\text{Y}/\text{Ba}]$ (Fig. 12).

$[\text{Y}/\text{Fe}]$ and $[\text{Ba}/\text{Fe}]$ of BD+04°2466 are obviously higher than other stars. We estimated the carbon abundance of this star as $[\text{C}/\text{Fe}] = 1.21$ dex. As mentioned in §2.3, this star is believed to belong to a binary system because of its radial velocity variation. Thus, this star would have obtained s-process-rich material from an AGB companion (Busso et al. 2001).

Both $[\text{Y}/\text{Fe}]$ and $[\text{Ba}/\text{Fe}]$ increase with increasing $[\text{Fe}/\text{H}]$ in the lower metallicity range ($[\text{Fe}/\text{H}] < -2$), while the ratios are approximately constant ($[\text{Y}/\text{Ba}] \sim 0$) at the higher metallicity. At lower metallicity, $[\text{Y}/\text{Ba}]$ increases with decreasing $[\text{Fe}/\text{H}]$ or $[\text{Ba}/\text{H}]$. The behaviors of Y and Ba are similar for $[\text{Fe}/\text{H}] > -2$. By contrast, no object having high $[\text{Y}/\text{Fe}]$ or $[\text{Ba}/\text{Fe}]$ is found in our sample in $[\text{Fe}/\text{H}] < -2$. Such under-abundance of neutron-capture elements in the low metallicity range is possibly a chemical property of outer halo stars. However, given the small number of stars studied here, we cannot derive any conclusion.

The bottom panel of Fig. 12 shows the $[Y/Ba]$ as a function of $[Ba/H]$. This can be divided into two parts: near solar abundance for $[Ba/H] > -2.5$ and increasing of $[Y/Ba]$ with barium decreasing at lower $[Ba/H]$. Honda et al. (2004) and Aoki et al. (2005) discussed that the “weak r-process” which contributes only to the light neutron-capture elements affects most stars with $[Fe/H] \gtrsim -3.5$. The feature in Fig. 12 indicates that the stars with $[Ba/H] < -2.5$ ($-3.25 < [Fe/H] < -2.25$) in our sample have been significantly affected by this process.

5.5. Magnesium as the metallicity indicator

Although the Fe abundance is adopted as the metallicity indicator in the above discussion as usual, the Mg abundance may provide better estimate of metallicity, because that is produced by hydrostatic burning processes in massive stars, while Fe production is sensitive to the supernova processes yet understood well. Shigeyama & Tsujimoto (1998) and Cayrel et al. (2004) also recommended that choosing this element as metallicity tracer. Thus, the abundances of odd-Z elements and α -elements relative to magnesium vs. $[Mg/H]$ are plotted in Fig. 13. It is clear that the behavior of Ti is different from other α -elements (Fig. 13). The reason is discussed in §5.1.

In the first plot of Fig. 13, we notice that a relatively large scatter in $[Na/Mg]$ is seen in giants which are in the metallicity range of $[Mg/H] < -1.5$, while the correlation of $[Na/Mg]$ vs. $[Mg/H]$ is tighter in the higher metallicity range ($[Mg/H] > -1.5$). As discussed in §5.2.1, some giants with large sodium abundances enhanced by dredging process cause higher $[Na/Mg]$ and, consequently, result in large scatter of $[Na/Mg]$ at lower $[Mg/H]$.

A strong metallicity dependence of abundance ratios of the odd-Z elements (Na, Sc) is seen in Fig. 13. The production of Na is thought to be controlled by the neutron flux which depends on the metallicity of the SN. Therefore, a statistic increase of $[Na/Mg]$ with increasing $[Mg/H]$ is expected. Besides, Sc is a product of explosive oxygen and neon burning (Woosley & Weaver 1995), the enhanced mechanism of the Sc is thought to be the surplus of neutrons in ^{22}Ne which is formed from ^{14}N by the CNO circle (Kobayashi et al. 2006). The low abundance ratios of Sc in low $[Mg/H]$ is the result of small amount of CNO elements.

6. Discussion

As mentioned in §5.1, the $[\alpha/Fe]$ vs. $[Fe/H]$ diagram obtained for our sample stars presents a finite slope, namely, decreasing $[\alpha/Fe]$ with increasing $[Fe/H]$ (Fig. 6). A similar

trend was also reported by SB02, who studied candidate outer-halo stars. Fig. 7 shows the abundance ratios of α -elements for our sample and that of SB02 as well as of Gratton et al. (2003). The stars of the present work and of SB02 show the decreasing trend and the presence of a large scatter in the $[\alpha/\text{Fe}]$ ratios at $[\text{Fe}/\text{H}] > -2$, compared with the objects studied by Gratton et al. (2003), most of which are inner halo stars. Thus, although the $[\alpha/\text{Fe}]$ ratios (in particular $[\text{Mg}/\text{Fe}]$) of the halo sample, usually dominated by the inner halo population, have been conventionally regarded to be constant, this is not the case for the outer halo stars.

Our measurements also suggest that the $[\text{Zn}/\text{Fe}]$ ratios of our sample are systematically lower than other halo stars previously studied. This element was not studied by SB02. Most of our objects with $-2 < [\text{Fe}/\text{H}] < -1$ have sub-solar $[\text{Zn}/\text{Fe}]$ values, while the bulk of halo stars previously studied (most of them would belong to the inner halo) have $[\text{Zn}/\text{Fe}] \sim 0$. The three most metal-poor stars ($[\text{Fe}/\text{H}] < -2.5$) in our sample have $[\text{Zn}/\text{Fe}] \sim 0$, lower than the trend found for other stars in this metallicity range previously.

We here investigate a possible correlation between abundance ratios and orbital parameters of our current sample stars. Figures 14 and 15 show the abundance ratios for Mg, Si, Ca and Zn as functions of Z_{max} and R_{apo} , respectively. In these plots, small and large marks correspond to $[\text{Fe}/\text{H}] < -2$ and > -2 , respectively. As is evident, no clear trend of $[\text{X}/\text{Fe}]$ against the orbital parameters is found for the three α elements. For $[\text{Fe}/\text{H}] < -2$ the $[\alpha/\text{Fe}]$ ratios remain larger than those for $[\text{Fe}/\text{H}] > -2$ and a star with highest $[\alpha/\text{Fe}]$ is located at large Z_{max} or R_{apo} . This suggests that metal-poor, outer halo stars with $[\text{Fe}/\text{H}] < -2$ are largely enriched by SNe II, without any dependence on their orbital parameters. Also the outer halo stars with $[\text{Fe}/\text{H}] > -2$ show roughly constant $[\alpha/\text{Fe}]$ ratios with increasing Z_{max} or R_{apo} . We note that HD 134439 having the lowest $[\alpha/\text{Fe}]$ has low Z_{max} , but has very high R_{apo} , and is classified into the outer halo. In contrast to $[\alpha/\text{Fe}]$, one may find a weak decreasing trend of $[\text{Zn}/\text{Fe}]$ with increasing Z_{max} and R_{apo} . However, the sample size is yet too small to derive any definitive conclusion for this trend.

These results indicate that, among our sample stars which reside in the outer halo component, there is no significant dependence of chemical abundances on kinematical parameters *within* this population. There is a signature of some systematic, chemical difference between the inner and outer halo: smaller $[\alpha/\text{Fe}]$ with large scatters at $[\text{Fe}/\text{H}] > -2$ (Fig. 7) and smaller $[\text{Zn}/\text{Fe}]$ at $[\text{Fe}/\text{H}] < -2$ (Fig. 9) for the outer halo than the inner one. However, in order to set tighter constraints on these chemical trends, a much larger sample of both inner and outer halo stars is clearly required.

The decreasing trend of $[\alpha/\text{Fe}]$ with increasing metallicity found for the outer halo stars recalls the chemical nature of dwarf spheroidal galaxies (dSphs) around the Galaxy (e.g.,

Shetrone et al. 2001, 2003). Lanfranchi & Matteucci (2004) studied abundance ratios of six dSph galaxies, and predicted a plateau for lower metallicity range ($[\text{Fe}/\text{H}] \lesssim -1.8$) and a sudden decrease for $[\text{Fe}/\text{H}] \gtrsim -1.8$ in the relationship between $[\alpha/\text{Fe}]$ and $[\text{Fe}/\text{H}]$. The production of α elements are mainly from SNe II explosions in a short time scale while Fe can be from SNe Ia and SNe II. The sharp decline of $[\alpha/\text{Fe}]$ implies intense galactic winds and contributions of SNe Ia to Fe from $[\text{Fe}/\text{H}] \sim -1.8$ in dSph galaxies (Lanfranchi & Matteucci 2004). If a merging and collision of certain dSph galaxies happened before significant contributions of SNe Ia, it should result in normal $[\alpha/\text{Fe}]$ in outer halo of the Galaxy. Indeed, in the simulation of Johnston et al. (2008), they suggested that α -rich stars in outer halo may come from dSph galaxies by merging at early epoch. On the other hand, mergers of dSph galaxies at later times would result in low $[\alpha/\text{Fe}]$ stars in the outer halo.

The lower $[\text{Zn}/\text{Fe}]$ values were also reported for stars belonging to the nearby dSph studied by Shetrone et al. (2001, 2003). Among their sample, majority of dSphs stars having metallicity of $-2 < [\text{Fe}/\text{H}] < -1$ show $[\text{Zn}/\text{Fe}] < 0$ similar to our sample of outer halo stars. For the more metal-poor stars ($[\text{Fe}/\text{H}] < -2$) in our sample, $[\text{Zn}/\text{Fe}]$ approximately follow the solar value as discussed in Section 5.3, except for one star showing $[\text{Zn}/\text{Fe}] > 0.4$. This behavior is similar to metal-poor stars in the ultra-faint dwarf spheroidal galaxies studied in Frebel et al. (2009). However, the sample size of stars in dwarf galaxies for which the Zn abundance is studied is too small to derive any conclusion. Further measurements of Zn abundances for dwarf galaxy stars as well as for outer halo objects would be a key to understanding the contributing of massive progenitors to the metal-enrichment in these systems.

We also remark that the $[\text{Mn}/\text{Fe}]$ ratios of the outer halos stars having an approximately constant value of ~ -0.4 dex agree well with those obtained for dSph stars (e.g., Shetrone et al. 2001, 2003). Thus, combined with the properties of $[\alpha/\text{Fe}]$ and $[\text{Zn}/\text{Fe}]$ ratios discussed above, it is consistent with the hypothesis that the outer halo is largely made up with late merging/accretion of dSphs which are similar to those currently observed.

In the analysis of Roederer (2009), a large spread (0.5 – 0.7 dex) in $[\text{Ni}/\text{Fe}]$ for the outer halo stars was noticed. However, in our sample, the scatter of $[\text{Ni}/\text{Fe}]$ of outer halo stars is 0.05 dex, which is similar to that of our inner halo ones (0.06 dex). The abundance ratios of Roederer (2009) were collected from different sources, therefore, the large scatter in his analysis is partially caused by different spectral qualities, different methods of stellar parameter determination and different structure of model atmospheres. Our consistency results do not support the claim about the difference of the abundance scatter between the inner and outer halo populations. Thus, a sample with larger size and from

single source is needed to probe whether Ni can be taken as another indicator for chemical inhomogeneity between inner and outer halo populations.

7. Summary

Elemental abundances and kinematics of 26 metal-poor halo stars in $-3.5 < [\text{Fe}/\text{H}] < -1.0$ were studied with high-resolution and high signal-to-noise ratio spectra taken from Subaru/HDS. Most objects have large values of Z_{max} and/or R_{apo} , indicating their outer halo population.

1. The α -elements (Mg, Si, Ca, Ti) to iron ratios are overabundant relative to the solar values, and increase with decreasing $[\text{Fe}/\text{H}]$. From the investigation of $[\alpha/\text{Fe}]$ with kinematics, it is concluded that the slope of $[\alpha/\text{Fe}]$ vs. $[\text{Fe}/\text{H}]$ is caused by outer halo stars. This result bears a resemblance to the abundance trend of α -elements found in dSph galaxies around the Milky Way, suggesting contributions of mergers of dSph galaxies at later times to the formation of the outer halo structure.

2. There exist low $[\text{Zn}/\text{Fe}]$ stars in the very low metallicity range, which is different from the trend of Zn abundances found by previous studies, but is rather similar to those of ultra-faint dwarf galaxies. A weak slope is displayed in the plots of $[\text{Zn}/\text{Fe}]$ against kinematic parameters. These signatures should be confirmed by future work based on a larger sample.

3. The neutron-capture elements Y and Ba are under-abundant, following the trend found for the bulk of field halo stars. No neutron-capture enhanced object was found in our sample, and that is a possible property of outer halo stars, though studies for a larger sample is also needed. Increasing Y with decreasing Ba in lower $[\text{Ba}/\text{H}]$ indicates that the stars with lower $[\text{Fe}/\text{H}]$ and $[\text{Ba}/\text{H}]$ in our sample have experienced the “weak r-process”.

4. Discrepancies of elemental abundances by the order of 0.15 dex between giant and dwarf stars are found for Sc, Cr and Mn. Our results support the recent study for these elements by Bonifacio et al. (2009), though the reasons for these discrepancies are still unclear. A discrepancy of 0.35 dex between giants and dwarfs is found for $[\text{Na}/\text{Fe}]$ in $[\text{Fe}/\text{H}] < -2$ even after non-LTE corrections, possibly reflecting abundance variations in several giants from their original composition.

LZ thanks Drs. J. R. Shi, Y. Q. Chen and J. S. Deng for useful suggestions and discussions. This work is supported by the NSFC under grant 10821061 and by the National Basic Research Program of China under grant 2007CB815103. MC acknowledges support from a Grant-in-Aid for Scientific Research (20340039) of the Ministry of Education, Culture,

Sports, Science and Technology in Japan.

REFERENCES

- Alonso, A., Arribas, S., Martínez-Roger, C., 1996, *A&A*, 313, 873
- Alonso, A., Arribas, S., Martínez-Roger, C., 1999, *A&AS*, 140, 261
- Anders, E., & Grevesse, N., 1989, *Geochim. Cosmochim. Acta*, 53, 197
- Andrievsky, S. M., Spite, M., Korotin, S. A., & Spite, F. et al., *A&A*, 464, 1081
- Aoki, W., Honda, S., Beers, T. C., et al., 2005, *ApJ*, 632, 611
- Aoki, W., Barklem, P. S., Beers, T. C., Christlieb, N., Inoue, S., Garcia Perez, A. E., Norris, J. E., & Carollo, D., 2009, *ApJ*, 698, 1803
- Aoki, W., et al., 2009, *A&A*, 502, 569
- Barklem, P. S., Christlieb, N., Beers, T. C., et al., 2005, *A&A*, 439, 129
- Baumüller, D., Butler, K., & Gehren, T., 1998, *A&A*, 338, 637
- Beers, T. C., Chiba, M., Yoshii, Y., Platais, I., Hanson, R. B., Fuchs, B. & Rossi, S., 2000, *AJ*, 119, 2866
- Beers, T. C., & Christlieb, N., 2005, *ARA&A*, 43, 531
- Booth, A. J., Blackwell, D. E., Petford, A. D., & Shallis, M. J., 1984, *MNRAS*, 208, 147
- Biéumont, E., & Godefroid, M. 1980, *A&A*, 84, 361
- Bonifacio, P., Spite, M., & Cayrel, R. et al., 2009, arXiv: 0903.4174
- Bullock, J. S., & Johnston, K. V., 2005, *ApJ*, 635, 931
- Busso, M., Gallino, R., Lambert, D.L., Travaglio, C., & Smith, V.V., 2001, *ApJ*, 557, 802
- Carney, B. W., Latham, D. W., Laird, J. B., & Aguilar, L. A., 1994, *AJ*, 107, 2240
- Carney, B. W., Latham, D. W., Stefanik, R. P., Laird, J. B., & Morse, J. A., 2003, *AJ*, 125, 293
- Carretta, E., Gratton, R., Cohen, J., et al., 2002, *ApJ*, 124, 481

- Castelli, F., Gratton, R. G., & Kurucz, R. L., 1997, *A&A*, 318, 841
- Castelli, F., & Kurucz, R. L. 2003, *Modelling of Stellar Atmospheres*, 210, 20P
- Carollo, D., et al., 2007, *Nature*, 450, 1020
- Cayrel, R. 1988, in *The impact of very high S/N spectroscopy on Stellar Physics*, ed. G. Cayrel de Strobel, & M. Spite (Kluwer), *Proc. IAU Symp.*, 132, 345
- Cayrel, R., Depagne, E., Spite, M., et al. 2004, *A&A*, 416, 1117
- Chiba, M., & Beers, T. C., 2000, *AJ*, 549, 325
- Cohen, J. G., Christlieb, N., Beers, T. C., et al., 2002, *ApJ*, 124, 470
- Frebel, A., Simon, J. D., Geha, M., & Willman, B., 2009, *arXiv:0902.2395*
- Fulbright, J. P., 2000, *AJ*, 120, 1841
- Fulbright, J. P., 2002, *AJ*, 123, 404
- Honda, S., Aoki, W., Kajino, T., et al., 2004, *ApJ*, 607, 474
- Heger, A., & Woosley, S. E., 2002, *ApJ*, 567, 532
- Gehren, T., Liang, Y. C., Shi, J. R., et al., 2004, *A&A*, 413, 1045
- Gehren, T., Shi, J. R., Zhang, H. W., et al., 2006, *A&A*, 451, 1065
- Gilmore, G., & Wyse, R. F. G., 1998, *AJ*, 116, 748
- Gratton, R. G., Carretta, E., Clementini, G., & Sneden, C. 1997, in *Proc. of the ESA Symposium: HipparcosVenice '97*, ESA SP-402 (Noordwijk: ESA), 339
- Gratton, R. G., Carretta, E., Claudi, R., Lucatello, S., & Barbieri, M., 2003, *A&A*, 404, 187
- Ibata, R. A., Gilmore, G., & Irwin, M. J., 1994, *Nature*, 370, 194
- Jorissen, A., Zacs, L., Udry, S., Lindgren, H., & Musaeff, F. A., 2005, *A&A*, 441, 1135
- Johnston, K. V., Bullock, J. S., Sharma, S., Font, A., Robertson, B. E., & Leitner, S. N., 2008, *ApJ*, 689, 936
- Kobayashi, C., Umeda, H., Nomoto, K., Tominaga, N., & Ohkubo, T., 2006, *ApJ*, 653, 1145
- Kurucz, R. L., 1993, CD-ROM No. 13, 18, Smithsonian Astrophysical Observatory

- Lai, D. K., Bolte, M., Johnson, Jennifer A., & Lucatello, S., et al., 2008, ApJ, 681, 1524
- Lanfranchi, G. A., & Matteucci, F., 2004, MNRAS, 351, 1338
- Latham, D. W., Stefanik, R. P., & Torres, G. et al., 2002 ApJ, 124, 1144
- Lawler, J. E., & Dakin, J. T., 1989, J. Opt. Soc. Am. B 6, 1457
- McWilliam, A., Preston, G. W., Sneden, C., & Searle, L., 1995, AJ, 109, 2757
- McWilliam A., 1998, AJ, 115, 1640
- Noguchi, K., Aoki, W., Kawanomoto, S., Ando, H., et al., 2002, PASJ, 54, 855
- Norris, J. E. 1994, ApJ, 431, 645
- Perryman, M. A. C., Lindegren, L., Kovalevsky, J., & Hoeg, E., et al., 1997, A&A, 323L, 49
- Preston, G. W., Beers, T. C., & Schectman, S. A., 1994, AJ, 108, 538
- Ramirez, I., & Meléndez, J., 2004, ApJ, 609, 417
- Reoderer, I. U., 2009, ApJ, 137, 272
- Ryan, S. G., & Norris, J. E., 1991, AJ, 101, 1865
- Ryan, S. G., Norris, J. E., Beers, T. C., 1996, ApJ, 471, 254
- Schlegel, D. J., Finkbeiner, D. P., & Davis, M., 1998, ApJ, 500, 525
- Shetron, M., Côté, P., & Sargent, W. L. W., 2001, ApJ, 548, 592
- Shetron, M., Venn, K. M., Tolstoy, E., Primas, F., Hill, V., & Kaufer, A., 2003, ApJ, 125, 684
- Shigeyama, T., & Tsujimoto, T., 1998, ApJ, 507, L135
- Sneden, C., McWilliam, A., Preston, G. W., et al., 1996, ApJ, 467, 819
- Sobeck, J. S., Lawler, J. E., & Sneden, C., 2007, ApJ, 667, 1267
- Sommer-Larsen, J. & Zhen, C., 1990, MNRAS, 242, 10
- Stephens, A., 1999, AJ, 117, 1771
- Stephens, A., & Boesgaard, A. M., 2002, AJ, 123, 1647

Tsujimoto, T., Nomoto, K., Yoshii, Y., Hashimoto, M., Yanagida, S., & Thielemann, F.-K.,
1995, MNRAS, 277, 94

Umeda, H., & Nomoto, K., 2005, ApJ, 619, 427

Woosley, S.E., & Weaver, T. A., 1995, ApJS, 101, 181

Zhao, G., & Magain, P., 1990, A&A, 238, 242

Zhao, G., & Magain, P., 1991, A&A, 244, 425

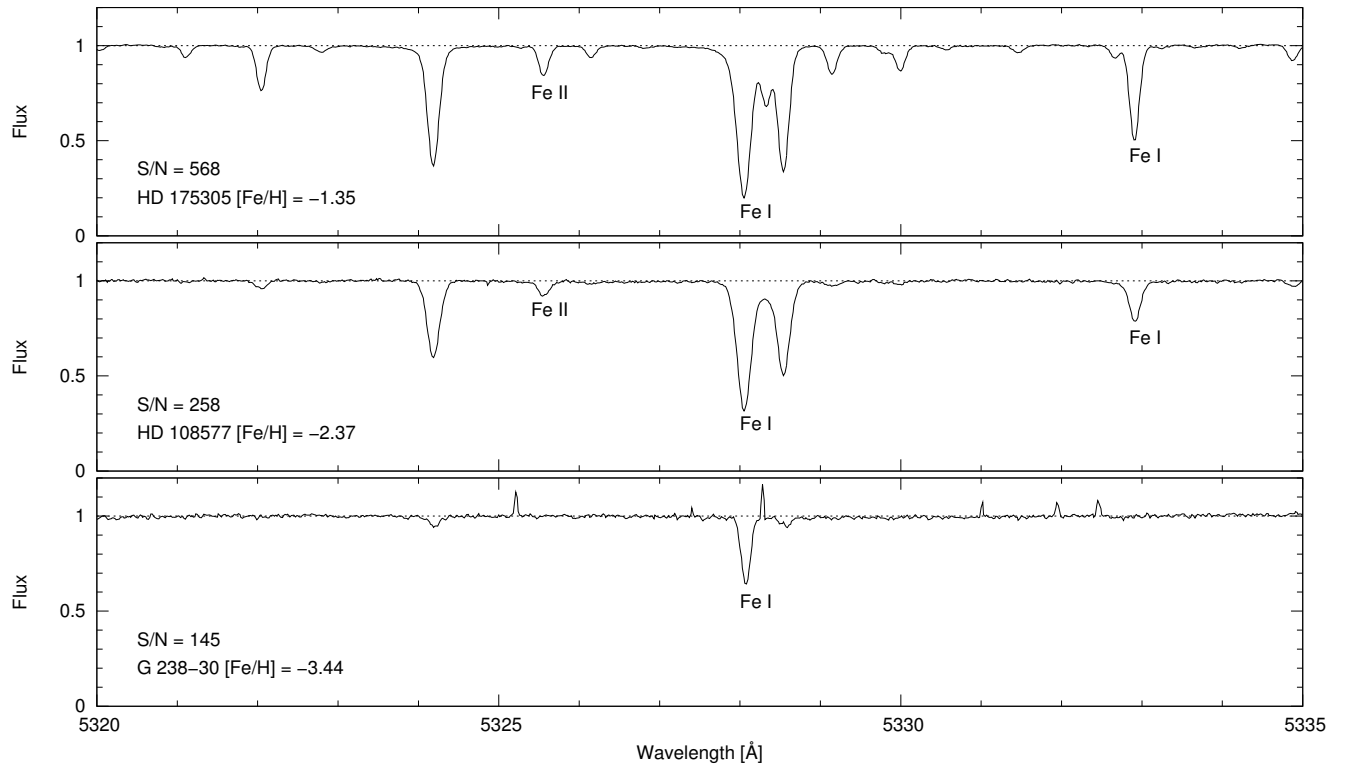


Fig. 1.— Examples of spectra obtained with Subaru/HDS for HD 175305 ($T_{\text{eff}} = 5035$, $\log g = 2.84$, $[\text{Fe}/\text{H}] = -1.35$) with $S/N \sim 568$, HD 108577 ($T_{\text{eff}} = 4800$, $\log g = 1.13$, $[\text{Fe}/\text{H}] = -2.37$) with $S/N \sim 270$ and G 238-30 ($T_{\text{eff}} = 5490$, $\log g = 3.57$, $[\text{Fe}/\text{H}] = -3.44$) with $S/N \sim 130$.

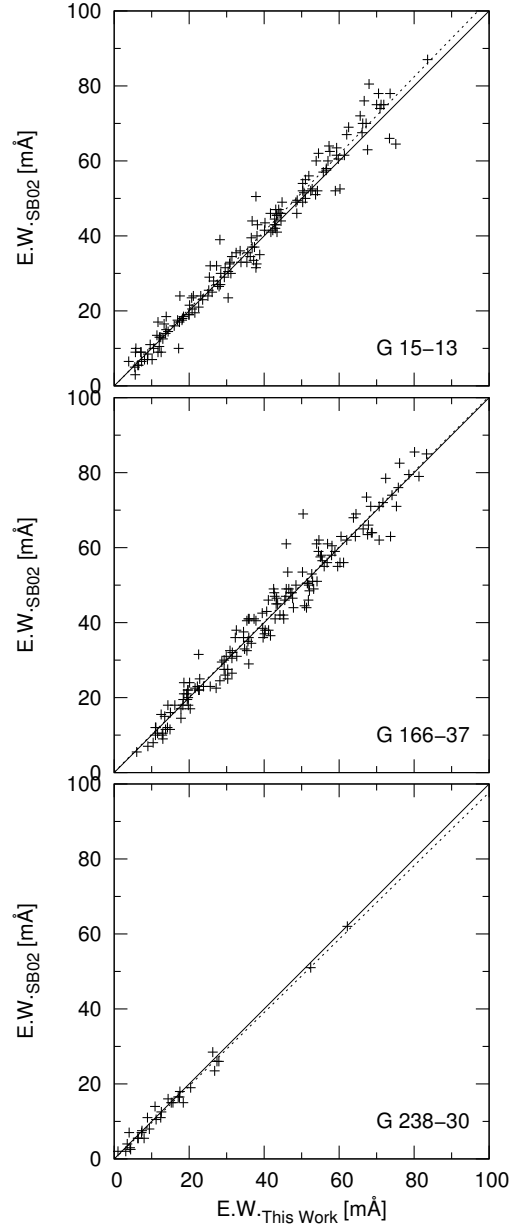


Fig. 2.— Comparison of the equivalent widths measured in this work with those of SB02. In all cases the solid line represents a one-to-one correlation and the dotted line represents a linear fit of the data.

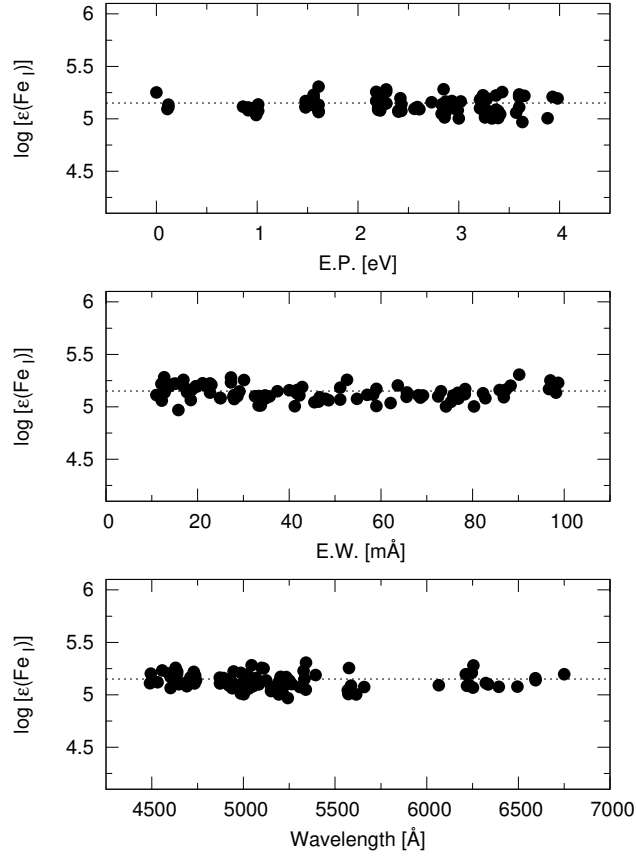


Fig. 3.— Fe I abundances derived from individual Fe I lines for HD 108577 as functions of excitation potential (E.P.), equivalent width (E.W.), and wavelength. The dashed line represents the mean value of iron abundance. The parameters are $T_{\text{eff}} = 4800\text{K}$, $\log g = 1.13$, $[\text{Fe}/\text{H}] = -2.37$, $\xi_t = 1.8 \text{ km}\cdot\text{s}^{-1}$.

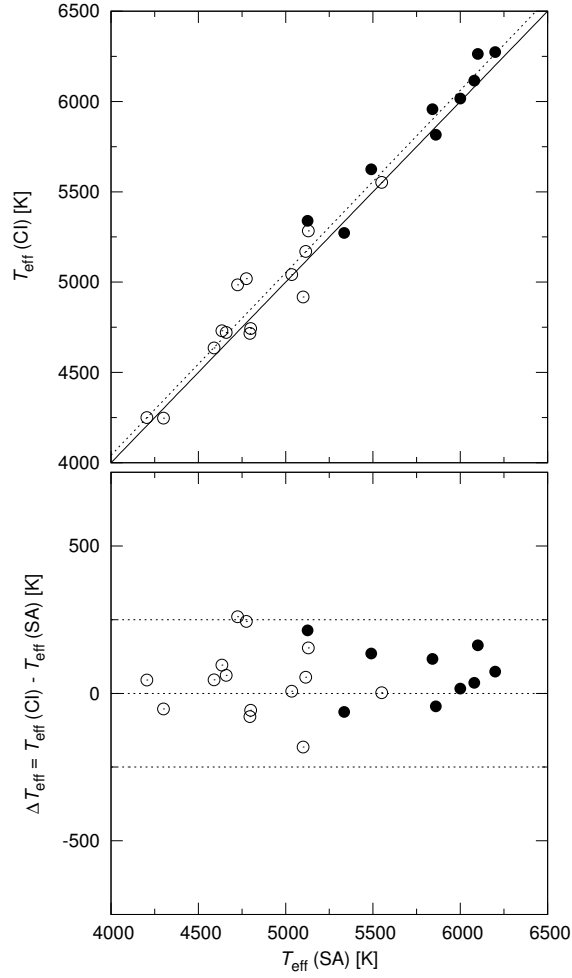


Fig. 4.— Comparison of T_{eff} adopted finally (SA) vs. those derived by color indices (CI). The solid line represents a one-to-one correlation while the dashed line represents a linear fit of the data. Filled circles represent dwarfs while open ones mean giants.

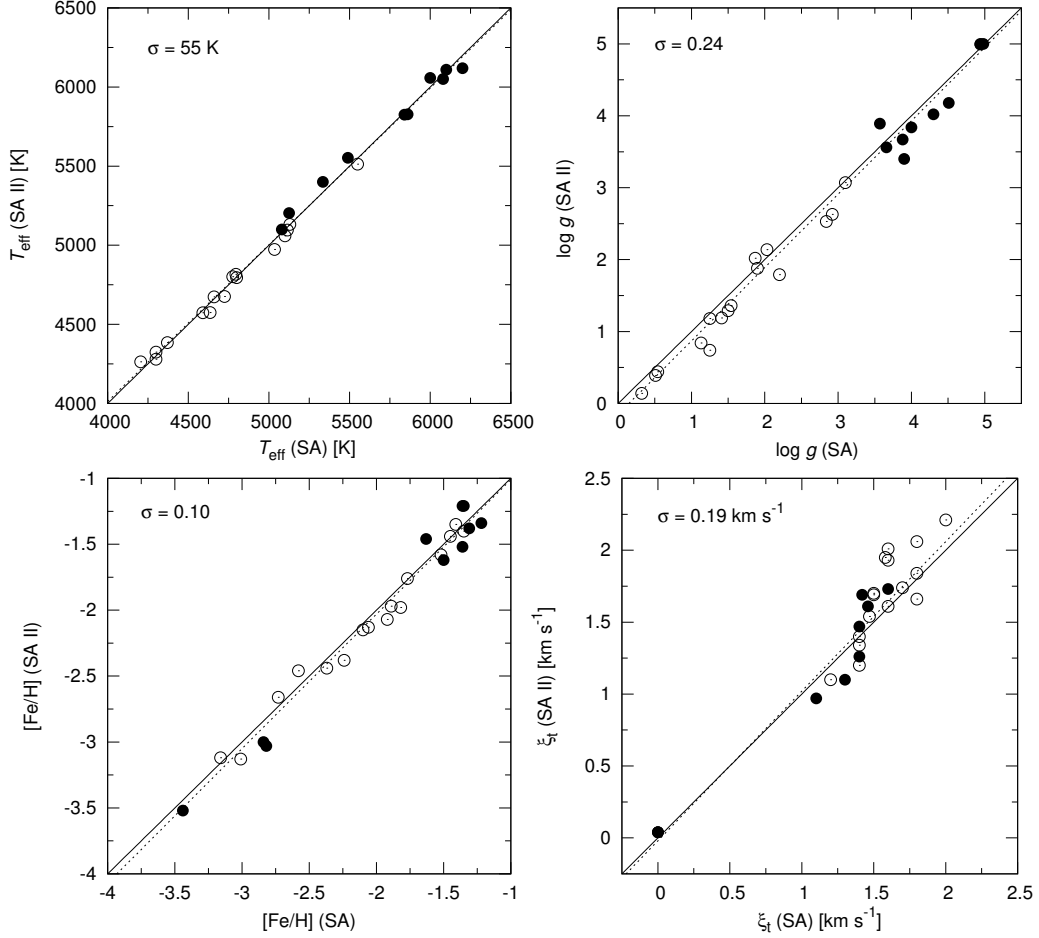


Fig. 5.— Comparison of atmospheric parameters adopted finally (SA) with those derived by an independent analysis (SA II; see text). The solid line represents a one-to-one correlation while the dashed line represents a linear fit of the data. The symbols are the same as in Fig. 4.

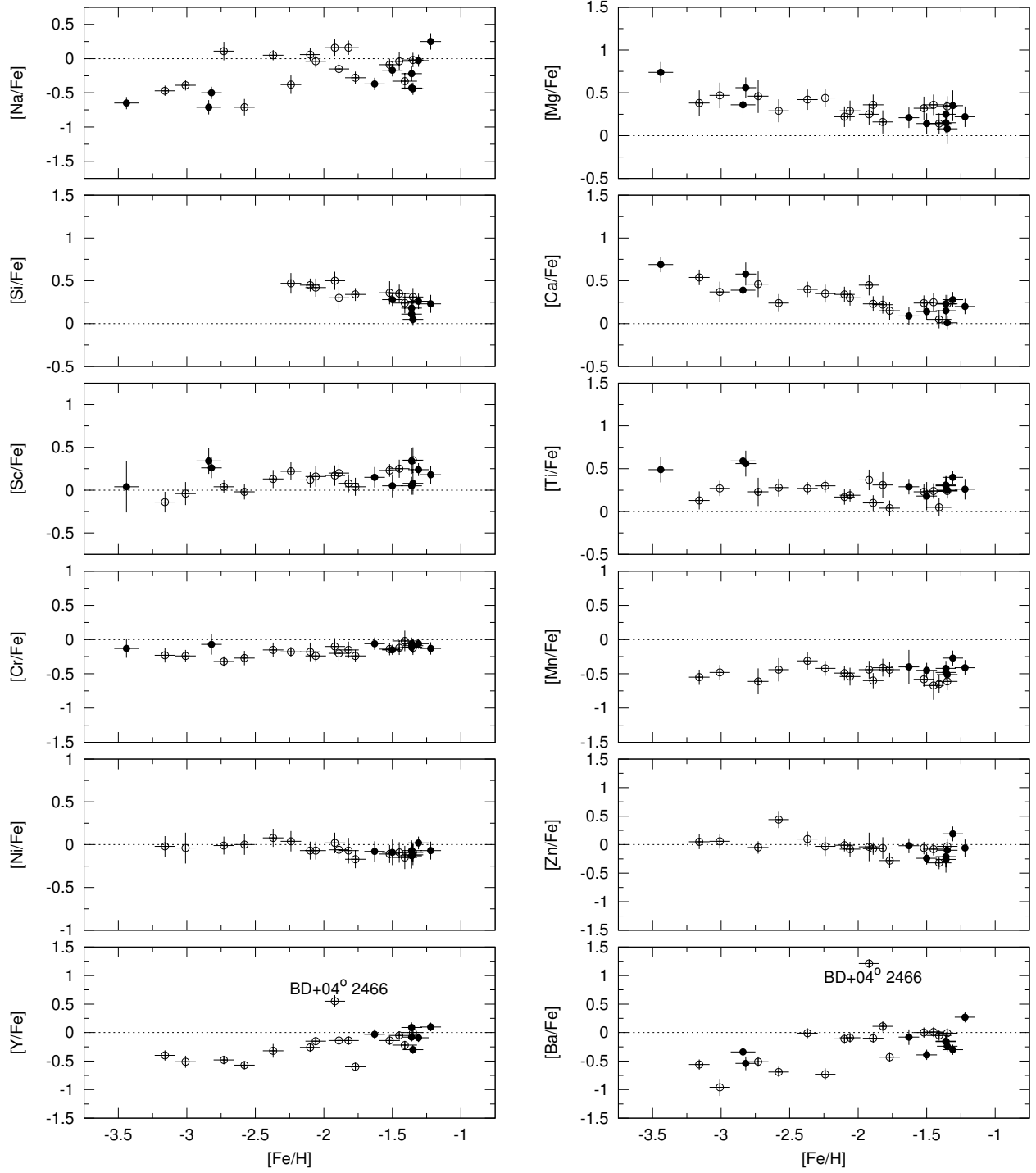


Fig. 6.— Plots of the elemental abundance ratios against metallicity. The symbols are the same as in Fig. 4.

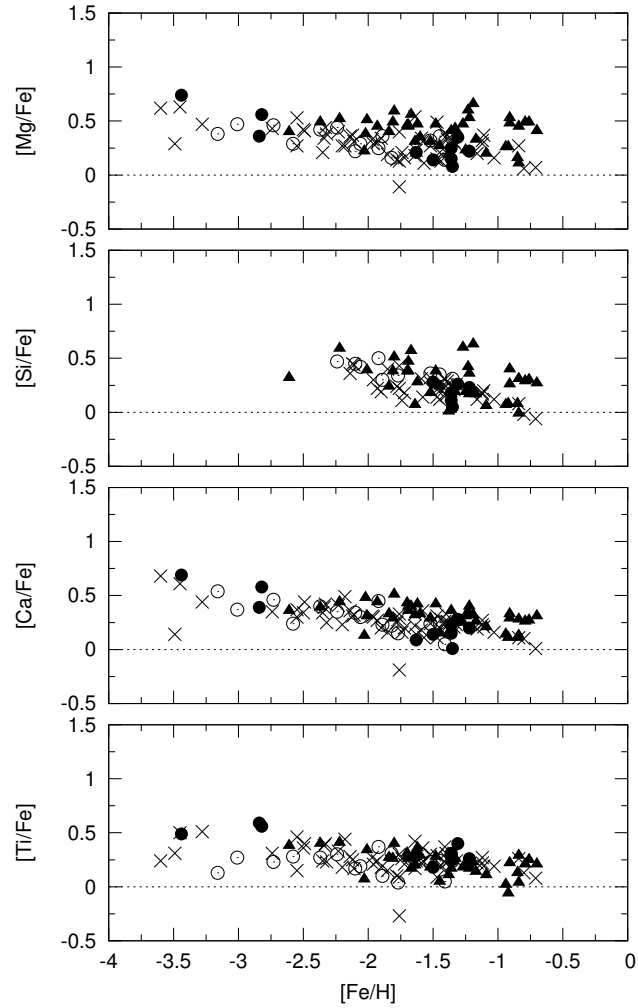


Fig. 7.— A plot of our observed $[\alpha/\text{Fe}]$ values (circles, same as Fig. 4) and previous abundance studies. The crosses represent the results of SB02, while filled triangles mean the results of halo samples from Gratton et al. (2003).

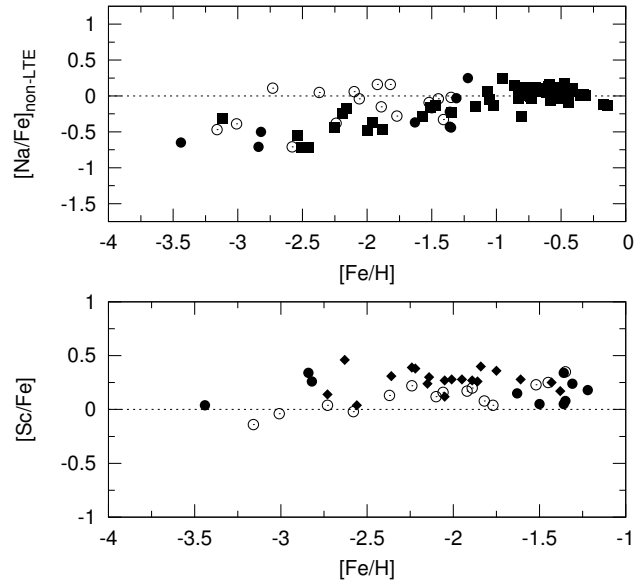


Fig. 8.— Same as Fig. 7, but for $[\text{Na}/\text{Fe}]$ and $[\text{Sc}/\text{Fe}]$. Filled squares are dwarfs from Gehren et al. (2006), and filled diamonds are dwarfs from Zhao & Magain (1990).

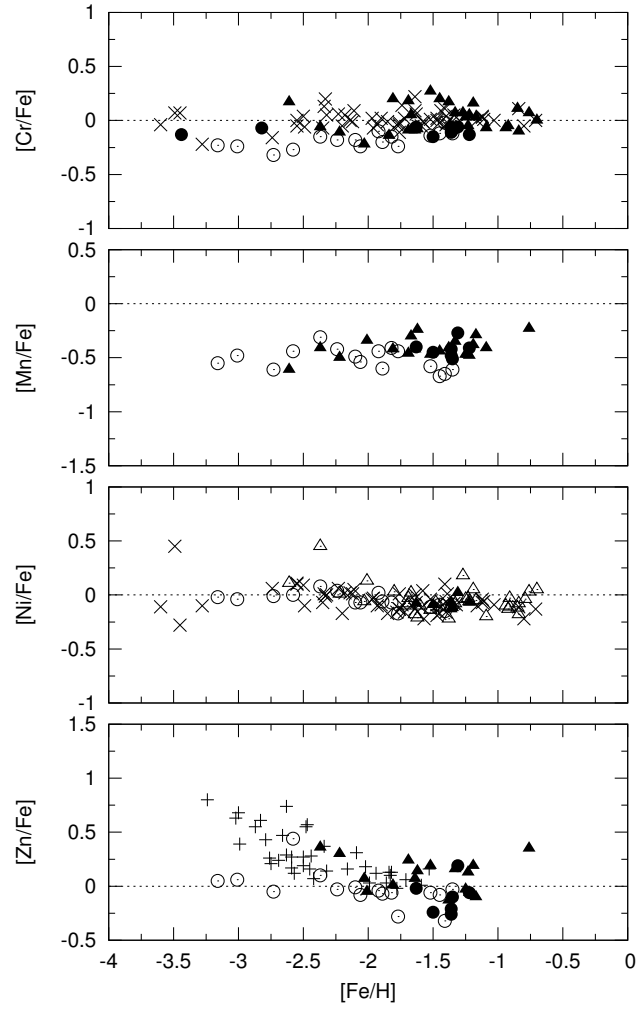


Fig. 9.— Same as Fig. 7, but for Fe-peak elements. Pluses represent the results of Barklem et al. (2005).

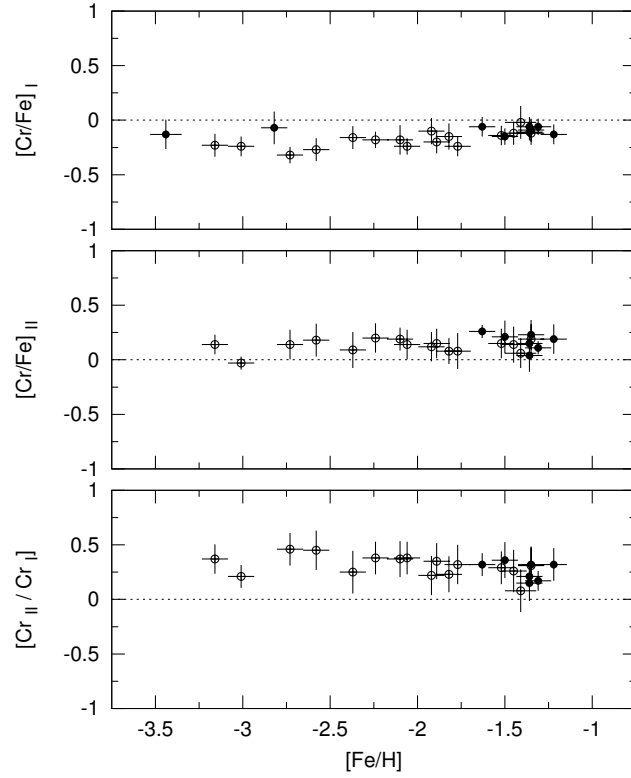


Fig. 10.— Cr abundance derived from Cr I and Cr II ($[\text{Cr}/\text{Fe}]_{\text{II}}$) against with $[\text{Fe}/\text{H}]$, along with $[\text{Cr II}/\text{Cr I}]$. The symbols are the same as in Fig. 4.

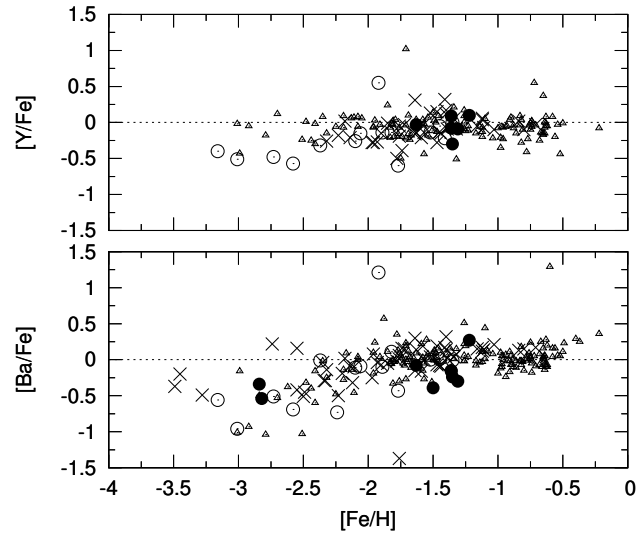


Fig. 11.— Same as Fig. 7, but for $[\text{Y}/\text{Fe}]$ and $[\text{Ba}/\text{Fe}]$. Small open triangles represent the results from Fulbright (2000).

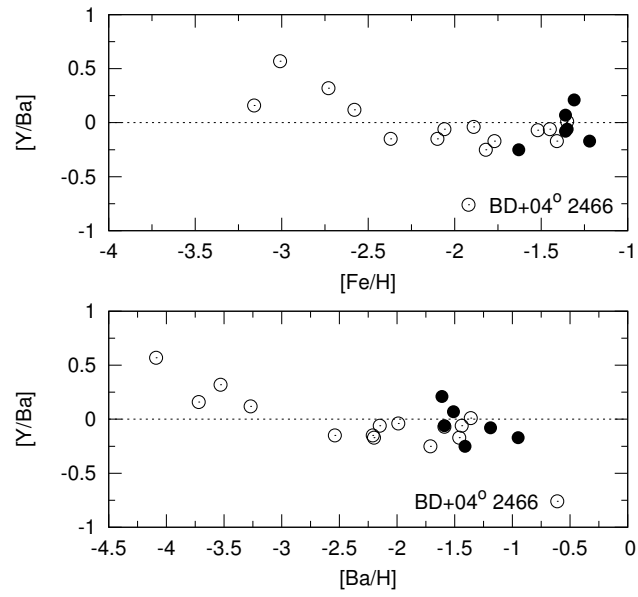


Fig. 12.— A plot of $[Y/Ba]$ vs. $[Fe/H]$ and $[Ba/H]$. The symbols are the same as in Fig. 4.

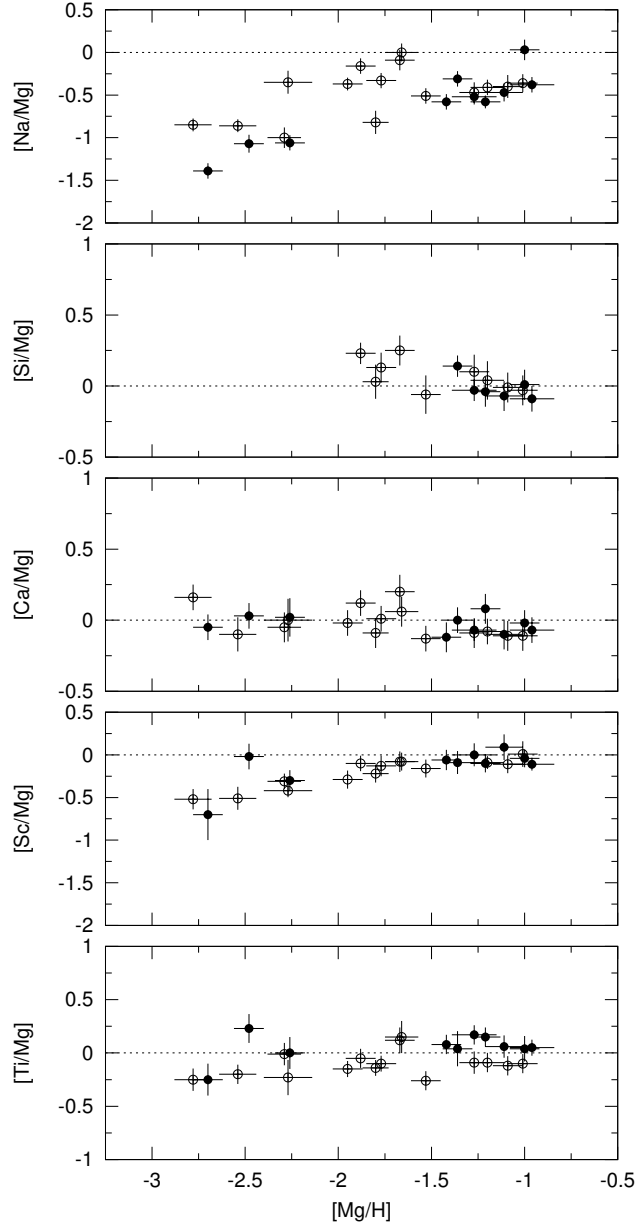


Fig. 13.— Same as Fig. 6, but for $[(Na, Si, Ca, Sc, Ti)/Mg]$ vs. $[Mg/H]$.

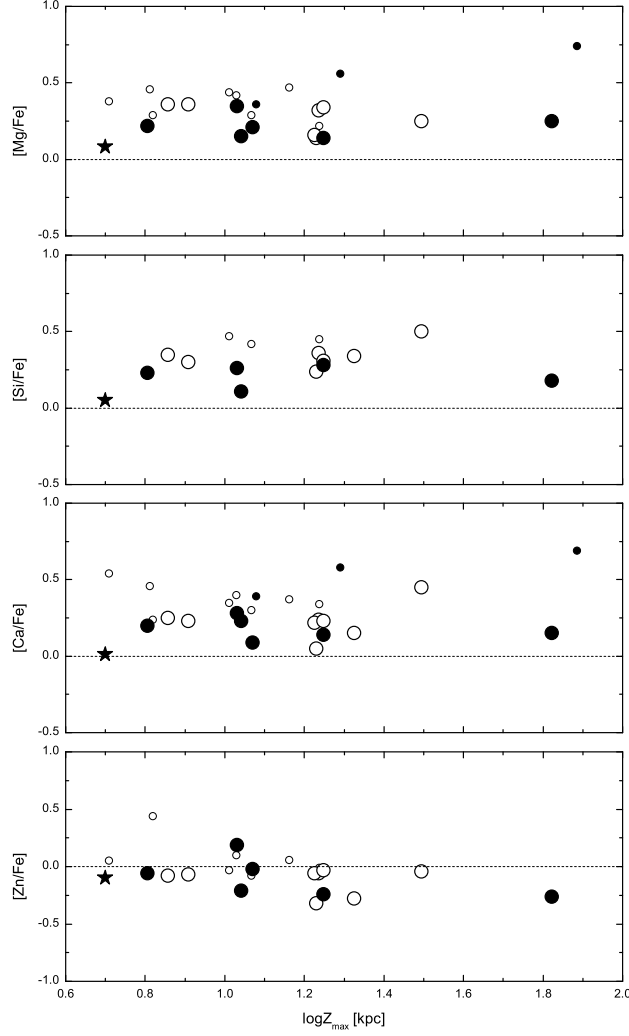


Fig. 14.— Plots of $[\alpha/\text{Fe}]$ and $[\text{Zn}/\text{Fe}]$ against the logarithm of Z_{max} . The symbols are the same as in Fig. 4. The black star is HD 134439 which has low Z_{max} , but it is classified into the outer halo because of its very high R_{apo} . Besides, the large circle means the stars with $[\text{Fe}/\text{H}] > -2$, while small ones are those with $[\text{Fe}/\text{H}] < -2$.

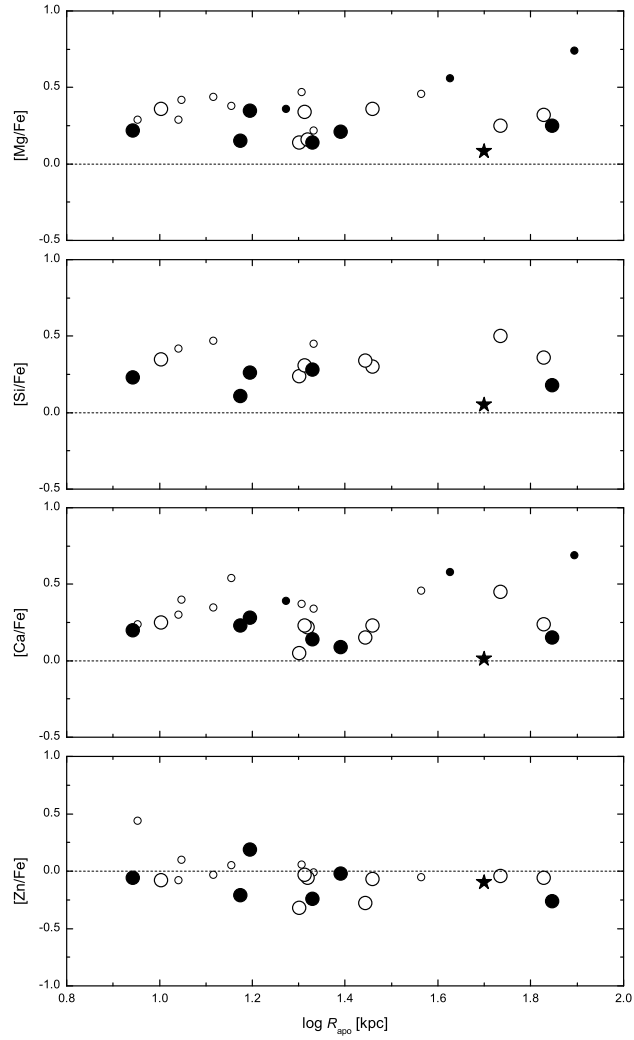


Fig. 15.— Plots of $[\alpha/\text{Fe}]$ and $[\text{Zn}/\text{Fe}]$ against the logarithm of R_{apo} . The symbols are the same as in Fig. 14.

Table 1. Log of the Subaru/HDS

Code	Name	RA (J2000)	DEC (J2000)	V^a	[Fe/H] ^a	Exp. [s]	N_{photon}^b	v_{rad}^c [km·s ⁻¹]	R_{apo} [kpc]	Z_{max} [kpc]
1	BD+04° 2466	11 26 49.20	+03 51 52.2	10.53	-1.88	1200	30511	37.1	54.26	31.20
2	BD+01° 3070	15 22 40.08	+01 15 52.9	10.06	-1.85	900	35921	-327.4	67.32	17.19
3	BD+09° 2870	14 16 29.98	+08 27 52.9	9.40	-2.39	900	40356	-119.7	36.62	6.48
4	BD+10° 2495	12 59 19.96	+09 14 35.4	9.72	-1.83	600	36539	251.5	21.49	17.30
5	BD+12° 2547	13 04 06.59	+11 26 16.3	9.92	-2.07	900	23928	6.6	28.79	8.09
6	BD+29° 2356	13 01 52.42	+29 11 17.8	11.50	-1.06	3600	20992	-207.3	10.06	7.19
7	BD+30° 2611	15 06 53.82	+30 00 37.0	9.13	-1.32	600	64797	-280.4	19.98	16.98
8	HD 33771	05 10 49.56	-37 49 02.9	9.45	-1.93	1500	29398	-12.8	10.97	11.67
9	HD 85773	09 53 39.25	-22 50 08.2	9.42	-2.27	1200	38485	148.2	8.97	6.59
10	HD 107752	12 22 52.75	+11 36 25.8	10.01	-2.74	1200	42834	220.4	14.29	5.11
11	HD 108577	12 28 16.91	+12 20 41.5	9.57	-2.56	600	38485	-111.0	11.15	10.67
12	HD 119516	13 43 26.76	+15 34 31.2	9.05	-2.49	600	51786	-284.5	20.86	16.78
13	HD 124358	14 13 21.38	-12 09 23.9	9.50	-1.98	600	38284	324.7	27.77	21.12
14	HD 128279	14 36 48.47	-29 06 43.6	8.02	-2.20	300	55752	-75.1	13.04	10.24
15	HD 175305	18 47 05.73	+74 43 30.8	7.18	-1.45	300	165037	-184.0	20.56	17.67
16	HD 237846	09 52 38.68	+57 54 58.7	9.93	-2.63	1200	23208	-303.1	20.24	14.49
17	HD 134439	15 10 13.09	-16 22 45.4	9.09	-1.57	600	63772	310.4	50.08	5.01
18	G 112-43	07 43 43.97	-00 04 00.9	10.22	-1.51	900	27629	-83.8	15.67	10.74
19	G 115-58	09 10 48.10	+46 22 36.6	12.08	-1.74	2400	14492	226.8	14.91	11.00
20	G 15-13	15 12 32.43	+06 01 44.3	12.32	-1.71	5400	23527	219.7	24.59	11.76
21	G 166-37	14 34 51.00	+25 09 54.0	12.67	-1.47	5400	17456	369.4	70.11	66.39
22	G 238-30	13 17 40.00	+64 15 00.0	12.91	-2.96	5400	17825	229.7	78.38	76.89
23	G 41-41	09 29 15.56	+08 38 00.6	11.15	-2.80	1800	19291	266.9	18.75	11.97
24	G 48-29	09 40 43.20	+01 00 29.6	10.48	-2.66	1200	19565	-56.4	42.30	19.53
25	G 53-41	10 27 24.25	+01 24 00.1	11.04	-1.34	1800	20473	88.2	8.76	6.38
26	LP 894-3	05 57 50.70	-30 53 48.7	11.26	-1.83	2400	18495	305.7	21.37	17.71

Note. — a: V band magnitude and metallicity are taken from Beers et al. (2000), Carney et al. (1994) or Ryan & Norris (1991); b: The signal-to-noise ratio and number of photon per unit pixel evaluated at $\sim 5800\text{\AA}$; c: Heliocentric radial velocities.

Table 2. Atomic data and measured equivalent widths

Element	λ (Å)	E.P.	$\log gf$	$\Delta\gamma_6$	1	2	3	4	5
Na I	5682.650	2.10	-0.82	2.0	6.9	12.1	3.0	7.1	6.9
Na I	5688.219	2.10	-0.37	2.0	14.6	19.9	6.2	11.2	15.3
Na I	5889.951	0.00	0.12	2.0	196.0
Na I	5895.924	0.00	-0.18	2.0	173.7
Na I	6154.227	2.10	-1.66	2.0	...	1.4	2.5
Na I	6160.751	2.10	-1.35	2.0	1.0	1.1
Mg I	4571.099	0.00	-5.59	2.5	64.3	84.2	...	81.8	116.6
Mg I	4702.996	4.34	-0.55	2.5	108.4	119.0	89.7	94.3	120.9
.
.
.

Note. — Table 2 is published in its entirety in the electronic edition of the *Astrophysical Journal*. A portion is shown here for guidance regarding its form and content.

Table 3. T_{eff} derived by different methods.

star	$E(B-V)$	T_{eff} [K]				T_{eff}^* [K]	
		$(V-K)$	$(J-H)$	$(J-K)$	Average	SA II	This Work
BD+04° 2466	0.042	5165	5120	5227	5170	5096	5115
BD+01° 3070	0.054	5352	5319	5181	5284	5132	5130
BD+09° 2870	0.029	...	4247	...	4247	4324	4300
BD+10° 2495	0.022	5042	5047	4968	5019	4801	4775
BD+12° 2547	0.029	4668	4580	4661	4636	4573	4590
BD+29° 2356	0.013	4648	4676	4824	4716	4816	4795
BD+30° 2611	0.019	4280	4300
HD 33771	0.030	4761	4717	4716	4731	4575	4635
HD 85773	0.047	...	4250	...	4250	4263	4205
HD 107752	0.030	4385	4370
HD 108577	0.027	...	4743	...	4743	4795	4800
HD 119516	0.026	5506	5565	5586	5552	5512	5550
HD 124358	0.064	4702	4677	4786	4721	4674	4660
HD 128279	0.047	...	4918	...	4918	5059	5100
HD 175305	0.034	5047	5068	5013	5042	4973	5035
HD 237846	0.010	...	4977	4994	4985	4676	4725
HD 134439	0.011	5100	5080
G 112–43	0.012	6003	6000	6046	6016	6057	6000
G 115–58	0.011	6126	6089	6134	6116	6050	6080
G 15–13	0.020	5046	5522	5450	5339	5203	5125
G 166–37	0.024	5314	5166	5335	5272	5401	5335
G 238–30	0.018	5372	5742	5762	5625	5553	5490
G 41–41	0.030	6444	6111	6233	6263	6109	6100
G 48–29	0.058	...	6345	6204	6274	6119	6200
G 53–41	0.040	5930	6011	5931	5957	5825	5840
LP 894–3	0.014	5755	5849	5825	5816	5827	5860

Note. — Column 3 to column 6 represent the values estimated by color indices. Last two columns represent the values derived by different spectroscopic analysis codes.

Table 4. Derived atmospheric parameters for the sample stars

star	Type	T_{eff} [K]	$\log g$	[Fe/H]	ξ [km.s ⁻¹]
BD+04° 2466	G	5115 ± 80	1.87 ± 0.23	-1.92 ± 0.05	1.70 ± 0.2
BD+01° 3070	G	5130 ± 110	3.10 ± 0.10	-1.52 ± 0.10	1.20 ± 0.1
BD+09° 2870	G	4300 ± 100	0.51 ± 0.15	-2.73 ± 0.13	1.60 ± 0.3
BD+10° 2495	G	4775 ± 100	1.90 ± 0.15	-2.10 ± 0.08	1.47 ± 0.3
BD+12° 2547	G	4590 ± 70	1.50 ± 0.15	-1.89 ± 0.10	1.50 ± 0.2
BD+29° 2356	G	4795 ± 60	2.03 ± 0.23	-1.45 ± 0.10	1.40 ± 0.2
BD+30° 2611	G	4300 ± 70	1.25 ± 0.10	-1.41 ± 0.09	1.80 ± 0.2
HD 33771	G	4635 ± 50	1.54 ± 0.15	-2.06 ± 0.07	1.60 ± 0.3
HD 85773	G	4205 ± 50	0.32 ± 0.20	-2.58 ± 0.10	1.60 ± 0.3
HD 107752	G	4370 ± 90	0.54 ± 0.20	-3.16 ± 0.10	1.58 ± 0.3
HD 108577	G	4800 ± 80	1.13 ± 0.10	-2.37 ± 0.09	1.80 ± 0.3
HD 119516	G	5550 ± 50	2.20 ± 0.20	-1.82 ± 0.10	2.00 ± 0.3
HD 124358	G	4660 ± 70	1.25 ± 0.20	-1.77 ± 0.12	1.80 ± 0.2
HD 128279	G	5100 ± 50	2.92 ± 0.10	-2.24 ± 0.10	1.40 ± 0.3
HD 175305	G	5035 ± 70	2.84 ± 0.10	-1.35 ± 0.10	1.40 ± 0.1
HD 237846	G	4725 ± 60	1.41 ± 0.10	-3.01 ± 0.10	1.50 ± 0.3
HD 134439	D	5080 ± 110	4.94 ± 0.22	-1.35 ± 0.08	0.00 ± 0.4
G 112-43	D	6000 ± 70	4.00 ± 0.10	-1.31 ± 0.10	1.40 ± 0.3
G 115-58	D	6080 ± 105	3.88 ± 0.24	-1.36 ± 0.12	1.40 ± 0.3
G 15-13	D	5125 ± 100	4.94 ± 0.31	-1.63 ± 0.09	0.00 ± 0.3
G 166-37	D	5335 ± 100	4.98 ± 0.30	-1.36 ± 0.08	0.00 ± 0.1
G 238-30	D	5490 ± 90	3.57 ± 0.31	-3.44 ± 0.21	1.46 ± 0.3
G 41-41	D	6100 ± 70	3.90 ± 0.30	-2.84 ± 0.16	1.42 ± 0.2
G 48-29	D	6200 ± 50	3.66 ± 0.10	-2.82 ± 0.08	1.60 ± 0.3
G 53-41	D	5840 ± 80	4.51 ± 0.24	-1.22 ± 0.10	1.10 ± 0.1
LP 894-3	D	5860 ± 80	4.30 ± 0.10	-1.50 ± 0.11	1.30 ± 0.1

Table 5. Abundance uncertainties linked to stellar parameters.

Star	Element Ration	$\Delta T_{\text{eff}}(\pm 100 \text{ K})$	$\Delta \log g(\pm 0.30)$	$\Delta[\text{Fe}/\text{H}](\pm 0.10)$	$\Delta\xi(\pm 0.30 \text{ km}\cdot\text{s}^{-1})$	Total Error
G166-37 (dwarf)	[Na/Fe]	∓ 0.03	± 0.00	± 0.00	± 0.01	± 0.03
	[Mg/Fe]	∓ 0.03	± 0.00	± 0.00	± 0.00	± 0.03
	[Si/Fe]	∓ 0.02	± 0.02	± 0.02	± 0.01	± 0.04
	[Ca/Fe]	∓ 0.02	± 0.00	± 0.00	± 0.00	± 0.02
	[Sc/Fe]	∓ 0.03	± 0.01	± 0.03	± 0.00	± 0.04
	[Ti/Fe]	± 0.00	∓ 0.03	∓ 0.01	± 0.01	± 0.03
	[Cr/Fe]	± 0.00	± 0.01	± 0.00	± 0.01	± 0.01
	[Mn/Fe]	∓ 0.02	± 0.02	± 0.03	± 0.02	± 0.05
	[Ni/Fe]	± 0.01	± 0.02	± 0.00	± 0.01	± 0.02
	[Zn/Fe]	∓ 0.00	± 0.02	± 0.01	± 0.00	± 0.02
	[Y /Fe]	∓ 0.01	± 0.02	± 0.01	± 0.00	± 0.02
	[Ba/Fe]	∓ 0.02	± 0.07	± 0.00	± 0.01	± 0.09
	[Fe/H] _I	± 0.07	∓ 0.05	± 0.02	± 0.00	± 0.08
	[Fe/H] _{II}	± 0.00	± 0.06	± 0.03	± 0.00	± 0.06
HD 175305 (giant)	[Na/Fe]	∓ 0.04	± 0.01	± 0.00	± 0.06	± 0.07
	[Mg/Fe]	± 0.00	∓ 0.04	± 0.00	± 0.02	± 0.04
	[Si/Fe]	∓ 0.06	± 0.03	± 0.00	± 0.07	± 0.09
	[Ca/Fe]	∓ 0.02	∓ 0.04	± 0.00	± 0.03	± 0.05
	[Sc/Fe]	∓ 0.04	± 0.01	± 0.01	± 0.00	± 0.04
	[Ti/Fe]	± 0.02	∓ 0.01	± 0.00	± 0.01	± 0.02
	[Cr/Fe]	± 0.01	∓ 0.02	∓ 0.01	∓ 0.01	± 0.03
	[Mn/Fe]	∓ 0.02	± 0.03	± 0.00	± 0.00	± 0.03
	[Ni/Fe]	∓ 0.01	± 0.02	± 0.01	± 0.04	± 0.04
	[Zn/Fe]	∓ 0.00	± 0.01	± 0.00	± 0.01	± 0.01
	[Y /Fe]	∓ 0.05	± 0.06	± 0.01	± 0.03	± 0.08
	[Ba/Fe]	∓ 0.03	± 0.04	± 0.01	∓ 0.01	± 0.05
	[Fe/H] _I	± 0.06	∓ 0.01	∓ 0.01	∓ 0.07	± 0.09
	[Fe/H] _{II}	± 0.01	± 0.09	± 0.03	∓ 0.09	± 0.11

Table 6. Comparisons of stellar parameters between the two analyses

star	ΔT_{eff}	$\Delta \log g$	$\Delta [\text{Fe}/\text{H}]$	$\Delta \xi$
BD+04° 2466	19	-0.15	0.15	-0.04
BD+01° 3070	-2	0.03	0.06	0.10
BD+09° 2870	-24	0.12	-0.07	-0.33
BD+10° 2495	-26	0.02	0.05	-0.07
BD+12° 2547	17	0.21	0.08	-0.20
BD+29° 2356	-21	-0.11	-0.01	0.00
BD+30° 2611	20	0.51	-0.06	0.14
HD 33771	60	0.18	0.07	-0.01
HD 85773	-58	0.18	-0.12	-0.41
HD 107752	-15	0.10	-0.04	-0.37
HD 108577	5	0.29	0.07	-0.26
HD 119516	38	0.41	0.16	-0.21
HD 124358	-14	0.07	-0.01	-0.04
HD 128279	41	0.29	0.14	0.06
HD 175305	62	0.31	0.05	0.20
HD 237846	49	0.22	0.12	-0.19
HD 134439	-20	-0.05	-0.14	-0.04
G 112-43	-57	0.16	0.07	0.14
G 115-58	30	0.21	0.16	-0.07
G 15-13	-78	-0.06	-0.17	-0.04
G 166-37	-66	-0.02	-0.15	-0.04
G 238-30	-63	-0.32	0.08	-0.15
G 41-41	-9	0.50	0.16	-0.27
G 48-29	81	0.10	0.21	-0.13
G 53-41	15	0.33	0.12	0.13
LP 894-3	33	0.28	0.12	0.20
$\overline{\Delta}$	0.65	0.15	0.04	-0.07
σ	43	0.20	0.11	0.17

Note. — $\Delta = \text{SA} - \text{SA II}$

Table 7. Comparisons of abundance results between the two analyses

Star	$\Delta[\text{Mg}/\text{Fe}]$	$\Delta[\text{Si}/\text{Fe}]$	$\Delta[\text{Ca}/\text{Fe}]$	$\Delta[\text{Ti}/\text{Fe}]$	$\Delta[\text{Cr}/\text{Fe}]$	$\Delta[\text{Mn}/\text{Fe}]$	$\Delta[\text{Ni}/\text{Fe}]$	$\Delta[\text{Zn}/\text{Fe}]$	$\Delta[\text{Y}/\text{Fe}]$	$\Delta[\text{Ba}/\text{Fe}]$
BD+04° 2466	-0.07	-0.01	-0.01	-0.03	0.07	0.13	-0.08	-0.06	-0.02	-0.09
BD+01° 3070	0.10	0.14	0.02	-0.08	-0.01	0.01	-0.02	0.04	..	0.05
BD+09° 2870	-0.01	..	0.07	0.10	0.04	0.03	0.02	-0.02	0.05	0.14
BD+10° 2495	-0.11	0.12	0.05	-0.03	-0.11	0.08	-0.01	0.03	-0.01	0.10
BD+12° 2547	-0.02	0.01	-0.05	-0.12	-0.05	-0.11	0.07	0.02	0.07	-0.05
BD+29° 2356	0.12	0.08	0.02	-0.12	0.00	-0.20	0.01	-0.03	-0.08	-0.12
BD+30° 2611	-0.14	0.12	-0.04	0.01	0.10	-0.34	0.15	0.10	-0.09	-0.03
HD 33771	-0.14	0.10	-0.01	0.02	-0.10	0.03	0.04	-0.07	0.03	0.12
HD 85773	0.04	..	0.06	0.18	-0.02	-0.12	-0.01	0.07	0.14	0.03
HD 107752	0.05	..	0.09	0.12	0.09	..	0.10	0.01	0.02	-0.04
HD 108577	0.03	..	0.01	0.07	0.05	0.12	-0.01	-0.01	0.09	0.14
HD 119516	0.02	..	-0.08	0.14	0.04	0.11	0.09	0.04	0.08	0.08
HD 124358	..	0.15	-0.01	-0.08	-0.05	0.07	0.03	0.01	0.02	-0.11
HD 128279	0.07	0.09	0.00	0.05	0.04	0.17	0.05	0.01	..	0.04
HD 175305	0.13	0.11	-0.01	-0.09	-0.01	-0.11	-0.01	0.07	0.06	-0.10
HD 237846	0.10	..	-0.01	0.08	0.16	-0.03	..	0.08
HD 134439	-0.06	-0.12	-0.08	-0.02	-0.02	-0.28	-0.12	-0.18
G 112-43	0.10	0.06	0.02	0.03	-0.01	0.11	0.01	0.01	0.06	-0.11
G 115-58	0.08	0.04	0.00	0.07	0.05	0.03	0.02	0.03	0.15	-0.14
G 15-13	0.04	0.05	-0.21	0.01	0.20	-0.18	-0.16
G 166-37	-0.11	0.01	..	0.01	0.05	-0.34	0.02	-0.09	-0.20	-0.10
G 238-30	-0.06	..	0.05	0.11	0.17
G 41-41	-0.07	..	-0.03	0.13	0.15
G 48-29	0.01	..	-0.01	-0.04	0.00	-0.01
G 53-41	0.04	-0.08	-0.04	0.03	-0.07	0.06	0.02	-0.01	-0.02	0.00
LP 894-3	-0.06	0.08	0.01	0.10	0.09	..	0.08	0.05	..	-0.14
$\overline{\Delta[\text{X}/\text{Fe}]}$	0.00	0.06	0.00	0.03	0.02	-0.04	0.02	0.02	0.01	-0.02
σ	0.08	0.08	0.04	0.08	0.07	0.14	0.06	0.07	0.10	0.11

Note. — $\Delta = \text{SA} - \text{SA II}$. $\Delta[\text{Na}/\text{Fe}]$ is not presented here because of no non-LTE correction adopted in SA II.

Table 8. Comparison of parameters of common stars with SB02

star	Parameters (TW)				Parameters (SB02)				Δ (TW-SB02)			
	T_{eff}	$\log g$	[Fe/H]	ξ	T_{eff}	$\log g$	[Fe/H]	ξ	ΔT_{eff}	$\Delta \log g$	Δ [Fe/H]	$\Delta \xi$
G 15-13	5125	4.94	-1.63	0.00	5082	4.61	-1.70	0.00	43	0.33	0.07	0.00
G 166-37	5335	4.98	-1.36	0.00	5350	4.71	-1.39	0.00	-15	0.27	0.03	0.00
G 238-30	5490	3.57	-3.44	1.46	5383	3.43	-3.60	1.19	107	0.15	0.16	0.27

Note. — Column 2 ~ column 5 are the results derived in this work (TW), the results of column 6 ~ column 9 are cited from SB02, and the last 4 columns represent the discrepancy of these two works.

Table 9. Comparison of abundances with SB02

Star	$\Delta[\text{Fe}/\text{H}]$	$\Delta[\text{Na}/\text{Fe}]$	$\Delta[\text{Mg}/\text{Fe}]$	$\Delta[\text{Si}/\text{Fe}]$	$\Delta[\text{Ca}/\text{Fe}]$	$\Delta[\text{Ti}/\text{Fe}]$	$\Delta[\text{Cr}/\text{Fe}]$	$\Delta[\text{Ni}/\text{Fe}]$	$\Delta[\text{Y}/\text{Fe}]$	$\Delta[\text{Ba}/\text{Fe}]$
	G 15–13 ^a	0.07	0.23	0.05	...	–0.11	0.08	0.08	0.08	0.00
G 166–37 ^a	0.03	0.13	0.04	0.02	–0.05	0.08	–0.10	0.09	–0.03	0.02
G 238–30 ^a	0.16	...	0.12	...	0.01	0.25	–0.09
G 5–19 ^b	0.02	–0.02	–0.08	0.05	–0.05	–0.06	0.06	–0.05	0.03	–0.07
G 9–36 ^b	0.03	0.01	–0.04	0.16	0.02	–0.01	0.07	0.08	–0.08	–0.06
G 215–47 ^b	0.00	–0.03	–0.11	–0.13	–0.09	–0.09	0.03	–0.16	0.09	–0.03
G 5–19 ^c	0.00	–0.02	–0.05	0.03	–0.02	–0.02	–0.01	0.00	–0.01	–0.05
G 9–36 ^c	0.00	0.00	–0.02	–0.05	0.02	0.02	0.03	–0.06	–0.04	–0.04
G 215–47 ^c	0.00	–0.02	–0.07	0.02	–0.03	0.00	–0.03	–0.03	0.02	–0.03

Note. — $\Delta = \text{TW} - \text{SB02}$; a: Abundances derived from our measured equivalent widths; b & c: Abundance derived from the equivalent widths presented by SB02: abundances of b were determined taking atmospheric parameters derived in this work, while abundances of c were determined taking parameters presented in SB02.

Table 10. Abundance ratios: Na, Mg, Si, and Ca

Star	[NaI/H]	N	[MgI/H]	N	[SiI/H]	N	[SiII/H]	N	[CaI/H]	N
BD+04°2466	-1.76 ± 0.08	2	-1.67 ± 0.08	1	-1.42 ± 0.07	2	-1.47 ± 0.08	21
BD+01°3070	-1.61 ± 0.06	3	-1.20 ± 0.09	3	-1.16 ± 0.09	3	-1.17 ± 0.06	1	-1.28 ± 0.06	19
BD+09°2870	-2.62 ± 0.09	2	-2.26 ± 0.13	2	-2.26 ± 0.10	25
BD+10°2495	-2.04 ± 0.06	2	-1.88 ± 0.08	1	-1.65 ± 0.05	3	-1.76 ± 0.06	23
BD+12°2547	-2.04 ± 0.06	1	-1.53 ± 0.08	1	-1.59 ± 0.09	2	-1.66 ± 0.06	21
BD+29°2356	-1.49 ± 0.09	3	-1.09 ± 0.08	1	-1.10 ± 0.07	3	-1.20 ± 0.04	1	-1.20 ± 0.07	18
BD+30°2611	-1.74 ± 0.08	2	-1.27 ± 0.08	1	-1.17 ± 0.08	3	-1.07 ± 0.05	1	-1.36 ± 0.07	12
HD 33771	-2.10 ± 0.06	2	-1.77 ± 0.08	1	-1.62 ± 0.07	2	-1.76 ± 0.06	19
HD 85773	-3.29 ± 0.08	1	-2.29 ± 0.09	3	-2.34 ± 0.07	17
HD 107752	-3.63 ± 0.05	1	-2.78 ± 0.10	2	-2.62 ± 0.06	15
HD 108577	-2.32 ± 0.05	2	-1.95 ± 0.08	2	-1.97 ± 0.06	20
HD 119516	-1.66 ± 0.07	2	-1.66 ± 0.09	3	-1.60 ± 0.07	19
HD 124358	-2.05 ± 0.06	2	-1.43 ± 0.05	3	-1.62 ± 0.07	19
HD 128279	-2.62 ± 0.09	2	-1.80 ± 0.07	2	-1.77 ± 0.08	2	-1.89 ± 0.07	20
HD 175305	-1.37 ± 0.07	2	-1.01 ± 0.08	1	-1.04 ± 0.10	3	-0.97 ± 0.05	1	-1.12 ± 0.07	19
HD 237846	-3.40 ± 0.05	1	-2.54 ± 0.10	2	-2.64 ± 0.08	14
HD 134439	-1.79 ± 0.06	1	-1.27 ± 0.12	2	-1.30 ± 0.05	3	-1.34 ± 0.05	19
G 112-43	-1.34 ± 0.06	1	-0.96 ± 0.12	1	-1.05 ± 0.06	3	-1.05 ± 0.05	1	-1.03 ± 0.06	23
G 115-58	-1.79 ± 0.05	3	-1.21 ± 0.08	2	-1.25 ± 0.07	2	-1.13 ± 0.07	14
G 15-13	-2.00 ± 0.06	2	-1.42 ± 0.08	1	-1.54 ± 0.07	19
G 166-37	-1.58 ± 0.05	2	-1.11 ± 0.07	2	-1.18 ± 0.07	2	-1.21 ± 0.05	20
G 238-30	-4.09 ± 0.06	2	-2.70 ± 0.08	1	-2.75 ± 0.06	3
G 41-41	-3.55 ± 0.07	2	-2.39 ± 0.08	1	-2.38 ± 0.06	2
G 48-29	-3.32 ± 0.06	2	-2.26 ± 0.08	1	-2.24 ± 0.09	5
G 53-41	-0.97 ± 0.08	2	-1.00 ± 0.08	1	-0.99 ± 0.07	2	-0.89 ± 0.04	1	-1.02 ± 0.06	22
LP 894-3	-1.67 ± 0.06	2	-1.36 ± 0.08	2	-1.22 ± 0.05	1	-1.36 ± 0.06	20

Table 11. Abundance ratios: Sc, Ti, Cr and Mn

star	[ScII/H]	N	[TiI/H]	N	[TiII/H]	N	[CrI/H]	N	[CrII/H]	N	[MnI/H]	N
BD+04°2466	-1.75 ± 0.08	4	-1.55 ± 0.08	33	-1.55 ± 0.08	8	-2.02 ± 0.08	14	-1.80 ± 0.09	5	-2.36 ± 0.04	2
BD+01°3070	-1.29 ± 0.05	7	-1.29 ± 0.06	32	-1.11 ± 0.08	8	-1.66 ± 0.06	14	-1.37 ± 0.09	5	-2.10 ± 0.03	2
BD+09°2870	-2.69 ± 0.05	6	-2.50 ± 0.11	32	-2.44 ± 0.10	9	-3.05 ± 0.05	12	-2.59 ± 0.09	5	-3.34 ± 0.07	2
BD+10°2495	-1.98 ± 0.06	9	-1.93 ± 0.06	32	-1.78 ± 0.08	7	-2.28 ± 0.09	14	-1.91 ± 0.07	5	-2.59 ± 0.03	2
BD+12°2547	-1.69 ± 0.07	3	-1.79 ± 0.06	29	-1.50 ± 0.09	7	-2.09 ± 0.07	15	-1.74 ± 0.09	5	-2.49 ± 0.03	2
BD+29°2356	-1.20 ± 0.07	2	-1.21 ± 0.06	27	-1.00 ± 0.10	6	-1.57 ± 0.07	14	-1.31 ± 0.11	5	-2.12 ± 0.08	2
BD+30°2611	-1.36 ± 0.07	9	-1.13 ± 0.08	2	-1.43 ± 0.10	3	-1.35 ± 0.09	2	-2.06 ± 0.04	2
HD 33771	-1.90 ± 0.08	4	-1.87 ± 0.05	31	-1.68 ± 0.08	8	-2.30 ± 0.05	12	-1.92 ± 0.09	5	-2.60 ± 0.04	2
HD 85773	-2.60 ± 0.06	4	-2.30 ± 0.07	21	-2.25 ± 0.08	7	-2.85 ± 0.07	12	-2.40 ± 0.10	4	-3.02 ± 0.06	2
HD 107752	-3.30 ± 0.08	7	-3.03 ± 0.07	14	-2.98 ± 0.07	11	-3.39 ± 0.07	10	-3.02 ± 0.06	2	-3.71 ± 0.03	1
HD 108577	-2.24 ± 0.07	10	-2.10 ± 0.05	25	-2.06 ± 0.08	8	-2.53 ± 0.07	14	-2.28 ± 0.11	3	-2.68 ± 0.04	2
HD 119516	-1.74 ± 0.07	8	-1.51 ± 0.10	20	-1.55 ± 0.08	8	-1.97 ± 0.08	12	-1.74 ± 0.08	5	-2.23 ± 0.04	2
HD 124358	-1.73 ± 0.07	3	-1.73 ± 0.06	27	-1.54 ± 0.08	5	-2.01 ± 0.06	12	-1.69 ± 0.11	4	-2.21 ± 0.03	1
HD 128279	-2.02 ± 0.07	9	-1.94 ± 0.05	21	-1.80 ± 0.07	11	-2.42 ± 0.05	12	-2.04 ± 0.09	3	-2.66 ± 0.03	2
HD 175305	-1.00 ± 0.10	5	-1.11 ± 0.06	30	-0.90 ± 0.08	8	-1.47 ± 0.07	13	-1.16 ± 0.09	5	-1.94 ± 0.05	2
HD 237846	-3.05 ± 0.09	7	-2.74 ± 0.06	19	-2.73 ± 0.07	11	-3.25 ± 0.06	10	-3.04 ± 0.04	1	-3.49 ± 0.03	2
HD 134439	-1.27 ± 0.09	6	-1.10 ± 0.06	26	-1.01 ± 0.08	8	-1.34 ± 0.07	15	-1.12 ± 0.09	5	-1.86 ± 0.03	1
G 112-43	-1.07 ± 0.05	9	-0.91 ± 0.05	27	-0.86 ± 0.07	2	-1.37 ± 0.05	13	-1.20 ± 0.04	2	-1.58 ± 0.03	2
G 115-58	-1.31 ± 0.07	8	-1.06 ± 0.06	18	-1.01 ± 0.08	10	-1.47 ± 0.05	11	-1.32 ± 0.10	4	-1.78 ± 0.03	2
G 15-13	-1.48 ± 0.08	8	-1.34 ± 0.06	27	-1.25 ± 0.06	9	-1.69 ± 0.06	19	-1.37 ± 0.04	1	-2.03 ± 0.10	2
G 166-37	-1.02 ± 0.06	8	-1.05 ± 0.05	26	-0.93 ± 0.08	10	-1.42 ± 0.06	15	-1.21 ± 0.04	2	-1.84 ± 0.06	1
G 238-30	-3.40 ± 0.20	4	-2.95 ± 0.10	3	-3.20 ± 0.09	3	-3.57 ± 0.09	2
G 41-41	-2.50 ± 0.10	6	-2.25 ± 0.09	3
G 48-29	-2.56 ± 0.08	4	-2.26 ± 0.10	3	-2.89 ± 0.10	2
G 53-41	-1.04 ± 0.07	8	-0.96 ± 0.08	29	-0.80 ± 0.08	11	-1.35 ± 0.06	14	-1.03 ± 0.09	5	-1.62 ± 0.03	2
LP 894-3	-1.45 ± 0.09	9	-1.32 ± 0.11	13	-1.19 ± 0.08	10	-1.65 ± 0.05	11	-1.29 ± 0.10	4	-1.95 ± 0.03	1

Table 12. Abundance ratios: Fe, Ni, Zn, Y and Ba

Star	[FeI/H]	N	[FeII/H]	N	[NiI/H]	N	[ZnI/H]	N	[YII/H]	N	[BaII/H]	N
BD+04°2466	-1.92 ± 0.05	80	-1.92 ± 0.09	12	-1.90 ± 0.08	15	-1.96 ± 0.10	3	-1.37 ± 0.05	1	-0.61 ± 0.05	3
BD+01°3070	-1.52 ± 0.05	91	-1.52 ± 0.06	12	-1.63 ± 0.07	22	-1.58 ± 0.03	3	-1.66 ± 0.05	2	-1.59 ± 0.06	3
BD+09°2870	-2.73 ± 0.05	85	-2.73 ± 0.06	12	-2.74 ± 0.07	15	-2.78 ± 0.03	2	-3.21 ± 0.05	2	-3.53 ± 0.06	3
BD+10°2495	-2.10 ± 0.05	89	-2.10 ± 0.06	12	-2.17 ± 0.07	21	-2.11 ± 0.03	3	-2.36 ± 0.05	2	-2.21 ± 0.06	3
BD+12°2547	-1.89 ± 0.05	77	-1.89 ± 0.06	9	-1.83 ± 0.07	22	-1.96 ± 0.03	2	-2.03 ± 0.05	2	-1.99 ± 0.06	3
BD+29°2356	-1.45 ± 0.05	74	-1.46 ± 0.06	10	-1.54 ± 0.08	22	-1.53 ± 0.03	3	-1.5 ± 0.05	2	-1.44 ± 0.06	3
BD+30°2611	-1.40 ± 0.06	55	-1.41 ± 0.08	7	-1.56 ± 0.09	15	-1.73 ± 0.03	2	-1.63 ± 0.05	1	-1.46 ± 0.06	3
HD 33771	-2.06 ± 0.05	85	-2.06 ± 0.06	10	-2.13 ± 0.07	16	-2.14 ± 0.04	3	-2.21 ± 0.05	1	-2.15 ± 0.06	3
HD 85773	-2.58 ± 0.05	60	-2.58 ± 0.05	9	-2.58 ± 0.08	15	-2.14 ± 0.05	3	-3.15 ± 0.05	1	-3.27 ± 0.06	4
HD 107752	-3.16 ± 0.05	84	-3.16 ± 0.05	12	-3.18 ± 0.08	9	-3.11 ± 0.04	3	-3.56 ± 0.06	2	-3.72 ± 0.06	4
HD 108577	-2.37 ± 0.05	87	-2.37 ± 0.07	12	-2.29 ± 0.07	15	-2.27 ± 0.04	2	-2.69 ± 0.08	2	-2.54 ± 0.06	3
HD 119516	-1.82 ± 0.05	82	-1.82 ± 0.07	10	-1.89 ± 0.10	6	-1.96 ± 0.07	3	-1.96 ± 0.05	2	-1.71 ± 0.06	3
HD 124358	-1.77 ± 0.05	68	-1.77 ± 0.06	9	-1.94 ± 0.07	23	-2.05 ± 0.04	6	-2.37 ± 0.05	1	-2.20 ± 0.06	3
HD 128279	-2.24 ± 0.05	85	-2.24 ± 0.06	11	-2.21 ± 0.08	11	-2.27 ± 0.06	3	-2.97 ± 0.07	3
HD 175305	-1.35 ± 0.09	80	-1.35 ± 0.11	11	-1.44 ± 0.07	22	-1.38 ± 0.04	3	-1.35 ± 0.09	2	-1.36 ± 0.06	3
HD 237846	-3.01 ± 0.05	77	-3.01 ± 0.06	12	-3.06 ± 0.12	5	-2.95 ± 0.04	2	-3.52 ± 0.07	2	-4.09 ± 0.10	3
HD 134439	-1.35 ± 0.05	70	-1.35 ± 0.08	11	-1.47 ± 0.08	21	-1.45 ± 0.03	2	-1.65 ± 0.05	1	-1.59 ± 0.06	4
G 112-43	-1.31 ± 0.05	95	-1.31 ± 0.06	13	-1.29 ± 0.05	14	-1.12 ± 0.04	3	-1.4 ± 0.05	2	-1.61 ± 0.06	3
G 115-58	-1.36 ± 0.05	71	-1.36 ± 0.06	9	-1.49 ± 0.10	8	-1.57 ± 0.07	2	-1.44 ± 0.05	2	-1.51 ± 0.10	4
G 15-13	-1.63 ± 0.05	78	-1.63 ± 0.08	11	-1.71 ± 0.08	19	-1.65 ± 0.04	2	-1.66 ± 0.06	2	-1.41 ± 0.09	4
G 166-37	-1.36 ± 0.08	86	-1.36 ± 0.07	12	-1.43 ± 0.03	18	-1.62 ± 0.04	2	-1.27 ± 0.06	2	-1.19 ± 0.10	4
G 238-30	-3.44 ± 0.06	20	-3.44 ± 0.09	3
G 41-41	-2.81 ± 0.06	50	-2.82 ± 0.07	6	-3.20 ± 0.06	1
G 48-29	-2.63 ± 0.05	24	-2.64 ± 0.07	7	-3.36 ± 0.08	2
G 53-41	-1.22 ± 0.05	93	-1.22 ± 0.06	12	-1.29 ± 0.07	17	-1.28 ± 0.05	3	-1.12 ± 0.05	2	-0.95 ± 0.06	3
LP 894-3	-1.50 ± 0.05	82	-1.50 ± 0.05	11	-1.59 ± 0.10	10	-1.74 ± 0.03	2	-1.70 ± 0.06	4

Table 13. Abundance relative to Fe: Na, Mg, Si, Ca, Sc, and Ti

Star	[Fe/H]	[Na/Fe]	[Mg/Fe]	[Si/Fe]	[Ca/Fe]	[Sc/Fe]	[Ti/Fe]
BD+04° 2466	-1.92 ± 0.05	0.16 ± 0.08	0.25 ± 0.08	0.50 ± 0.07	0.45 ± 0.08	0.17 ± 0.08	0.37 ± 0.08
BD+01° 3070	-1.52 ± 0.05	-0.09 ± 0.06	0.32 ± 0.09	0.36 ± 0.09	0.24 ± 0.06	0.23 ± 0.05	0.23 ± 0.06
BD+09° 2870	-2.73 ± 0.05	0.11 ± 0.09	0.46 ± 0.13	...	0.46 ± 0.10	0.04 ± 0.05	0.23 ± 0.11
BD+10° 2495	-2.10 ± 0.05	0.06 ± 0.06	0.22 ± 0.08	0.45 ± 0.05	0.34 ± 0.06	0.12 ± 0.06	0.17 ± 0.06
BD+12° 2547	-1.89 ± 0.05	-0.15 ± 0.06	0.36 ± 0.08	0.30 ± 0.09	0.23 ± 0.06	0.2 ± 0.07	0.10 ± 0.06
BD+29° 2356	-1.45 ± 0.05	-0.04 ± 0.09	0.36 ± 0.08	0.35 ± 0.07	0.25 ± 0.07	0.25 ± 0.07	0.24 ± 0.06
BD+30° 2611	-1.41 ± 0.06	-0.33 ± 0.08	0.14 ± 0.08	0.24 ± 0.08	0.05 ± 0.07	...	0.05 ± 0.07
HD 33771	-2.06 ± 0.05	-0.04 ± 0.06	0.29 ± 0.08	0.42 ± 0.07	0.30 ± 0.06	0.16 ± 0.08	0.19 ± 0.05
HD 85773	-2.58 ± 0.05	-0.71 ± 0.08	0.29 ± 0.09	...	0.24 ± 0.07	-0.02 ± 0.06	0.28 ± 0.07
HD 107752	-3.16 ± 0.05	-0.47 ± 0.05	0.38 ± 0.10	...	0.54 ± 0.06	-0.14 ± 0.08	0.13 ± 0.07
HD 108577	-2.37 ± 0.05	0.05 ± 0.05	0.42 ± 0.08	...	0.40 ± 0.06	0.13 ± 0.07	0.27 ± 0.05
HD 119516	-1.82 ± 0.05	0.16 ± 0.07	0.16 ± 0.09	...	0.22 ± 0.07	0.08 ± 0.07	0.31 ± 0.10
HD 124358	-1.77 ± 0.05	-0.28 ± 0.06	...	0.34 ± 0.05	0.15 ± 0.07	0.04 ± 0.07	0.04 ± 0.06
HD 128279	-2.24 ± 0.05	-0.38 ± 0.09	0.44 ± 0.07	0.47 ± 0.08	0.35 ± 0.07	0.22 ± 0.07	0.30 ± 0.05
HD 175305	-1.35 ± 0.09	-0.02 ± 0.07	0.34 ± 0.08	0.31 ± 0.10	0.23 ± 0.07	0.35 ± 0.10	0.24 ± 0.07
HD 237846	-3.01 ± 0.05	-0.39 ± 0.05	0.47 ± 0.10	...	0.37 ± 0.08	-0.04 ± 0.09	0.27 ± 0.06
HD 134439	-1.35 ± 0.05	-0.44 ± 0.06	0.08 ± 0.12	0.05 ± 0.05	0.01 ± 0.05	0.08 ± 0.09	0.25 ± 0.06
G 112-43	-1.31 ± 0.05	-0.03 ± 0.06	0.35 ± 0.12	0.26 ± 0.06	0.28 ± 0.06	0.24 ± 0.05	0.40 ± 0.05
G 115-58	-1.36 ± 0.05	-0.43 ± 0.05	0.15 ± 0.08	0.11 ± 0.07	0.23 ± 0.07	0.05 ± 0.07	0.30 ± 0.06
G 15-13	-1.63 ± 0.05	-0.37 ± 0.06	0.21 ± 0.08	...	0.09 ± 0.07	0.15 ± 0.08	0.24 ± 0.06
G 166-37	-1.36 ± 0.08	-0.22 ± 0.05	0.25 ± 0.07	0.18 ± 0.07	0.15 ± 0.05	0.34 ± 0.06	0.17 ± 0.06
G 238-30	-3.44 ± 0.06	-0.65 ± 0.06	0.74 ± 0.08	...	0.69 ± 0.06	0.04 ± 0.20	0.49 ± 0.10
G 41-41	-2.84 ± 0.06	-0.71 ± 0.07	0.36 ± 0.08	...	0.39 ± 0.06	0.34 ± 0.10	0.59 ± 0.09
G 48-29	-2.82 ± 0.05	-0.50 ± 0.06	0.56 ± 0.08	...	0.58 ± 0.09	0.26 ± 0.08	0.56 ± 0.10
G 53-41	-1.22 ± 0.05	0.25 ± 0.08	0.22 ± 0.08	0.23 ± 0.07	0.20 ± 0.06	0.18 ± 0.07	0.26 ± 0.08
LP 894-3	-1.50 ± 0.05	-0.17 ± 0.06	0.14 ± 0.08	0.28 ± 0.05	0.14 ± 0.06	0.05 ± 0.09	0.18 ± 0.11

Table 14. Abundance relative to Fe: Cr, Mn, Ni, Zn, Y, and Ba

Star	[Fe/H]	[Cr/Fe]	[Mn/Fe]	[Ni/Fe]	[Zn/Fe]	[Y/Fe]	[Ba/Fe]
BD+04° 2466	-1.92 ± 0.05	-0.10 ± 0.08	-0.44 ± 0.04	0.02 ± 0.08	-0.04 ± 0.10	0.55 ± 0.05	1.31 ± 0.05
BD+01° 3070	-1.52 ± 0.05	-0.14 ± 0.06	-0.58 ± 0.03	-0.11 ± 0.07	-0.06 ± 0.03	-0.14 ± 0.05	-0.07 ± 0.06
BD+09° 2870	-2.73 ± 0.05	-0.32 ± 0.05	-0.61 ± 0.07	-0.01 ± 0.07	-0.05 ± 0.03	-0.48 ± 0.05	-0.80 ± 0.06
BD+10° 2495	-2.10 ± 0.05	-0.18 ± 0.09	-0.49 ± 0.03	-0.07 ± 0.07	-0.01 ± 0.03	-0.26 ± 0.05	-0.11 ± 0.06
BD+12° 2547	-1.89 ± 0.05	-0.20 ± 0.07	-0.60 ± 0.03	-0.06 ± 0.07	-0.07 ± 0.03	-0.14 ± 0.05	-0.10 ± 0.06
BD+29° 2356	-1.45 ± 0.05	-0.12 ± 0.07	-0.67 ± 0.08	-0.09 ± 0.08	-0.08 ± 0.03	-0.05 ± 0.05	0.01 ± 0.06
BD+30° 2611	-1.41 ± 0.06	-0.02 ± 0.10	-0.65 ± 0.04	-0.15 ± 0.09	-0.32 ± 0.03	-0.22 ± 0.05	-0.05 ± 0.06
HD 33771	-2.06 ± 0.05	-0.24 ± 0.05	-0.54 ± 0.04	-0.07 ± 0.07	-0.08 ± 0.04	-0.15 ± 0.05	-0.09 ± 0.06
HD 85773	-2.58 ± 0.05	-0.27 ± 0.07	-0.44 ± 0.06	0.00 ± 0.08	0.44 ± 0.05	-0.57 ± 0.05	-0.69 ± 0.06
HD 107752	-3.16 ± 0.05	-0.23 ± 0.07	-0.55 ± 0.03	-0.02 ± 0.08	0.05 ± 0.04	-0.40 ± 0.06	-0.56 ± 0.06
HD 108577	-2.37 ± 0.05	-0.15 ± 0.07	-0.31 ± 0.04	0.08 ± 0.07	0.10 ± 0.04	-0.32 ± 0.08	-0.17 ± 0.06
HD 119516	-1.82 ± 0.05	-0.15 ± 0.08	-0.41 ± 0.04	-0.07 ± 0.10	-0.06 ± 0.07	-0.14 ± 0.05	0.11 ± 0.06
HD 124358	-1.77 ± 0.05	-0.24 ± 0.06	-0.44 ± 0.03	-0.17 ± 0.07	-0.28 ± 0.04	-0.60 ± 0.05	-0.43 ± 0.06
HD 128279	-2.24 ± 0.05	-0.18 ± 0.05	-0.42 ± 0.03	0.04 ± 0.08	-0.03 ± 0.06	...	-0.73 ± 0.07
HD 175305	-1.35 ± 0.09	-0.12 ± 0.07	-0.61 ± 0.05	-0.09 ± 0.07	-0.03 ± 0.04	0.00 ± 0.09	-0.01 ± 0.06
HD 237846	-3.01 ± 0.05	-0.24 ± 0.06	-0.48 ± 0.03	-0.04 ± 0.12	0.06 ± 0.04	-0.51 ± 0.07	-1.08 ± 0.10
HD 134439	-1.35 ± 0.05	-0.09 ± 0.07	-0.51 ± 0.03	-0.12 ± 0.08	-0.10 ± 0.03	-0.30 ± 0.05	-0.24 ± 0.06
G 112-43	-1.31 ± 0.05	-0.06 ± 0.05	-0.27 ± 0.03	0.02 ± 0.05	0.19 ± 0.04	-0.09 ± 0.05	-0.30 ± 0.06
G 115-58	-1.36 ± 0.05	-0.11 ± 0.05	-0.42 ± 0.03	-0.13 ± 0.10	-0.21 ± 0.07	-0.08 ± 0.05	-0.15 ± 0.10
G 15-13	-1.63 ± 0.05	-0.06 ± 0.06	-0.40 ± 0.10	-0.08 ± 0.08	-0.02 ± 0.04	-0.03 ± 0.06	0.22 ± 0.09
G 166-37	-1.36 ± 0.08	-0.06 ± 0.06	-0.48 ± 0.07	-0.07 ± 0.03	-0.26 ± 0.05	0.09 ± 0.06	0.16 ± 0.10
G 238-30	-3.44 ± 0.06	-0.13 ± 0.09
G 41-41	-2.84 ± 0.06	-0.36 ± 0.06
G 48-29	-2.82 ± 0.05	-0.07 ± 0.10	-0.54 ± 0.08
G 53-41	-1.22 ± 0.05	-0.13 ± 0.06	-0.41 ± 0.03	-0.07 ± 0.07	-0.06 ± 0.05	0.10 ± 0.05	0.27 ± 0.06
LP 894-3	-1.50 ± 0.05	-0.15 ± 0.05	-0.45 ± 0.03	-0.09 ± 0.10	-0.24 ± 0.03	...	-0.20 ± 0.06

Table 1. Atomic data and measured equivalent widths

Element	λ (Å)	E.P.	$\log gf$	$\Delta\gamma_6$	1	2	3	4	5	6	7	8	9	10	11	12	13
Na I	5682.650	2.10	-0.82	2.0	6.9	12.1	3.0	7.1	6.9	20.4	29.6	7.8	2.1	8.3
Na I	5688.219	2.10	-0.37	2.0	14.6	19.9	6.2	11.2	15.3	36.8	48.9	12.1	6.4	1.4	5.7	6.4	13.4
Na I	5889.951	0.00	0.12	2.0	196.0	225.1	151.7	194.9	194.3	...
Na I	5895.924	0.00	-0.18	2.0	173.7	195.5	132.1	171.2	162.7	...
Na I	6154.227	2.10	-1.66	2.0	...	1.4	2.5	1.6	7.2
Na I	6160.751	2.10	-1.35	2.0	1.0	1.1	...	6.1	10.5	...	1.9
Mg I	4571.099	0.00	-5.59	2.5	64.3	84.2	...	81.8	116.6	84.4	181.3	104.8	116.9	50.3	62.6	24.2	110.6
Mg I	4702.996	4.34	-0.55	2.5	108.4	119.0	89.7	94.3	120.9	135.2	161.4	111.4	90.6	51.1	85.6	81.6	119.3
Mg I	4730.026	4.34	-2.37	2.5	...	13.0	4.7	7.2	12.6	23.3	36.2	7.0	4.5	...	4.6	2.6	12.7
Si I	5772.148	5.08	-1.75	1.3	...	11.6	5.0	5.5	8.1	17.4	23.3	7.2	3.1	2.1	11.0
Si I	5948.545	5.08	-1.23	1.3	19.5	25.2	12.9	15.1	24.9	41.3	53.6	17.6	14.2	...	12.6	16.2	27.6
Si I	6155.141	5.62	-0.84	1.3	11.4	17.0	7.5	9.9	12.1	26.3	29.8	13.1	5.6	...	7.9	5.0	18.0
Si II	6347.100	8.12	0.32	2.5	...	6.9	1.4	2.9	3.2	8.4	7.4	7.6	6.4
Ca I	4526.934	2.71	-0.49	1.8	23.2	34.0	12.3	21.4	27.8	46.0	69.6	25.9	14.7	9.8	34.6
Ca I	4578.551	2.52	-0.63	1.8	22.6	38.4	15.4	22.8	36.5	52.8	...	29.4	14.4	7.2	13.8	14.2	32.5
Ca I	4685.268	2.93	-0.88	1.8	19.0	5.7	4.4	10.8	15.4	27.3	48.4	11.5	3.1	2.9	8.3	1.0	14.1
Ca I	5261.707	2.52	-0.65	1.8	33.2	46.4	21.9	30.6	7.8	11.9	98.6	40.6	23.3	10.6	19.5	16.2	46.5
Ca I	5262.241	2.52	-0.60	1.8	64.2	77.4	55.0	59.4	44.9	62.1	156.0	83.9	69.4	22.8	49.3	39.0	98.4
Ca I	5512.980	2.93	-0.37	1.8	95.7	114.8
Ca I	5581.968	2.52	-0.63	1.8	28.5	47.9	23.1	30.6	49.8	64.5	96.1	40.5	24.3	10.9	21.2	18.7	47.2
Ca I	5588.755	2.53	0.28	1.8	80.7	89.7	68.2	76.4	95.8	110.2	141.3	86.0	70.5	40.3	64.0	67.8	99.1
Ca I	5590.117	2.52	-0.64	1.8	30.2	45.6	22.8	31.3	45.6	63.4	93.1	39.1	21.5	9.0	19.9	18.5	46.5
Ca I	5594.466	2.52	0.02	1.8	72.4	80.4	52.3	62.4	84.9	73.6	57.7	30.1	51.0	49.8	91.2
Ca I	5598.480	2.52	-0.22	1.8	61.6	50.5	46.4	58.9	54.2	22.0	42.7	46.0	...
Ca I	5601.277	2.53	-0.69	1.8	38.9	66.9	24.8	31.4	46.4	69.9	97.7	40.9	26.4	10.6	21.5	19.9	49.1
Ca I	5857.451	2.93	0.24	1.8	54.7	1.7	39.4	50.1	66.5	82.6	15.8	55.8	31.9	19.3	37.8	31.1	69.5
Ca I	6122.217	1.89	-0.32	1.8	93.2	103.8	89.0	91.3	117.0	125.5	173.8	106.4	99.0	53.9	78.6	74.5	120.5
Ca I	6162.173	1.90	-0.09	1.8	103.6	116.5	98.6	102.3	122.0	135.5	188.8	110.6	108.1	67.2	94.5	88.7	133.7
Ca I	6163.755	2.52	-1.29	1.8	9.9	17.8	8.1	12.1	19.8	14.8	...	1.6	...	7.1	...
Ca I	6166.440	2.52	-1.14	1.8	11.1	22.5	10.6	13.5	22.1	35.0	65.3	16.4	9.3	1.2	5.9	4.5	21.4
Ca I	6169.042	2.52	-0.80	1.8	25.0	38.2	18.3	23.9	39.7	52.9	89.4	31.5	20.9	8.3	12.5	12.5	39.6
Ca I	6169.562	2.53	-0.37	1.8	36.6	53.0	28.1	36.8	55.1	70.1	107.0	46.2	31.6	13.4	26.2	20.6	53.4
Ca I	6449.810	2.52	-0.50	1.8	37.6	54.0	31.2	34.5	53.7	71.8	...	47.0	30.4	13.5	26.3	20.3	52.1
Ca I	6462.569	2.52	0.29	1.8	93.8	113.1	88.1	87.3	149.9	176.3	250.7	124.5	109.2	41.7	76.3	60.7	146.1
Ca I	6471.661	2.53	-0.64	1.8	30.5	42.4	21.1	28.5	46.1	63.5	95.2	37.1	24.6	11.7	19.0	15.0	46.1

Table 1—Continued

Element	λ (Å)	E.P.	$\log gf$	$\Delta\gamma_6$	1	2	3	4	5	6	7	8	9	10	11	12	13
Ca I	6493.781	2.52	0.02	1.8	58.2	73.2	55.6	56.8	78.6	94.5	131.9	69.2	51.0	25.5	46.9	41.4	74.6
Ca I	6499.650	2.52	-0.82	1.8	25.9	35.9	16.7	24.3	38.2	58.4	90.2	27.8	21.8	10.3	14.5	15.7	37.6
Ca I	6717.686	2.71	-0.57	1.8	34.6	41.3	20.4	28.9	44.2	70.2	108.2	...	23.7	8.6	21.1	13.6	48.1
Sc II	4246.837	0.32	0.24	2.5	126.6	142.3	...	108.3	144.4	144.2	...
Sc II	4314.095	0.62	-0.10	2.5	107.3	95.5	117.2	109.0	150.2
Sc II	4320.732	0.61	-0.25	2.5	...	85.6	...	89.0	121.9	62.2	104.4	96.0	132.6
Sc II	4324.996	0.60	-0.44	2.5	105.5	131.3	122.6	65.7	98.0	91.4	...
Sc II	4354.598	0.61	-1.58	2.5	...	43.5	39.3	...	63.8	...	110.9	56.6	49.6	13.5	29.7	15.6	66.4
Sc II	4374.457	0.62	-0.42	2.5	...	83.0	93.0	84.7	137.3	103.8	101.7	55.5	94.3	82.4	116.6
Sc II	4400.399	0.61	-0.54	2.5	...	74.1	90.7	81.1	100.7	111.7	52.3	89.6	78.8	121.9
Sc II	4415.563	0.60	-0.67	2.5	82.9	76.6	87.0	75.2	143.4	94.0	98.4	47.1	81.7	68.0	109.4
Sc II	4670.417	1.36	-0.58	2.5	42.6	38.5	44.0	35.9	66.0	72.7	112.9	54.0	56.1	13.5	40.0	29.6	71.7
Sc II	5031.021	1.36	-0.40	2.5	56.8	46.2	48.7	44.6	69.6	78.3	104.8	59.0	61.0	9.0	47.4	36.0	79.1
Ti I	4512.733	0.84	-0.42	2.5	30.3	35.2	23.5	25.0	50.6	65.5	106.8	36.0	41.3	8.3	19.4	9.7	47.6
Ti I	4518.023	0.83	-0.27	2.5	29.9	42.6	30.8	34.8	56.9	69.9	115.1	47.1	50.3	10.7	22.4	13.6	56.7
Ti I	4527.305	0.81	-0.47	2.5	77.0	40.8	25.0	33.2	60.9	...	148.4	46.9	40.7	8.8	...	15.1	58.0
Ti I	4533.239	0.85	0.53	2.5	64.5	73.7	69.5	65.4	93.2	101.4	...	84.0	92.6	39.0	59.4	47.1	96.0
Ti I	4534.778	0.84	0.34	2.5	54.4	64.7	59.7	57.9	80.1	92.3	134.7	72.8	78.3	32.3	50.3	36.6	86.9
Ti I	4535.570	0.83	0.12	2.5	50.1	...	52.2	52.5	84.9	100.5	23.5	43.1	31.4	97.7
Ti I	4544.688	0.82	-0.52	2.5	26.1	41.6	25.4	30.5	57.6	77.3	146.3	44.2	42.3	9.4	17.2	14.7	59.1
Ti I	4552.456	0.84	-0.34	2.5	27.7	44.9	13.7
Ti I	4555.485	0.85	-0.43	2.5	26.8	33.4	23.7	25.5	48.4	62.9	108.8	38.0	34.6	8.2	16.0	7.4	45.1
Ti I	4617.254	1.75	0.45	2.5	16.3	27.5	15.0	17.8	32.8	50.7	83.5	28.5	21.7	4.8	13.8	10.3	32.6
Ti I	4656.468	0.00	-1.29	2.5	21.1	39.0	32.6	30.4	59.7	72.4	133.6	49.2	56.3	9.9	23.1	10.9	60.3
Ti I	4681.908	0.05	-1.01	2.5	33.9	49.1	45.6	42.5	74.3	80.9	...	59.7	70.6	14.2	29.0	...	69.4
Ti I	4840.874	0.90	-0.45	2.5	20.3	31.6	20.9	23.3	44.9	55.8	105.9	35.5	36.0	6.5	15.4	10.2	41.3
Ti I	4885.082	1.89	0.41	2.5	12.6	20.6	10.2	14.1	27.7	44.2	83.2	22.6	17.3	2.0	11.3	4.8	25.3
Ti I	4913.616	1.87	0.22	2.5	...	18.2	...	12.0	19.7	32.3	68.5	14.3	...	3.3	9.9	...	17.2
Ti I	4981.732	0.85	0.56	2.5	73.3	79.8	76.1	75.7	101.3	106.7	165.2	88.8	97.8	41.2	68.2	49.9	103.1
Ti I	4991.067	0.84	0.44	2.5	67.4	...	71.3	70.5	93.1	39.4	69.7	51.8	...
Ti I	4999.504	0.82	0.31	2.5	86.9	71.6	63.7	65.3	96.4	103.7	174.2	84.2	87.9	33.0	56.9	40.4	96.0
Ti I	5016.162	0.85	-0.52	2.5	19.8	32.2	23.8	23.8	47.4	61.7	112.7	36.4	37.7	10.7	15.4	7.8	44.6
Ti I	5020.028	0.84	-0.36	2.5	28.6	42.7	32.7	33.1	57.8	73.4	122.4	47.2	45.8	10.7	22.6	14.8	54.9
Ti I	5022.871	0.83	-0.38	2.5	31.0	40.1	29.7	33.3	58.4	68.9	125.5	46.9	48.1	9.9	19.9	11.7	56.3
Ti I	5035.907	1.46	0.26	2.5	31.3	47.7	27.4	32.6	61.1	79.4	129.7	46.5	45.0	4.2	21.7	16.1	56.4

Table 1—Continued

Element	λ (Å)	E.P.	$\log gf$	$\Delta\gamma_6$	1	2	3	4	5	6	7	8	9	10	11	12	13
Ti I	5036.468	1.44	0.19	2.5	22.4	33.7	20.1	22.3	44.2	58.6	...	34.3	33.1	6.2	17.1	7.5	42.6
Ti I	5038.399	1.43	0.07	2.5	17.4	29.1	17.6	20.0	36.4	30.6	25.9	3.5	13.7	8.3	...
Ti I	5039.959	0.02	-1.13	2.5	33.7	48.4	47.7	36.4	70.9	81.6	148.1	61.2	69.7	15.7	28.5	14.0	69.7
Ti I	5064.654	0.05	-0.86	2.5	41.9	56.4	53.5	47.6	78.0	...	155.7	65.7	78.4	18.8	32.8	17.8	76.4
Ti I	5192.969	0.02	-0.95	2.5	45.2	59.4	54.0	50.2	84.2	97.2	191.3	70.5	88.1	...	36.4	23.1	75.1
Ti I	5210.386	0.05	-0.83	2.5	46.7	62.7	59.2	54.7	88.2	94.7	169.9	76.0	88.3	23.5	41.0	18.4	84.6
Ti I	5679.937	2.47	-0.57	2.5	1.2	1.5	6.8
Ti I	5953.162	1.89	-0.27	2.5	3.9	13.0	4.0	5.0	10.2	19.1	53.8	4.5	6.5	4.4	9.0
Ti I	5965.828	1.89	-0.35	2.5	3.0	8.9	...	2.1	8.9	16.3	48.6	6.8	7.5	7.7
Ti I	5978.543	1.87	-0.44	2.5	2.6	4.7	2.1	4.6	8.1	12.9	41.8	4.4	5.8	5.3
Ti I	6258.104	1.44	-0.36	2.5	8.5	15.1	9.2	9.9	22.9	36.1	89.3	18.3	17.4	4.5	6.4	...	27.4
Ti I	6258.709	1.44	-0.30	2.5	13.2	20.4	10.7	10.4	26.1	51.0	111.7	24.8	22.3	5.6	8.7	5.4	29.3
Ti I	6261.101	1.43	-0.42	2.5	7.4	14.7	7.3	10.5	20.8	34.5	90.5	17.2	16.1	1.8	4.6	...	17.5
Ti II	4501.272	1.12	-0.75	2.5	128.5	113.7	130.1	114.9	143.9	143.1	183.7	137.1	159.8	99.7	132.2	138.5	162.5
Ti II	4563.761	1.22	-0.96	2.5	125.2	104.8	124.9	109.1	135.6	139.6	183.3	126.4	154.1	92.6	127.8	130.5	152.8
Ti II	4571.968	1.57	-0.53	2.5	139.1	111.3	125.8	115.0	141.0	132.2	153.9	92.0	131.7	137.1	161.1
Ti II	4589.958	1.24	-1.79	2.5	81.4	71.3	82.1	74.0	97.8	99.4	123.1	91.1	105.2	49.6	83.4	74.4	105.5
Ti II	4657.203	1.24	-2.23	2.5	46.7	40.5	48.5	41.5	67.2	72.2	...	61.3	70.0	20.3	45.2	35.1	77.1
Ti II	4779.985	2.05	-1.37	2.5	52.0	46.2	45.0	44.0	65.0	73.9	92.6	58.3	59.5	19.0	45.8	40.7	72.0
Ti II	4805.085	2.06	-1.10	2.5	72.0	61.5	60.7	58.7	77.7	...	87.4	114.1	73.9	73.1	30.0	62.3	60.6
Ti II	5129.152	1.89	-1.39	2.5	68.3	56.2	58.0	52.5	77.7	72.0	75.5	24.4	58.4	49.8	...
Ti II	5154.070	1.57	-1.92	2.5	58.6	52.2	59.4	51.9	76.1	80.3	111.4	67.0	76.9	25.5	54.1	42.6	82.3
Ti II	5188.680	1.58	-1.21	2.5	107.3	...	98.1	98.2	130.8	127.6	61.8	105.3	105.0	...
Ti II	5336.781	1.58	-1.66	2.5	65.1	57.5	64.2	59.4	81.4	...	113.0	72.9	76.9	...	63.8	50.6	100.1
Ti II	5418.770	1.58	-2.11	2.5	37.4	32.2	38.7	33.9	55.4	60.6	85.0	47.5	54.9	13.3	33.4	23.9	63.7
Cr I	4496.842	0.94	-1.15	2.5	74.2	119.5	137.8	183.5	51.1	39.8	111.0
Cr I	4540.734	3.10	0.03	2.5	...	11.5	5.0	8.1	12.6	22.0	43.8	...	3.2	1.4	12.7
Cr I	4545.945	0.94	-1.37	2.5	27.2	42.3	26.0	33.8	58.1	69.2	122.5	40.1	49.0	11.1	19.7	13.0	63.6
Cr I	4591.389	0.97	-1.74	2.5	10.9	26.4	14.2	17.7	38.1	52.6	117.4	26.4	28.7	5.3	10.0	7.4	41.9
Cr I	4600.741	1.00	-1.26	2.5	26.4	43.5	25.9	32.6	58.4	72.7	...	46.7	50.0	11.0	22.4	15.6	63.4
Cr I	4616.120	0.98	-1.19	2.5	35.1	48.2	33.6	38.1	63.7	74.6	124.0	51.5	53.0	13.4	24.3	17.7	67.8
Cr I	4626.174	0.97	-1.32	2.5	24.0	38.0	27.3	31.8	57.1	67.4	116.6	43.7	47.5	11.3	20.6	15.3	56.8
Cr I	4646.148	1.03	-0.70	2.5	50.4	65.3	52.1	56.8	80.5	87.5	146.2	71.9	75.5	26.8	46.2	31.9	87.3
Cr I	4651.282	0.98	-1.46	2.5	24.2	37.1	20.9	27.7	51.0	63.5	117.0	38.2	37.5	8.7	16.9	10.7	54.1
Cr I	4652.152	1.00	-1.03	2.5	43.6	54.7	38.0	44.5	70.7	82.9	132.1	58.1	61.9	18.2	29.9	21.4	76.0

Table 1—Continued

Element	λ (Å)	E.P.	$\log gf$	$\Delta\gamma_6$	1	2	3	4	5	6	7	8	9	10	11	12	13
Cr I	4718.426	3.20	0.09	2.5	12.6	14.3	4.4	11.8	16.4	30.2	64.6	8.1	4.0	19.4
Cr I	5206.038	0.94	0.02	2.5	99.7	105.8	101.7	96.0	126.5	134.0	...	112.3	131.9	71.6	92.7	90.4	135.8
Cr I	5208.419	0.94	0.16	2.5	114.8	335.5	105.7	128.0	...
Cr I	5247.566	0.96	-1.64	2.5	16.8	32.9	20.9	24.6	48.2	60.7	122.4	33.5	38.4	7.5	14.7	7.7	50.9
Cr I	5345.801	1.00	-0.98	2.5	47.4	61.0	47.6	51.7	83.4	90.9	159.0	64.7	79.0	22.0	37.0	24.8	84.5
Cr I	5348.312	1.00	-1.29	2.5	25.3	46.7	31.5	37.0	64.2	74.6	137.5	49.3	55.9	12.8	23.2	14.3	67.9
Cr I	5409.772	1.03	-0.71	2.5	55.6	74.3	61.5	64.1	96.8	115.6	172.6	82.9	93.1	31.0	52.1	38.7	100.9
Cr I	6330.093	0.94	-2.92	2.5	...	3.6	...	4.1	7.1	13.2	55.9	...	6.4	7.2
Cr II	4558.650	4.07	-0.66	2.5	50.4	42.5	32.7	38.0	53.2	62.2	...	45.8	45.4	17.3	41.0	51.4	68.3
Cr II	4588.199	4.07	-0.63	2.5	35.4	33.5	20.5	30.8	41.2	50.1	62.4	37.3	36.1	10.6	31.6	41.2	54.6
Cr II	4634.070	4.07	-1.24	2.5	22.9	21.6	11.4	17.0	28.5	40.7	67.5	21.3	...	4.8	17.3	21.3	32.1
Cr II	4848.235	3.86	-1.14	2.5	29.5	25.1	15.9	22.8	33.6	42.3	...	23.6	25.4	...	23.6	25.9	43.9
Cr II	5237.329	4.07	-1.16	2.5	20.8	17.6	10.6	15.5	24.0	30.2	44.7	19.8	13.9	5.1	13.6	17.9	31.3
Mn I	4754.040	2.28	-0.09	2.5	24.7	45.1	23.6	32.9	61.2	80.2	130.3	45.3	45.1	...	26.0	16.5	72.6
Mn I	4823.496	2.32	0.14	1.5	37.0	51.5	23.0	42.1	69.3	78.8	134.0	52.8	63.3	10.8	31.2	21.7	...
Fe I	4489.739	0.12	-3.93	2.0	70.4	76.4	96.5	80.7	110.3	106.4	179.2	99.7	133.8	63.6	68.2	42.3	117.5
Fe I	4494.563	2.20	-1.14	2.0	91.5	95.8	99.3	89.8	120.6	132.7	205.1	110.8	120.5	68.7	88.3	79.2	128.6
Fe I	4528.614	2.17	-0.88	2.0	...	110.3	117.9	111.9	161.6	...	350.9	135.0	159.3	85.7	113.7	105.9	190.9
Fe I	4531.148	1.48	-2.13	2.0	82.2	81.4	96.3	85.8	118.8	107.4	132.2	65.6	78.3	67.6	119.6
Fe I	4556.126	3.60	-0.79	2.0	27.5	50.9	29.1	39.7	60.6	70.8	...	48.2	...	11.8	27.3
Fe I	4592.651	1.56	-2.46	2.0	62.4	...	81.5	78.0	108.8	...	204.0	91.0	115.7	44.9	63.7	48.4	124.3
Fe I	4602.000	1.61	-3.14	2.0	20.4	37.6	34.5	32.7	59.5	68.3	118.3	45.9	55.3	12.7	18.5	12.4	65.2
Fe I	4602.941	1.48	-2.21	2.0	76.0	...	93.0	83.5	110.1	111.1	173.9	99.9	122.3	64.0	78.4	62.3	119.1
Fe I	4619.287	3.60	-1.12	2.0	18.5	34.1	17.1	24.1	39.9	55.6	89.6	29.8	26.9	6.3	14.8	15.1	46.3
Fe I	4625.044	3.24	-1.34	2.0	...	42.9	24.4	31.1	53.9	63.9	...	41.2	35.5	10.6	21.1	18.9	59.0
Fe I	4630.120	2.28	-2.59	2.0	24.7	32.3	23.4	26.8	52.4	65.3	122.8	38.8	43.0	9.5	16.9	11.5	57.9
Fe I	4637.503	3.28	-1.39	2.0	27.0	38.6	20.7	26.3	47.9	60.8	100.1	36.8	31.6	8.1	17.0	14.2	53.0
Fe I	4638.010	3.60	-1.12	2.0	24.1	35.7	16.7	24.7	44.0	54.6	96.4	31.4	...	6.7	15.2	12.6	46.0
Fe I	4647.434	2.95	-1.33	2.0	49.0	53.8	39.9	43.5	70.3	78.9	141.5	58.7	54.6	17.0	32.5	27.2	76.6
Fe I	4669.171	3.65	-1.31	2.0	14.2	24.9	8.2	16.8	33.0	44.7	...	22.5	...	6.1
Fe I	4678.846	3.60	-0.75	2.0	29.1	52.4	28.1	42.8	60.6	72.5	106.1	50.9	...	14.0	27.9	27.1	62.8
Fe I	4691.411	2.99	-1.49	2.0	32.7	54.4	35.0	40.7	73.1	94.3	164.7	58.2	51.8	13.1	25.0	21.2	77.0
Fe I	4710.283	3.02	-1.61	2.0	38.1	44.3	26.4	30.8	63.0	81.0	...	47.9	39.4	10.4	18.8	14.8	63.2
Fe I	4728.546	3.65	-1.17	2.0	...	29.8	12.8	20.0	35.0	54.8	...	25.6	22.5	2.2	12.1	13.2	41.9
Fe I	4733.591	1.48	-2.99	2.0	46.0	56.2	55.1	50.2	80.9	85.6	146.5	67.7	81.0	24.4	34.7	21.1	86.7

Table 1—Continued

Element	λ (Å)	E.P.	$\log gf$	$\Delta\gamma_6$	1	2	3	4	5	6	7	8	9	10	11	12	13
Fe I	4736.773	3.21	-0.75	2.0	...	71.1	56.7	61.5	86.0	91.8	139.8	75.6	76.9	31.0	51.1	45.8	95.1
Fe I	4741.529	2.83	-1.88	2.0	...	30.0	19.4	22.1	41.0	53.8	93.4	31.2	26.4	5.7	12.8	11.6	45.4
Fe I	4871.318	2.87	-0.39	2.0	95.1	103.3	91.7	95.4	119.3	128.0	177.6	104.8	112.8	64.2	87.3	84.1	127.1
Fe I	4872.137	2.88	-0.58	2.0	82.7	90.3	81.4	84.8	109.0	95.0	103.8	52.7	75.8	70.5	119.7
Fe I	4882.144	3.42	-1.64	2.0	20.1	23.6	10.4	14.9	30.8	43.6	83.4	22.1	16.3	6.0	8.7	7.9	34.3
Fe I	4890.755	2.88	-0.41	2.0	109.4	101.9	90.0	93.8	119.9	127.9	183.3	110.0	110.6	62.5	85.9	82.5	126.1
Fe I	4891.492	2.85	-0.13	2.0	104.3	115.7	102.7	102.4	128.6	129.4	195.2	117.4	122.8	74.2	98.2	98.3	135.3
Fe I	4918.994	2.87	-0.36	2.0	95.0	106.4	92.5	90.0	120.7	129.1	...	108.0	110.8	66.0	86.8	84.5	130.1
Fe I	4920.503	2.83	0.06	2.0	113.7	116.0	141.7	87.0	114.0	115.6	157.8
Fe I	4924.770	2.28	-2.23	2.0	35.3	52.3	42.4	45.5	72.3	80.6	127.3	57.3	64.1	17.5	29.1	20.8	78.0
Fe I	4938.814	2.88	-1.08	2.0	54.2	69.0	59.2	60.4	80.3	86.9	138.6	72.2	74.7	31.0	48.6	42.8	89.5
Fe I	4939.687	0.86	-3.31	2.0	60.8	72.8	86.6	71.6	101.8	100.5	175.4	89.0	115.0	48.8	58.3	35.0	107.9
Fe I	4946.385	3.37	-1.17	2.0	45.9	44.0	21.8	31.7	54.3	67.1	109.7	45.0	38.1	9.6	22.7	19.3	62.0
Fe I	4985.253	3.93	-0.56	2.0	26.2	43.1	21.5	32.0	46.9	63.3	...	40.8	56.7	8.4	21.4	22.4	53.9
Fe I	4985.547	2.86	-1.33	2.0	38.6	56.6	41.9	48.3	70.8	79.9	...	62.0	...	19.3	33.3	29.4	81.6
Fe I	4994.130	0.91	-2.97	2.0	68.0	79.4	94.5	...	112.8	107.9	168.1	96.6	...	59.2	69.2	49.2	118.5
Fe I	5001.862	3.88	0.01	2.0	50.6	64.1	38.3	52.0	71.8	82.2	115.6	62.5	54.7	22.2	41.2	42.4	80.2
Fe I	5006.119	2.83	-0.64	2.0	80.8	93.3	84.6	86.0	109.7	113.7	165.0	97.9	101.2	55.3	75.3	70.1	117.0
Fe I	5012.068	0.86	-2.62	2.0	91.8	104.6	120.8	101.5	134.8	137.9	212.7	121.5	149.3	88.3	100.0	82.8	146.6
Fe I	5022.236	3.98	-0.53	2.0	29.1	43.4	22.5	30.4	49.2	61.8	97.2	39.6	29.6	9.0	19.9	21.6	56.5
Fe I	5028.127	3.57	-1.12	2.0	18.8	32.9	15.7	20.4	36.1	49.1	91.4	29.5	...	5.0	12.2	11.4	43.8
Fe I	5044.212	2.85	-2.06	2.0	...	27.3	17.9	20.0	40.2	49.0	96.0	27.1	26.1	5.2	12.7	6.1	42.0
Fe I	5049.819	2.28	-1.35	2.0	80.4	83.0	86.2	82.0	109.6	110.8	172.8	97.8	108.9	53.1	73.1	61.6	116.0
Fe I	5051.635	0.91	-2.76	2.0	82.7	93.7	108.8	92.7	127.6	130.2	...	113.1	140.2	75.6	82.8	67.6	135.0
Fe I	5068.766	2.94	-1.13	2.0	57.7	68.4	54.0	60.4	83.4	91.5	131.2	71.7	72.5	29.4	41.7	36.8	90.4
Fe I	5079.224	2.20	-2.09	2.0	48.1	64.0	57.0	58.0	84.8	91.0	...	74.2	79.2	26.9	41.6	32.3	...
Fe I	5079.740	0.99	-3.23	2.0	81.4	70.9	81.3	72.7	93.1	111.0	46.6	57.0	34.3	...
Fe I	5083.339	0.96	-2.84	2.0	76.5	81.8	99.8	83.0	112.5	112.6	180.2	103.4	126.5	65.2	72.5	52.7	120.2
Fe I	5098.697	2.17	-2.03	2.0	59.6	...	67.9	69.1	108.4	89.8	97.8	34.7	52.6	45.5	126.1
Fe I	5110.413	0.00	-3.76	2.0	89.2	102.5	124.1	104.9	138.6	137.4	230.3	123.5	152.9	92.0	97.0	70.2	147.3
Fe I	5123.720	1.01	-3.06	2.0	99.7	78.9	89.8	80.9	115.1	116.1	...	101.6	121.6	57.4	65.7	44.0	121.3
Fe I	5150.840	0.99	-3.02	2.0	...	75.9	86.0	74.8	104.1	105.3	176.7	91.6	108.9	49.5	62.1	42.0	112.8
Fe I	5151.911	1.01	-3.32	2.0	74.0	67.4	74.7	64.6	95.8	99.0	...	82.8	100.2	37.1	47.9	29.3	104.2
Fe I	5192.344	3.00	-0.42	2.0	80.3	93.6	81.5	81.8	105.3	115.1	...	93.3	...	47.7	74.2	73.4	103.3
Fe I	5194.942	1.56	-2.06	2.0	79.8	88.5	102.7	89.1	113.5	114.2	186.2	76.0	82.3	67.1	120.5

Table 1—Continued

Element	λ (Å)	E.P.	$\log gf$	$\Delta\gamma_6$	1	2	3	4	5	6	7	8	9	10	11	12	13
Fe I	5198.711	2.22	-2.11	2.0	39.4	57.8	52.8	51.2	...	86.2	139.4	24.1	34.8	26.0	84.6
Fe I	5202.336	2.18	-1.85	2.0	61.7	82.7	74.6	76.7	103.8	...	177.6	92.6	96.0	40.5	59.0	47.1	117.6
Fe I	5215.182	3.27	-0.87	2.0	41.3	57.8	39.7	48.3	70.8	79.9	115.9	59.3	56.9	18.6	33.8	29.9	77.0
Fe I	5216.274	1.61	-2.11	2.0	73.9	82.4	92.9	84.8	112.0	110.7	174.3	101.9	119.2	63.2	76.8	60.3	119.9
Fe I	5217.390	3.21	-1.11	2.0	36.9	53.0	36.2	42.5	65.6	75.9	116.8	53.5	46.9	16.1	28.7	24.5	72.9
Fe I	5225.525	0.11	-4.77	2.0	25.4	47.6	59.7	45.6	83.6	85.8	164.6	69.3	93.7	23.9	27.8	9.4	87.0
Fe I	5227.190	1.56	-1.23	2.0	120.8	134.1	143.1	129.8	163.5	164.3	...	148.4	...	111.9	131.3	125.0	173.5
Fe I	5232.940	2.94	-0.10	2.0	99.5	118.3	103.7	104.2	127.0	135.3	198.5	115.9	119.8	75.8	96.7	94.4	140.0
Fe I	5242.491	3.63	-0.90	2.0	23.4	37.9	17.9	28.7	42.2	57.8	93.9	34.0	25.6	6.5	15.8	16.0	51.9
Fe I	5250.210	0.12	-4.92	2.0	18.7	39.8	50.7	36.6	73.7	74.9	160.5	55.6	77.7	18.7	22.7	6.7	79.0
Fe I	5250.646	2.20	-2.11	2.0	46.3	62.4	57.0	56.1	83.4	86.2	...	69.1	73.3	27.0	42.2	29.7	91.8
Fe I	5263.305	3.27	-0.92	2.0	43.0	61.9	39.5	48.3	72.4	71.9	132.4	61.9	56.3	19.4	33.4	29.9	79.2
Fe I	5269.537	0.86	-1.32	2.0	144.0	173.1	176.5	159.8	203.9	217.1	393.5	182.2	214.8	145.5	158.7	150.9	214.1
Fe I	5307.361	1.61	-2.95	2.0	31.2	50.4	48.7	45.7	77.0	81.1	136.3	61.1	72.7	18.3	28.0	17.3	81.5
Fe I	5328.039	0.92	-1.47	2.0	139.4	158.3	167.3	147.7	188.1	171.9	200.1	136.2	152.8	150.8	201.5
Fe I	5328.532	1.56	-1.85	2.0	93.6	102.6	113.3	101.9	133.2	120.2	138.5	83.9	98.7	91.5	146.5
Fe I	5332.900	1.56	-2.86	2.0	39.3	58.2	58.9	52.4	83.9	82.7	...	71.5	81.1	26.3	37.4	23.9	89.3
Fe I	5339.930	3.27	-0.68	2.0	57.5	70.1	51.9	60.3	81.8	...	134.2	66.6	70.1	27.9	46.4	42.6	102.3
Fe I	5341.024	1.61	-2.01	2.0	89.3	...	105.4	96.3	125.2	131.7	...	109.5	135.0	74.9	90.2	...	137.1
Fe I	5373.698	4.47	-0.86	2.0	...	12.2	3.3	8.1	13.8	23.4	46.0	11.1	5.9	5.7	15.5
Fe I	5379.573	3.70	-1.50	2.0	...	14.6	4.4	...	18.9	28.5	61.8	11.7	...	2.0	20.6
Fe I	5393.167	3.24	-0.81	2.0	53.4	69.4	50.1	58.7	82.2	88.4	137.7	69.2	70.6	25.8	42.8	40.5	90.4
Fe I	5405.775	0.99	-1.85	2.0	117.6	125.4	149.2	126.3	168.3	172.0	259.4	159.2	190.1	121.5	128.4	116.9	175.3
Fe I	5429.696	0.96	-1.88	2.0	117.7	134.2	150.9	128.7	167.8	172.6	...	149.1	175.3	118.0	131.8	121.9	...
Fe I	5434.524	1.01	-2.12	2.0	106.5	112.6	132.7	...	163.9	136.9	233.9	140.0	133.4	...	114.6	100.2	...
Fe I	5455.609	1.01	-2.09	2.0	327.4	...	204.7	98.6	135.7	133.6	...
Fe I	5560.207	4.43	-1.19	2.0	3.1	7.6	3.2	5.1	9.0	15.3	33.6	5.1	3.9	10.1
Fe I	5569.618	3.42	-0.51	2.0	48.7	71.7	52.9	59.2	81.4	94.3	135.5	71.8	68.7	26.9	45.5	42.4	87.3
Fe I	5572.841	3.40	-0.29	2.0	66.4	81.7	64.8	68.4	95.4	103.9	...	83.1	86.5	37.9	59.0	54.6	103.9
Fe I	5576.090	3.43	-1.00	2.0	38.1	54.4	33.8	42.5	64.6	77.1	117.2	54.4	49.0	15.5	30.1	28.8	71.5
Fe I	5586.756	3.37	-0.14	2.0	78.6	92.3	75.2	80.6	106.7	114.1	160.0	93.7	93.4	48.2	68.6	66.7	114.6
Fe I	5615.644	3.33	-0.04	2.0	77.1	100.6	88.4	88.8	112.7	122.0	180.3	101.3	104.2	57.2	80.3	75.8	123.1
Fe I	5658.816	3.40	-0.84	2.0	42.7	60.3	41.9	49.0	76.7	61.3	57.1	17.6	33.5	31.6	78.8
Fe I	5679.025	4.65	-0.92	2.0
Fe I	5717.835	4.29	-1.13	2.0	8.7	10.2	3.5	5.8	14.7	23.4	46.3	10.5	4.1	1.3	14.5

Table 1—Continued

Element	λ (Å)	E.P.	$\log gf$	$\Delta\gamma_6$	1	2	3	4	5	6	7	8	9	10	11	12	13
Fe I	5775.080	4.22	-1.30	2.0	4.3	10.4	4.7	6.4	11.7	20.5	45.8	...	7.9	13.1
Fe I	6012.204	2.22	-4.04	2.0	...	3.4	1.6	1.7	5.6	9.0	36.5	5.4
Fe I	6016.604	3.55	-1.82	2.0	...	8.5	10.7	22.7	68.4	7.3	11.3	15.3
Fe I	6027.048	4.08	-1.15	2.0	8.3	16.6	5.5	9.7	14.9	27.8	58.2	10.9	7.0	1.9	...	3.6	21.8
Fe I	6055.992	4.73	-0.46	2.0	8.6	15.1	6.7	12.7	15.3	26.4	47.9	10.7	5.4	3.2	6.9	9.3	18.4
Fe I	6065.481	2.61	-1.47	2.0	51.3	68.5	61.2	62.9	90.5	96.7	153.6	77.3	83.6	28.7	46.6	36.1	97.8
Fe I	6078.999	4.65	-1.12	2.0	...	8.4	...	3.5	5.5	10.5	24.7	...	2.3	7.6
Fe I	6082.709	2.22	-3.57	2.0	...	7.0	2.1	4.0	10.9	20.4	62.8	7.9	7.4	13.8
Fe I	6127.904	4.14	-1.40	2.0	3.3	7.6	3.2	...	9.7	15.8	36.8	3.5	2.1
Fe I	6151.618	2.18	-3.30	2.0	4.6	...	8.8	10.3	21.2	31.2	86.2	14.6	15.2	3.7	4.6	3.1	22.2
Fe I	6157.725	4.08	-1.26	2.0	10.1	14.0	5.1	8.2	16.6	28.3	63.4	11.3	18.4
Fe I	6173.341	2.22	-2.88	2.0	13.3	26.1	18.6	...	43.3	53.2	107.7	32.6	35.6	7.2	...	6.1	47.4
Fe I	6180.203	2.73	-2.62	2.0	...	13.4	6.7	8.7	19.7	30.1	80.3	14.5	14.9	5.2	23.0
Fe I	6213.429	2.22	-2.57	2.0	22.9	42.3	32.3	34.9	58.9	68.3	125.0	47.9	48.6	11.4	19.6	14.6	66.7
Fe I	6219.280	2.20	-2.43	2.0	28.1	48.3	41.0	40.9	68.7	75.9	134.4	54.5	58.3	15.2	24.9	18.8	75.7
Fe I	6230.723	2.56	-1.28	2.0	67.7	84.7	81.6	80.8	106.4	111.2	193.7	94.1	106.2	47.1	65.6	56.0	116.4
Fe I	6240.645	2.22	-3.20	2.0	4.1	12.6	9.4	9.0	21.8	29.0	83.9	...	16.2	1.5	22.2
Fe I	6246.318	3.60	-0.88	2.0	31.7	52.0	30.0	37.3	60.4	68.1	112.3	45.5	42.1	11.8	23.0	22.2	63.5
Fe I	6252.555	2.40	-1.73	2.0	55.3	74.2	69.7	69.8	97.3	98.0	159.6	84.4	93.6	34.4	51.1	40.9	102.1
Fe I	6254.257	2.28	-2.44	2.0	30.7	52.7	37.8	39.7	73.0	82.1	135.3	57.5	64.1	13.6	27.3	19.3	73.7
Fe I	6322.684	2.59	-2.44	2.0	12.7	...	22.0	21.0	41.3	56.5	101.5	30.6	31.9	5.7	11.0	10.2	48.8
Fe I	6335.330	2.20	-2.20	2.0	36.5	57.8	54.5	53.8	81.9	89.9	147.0	68.7	77.7	21.7	35.7	25.7	87.2
Fe I	6344.148	2.43	-2.90	2.0	...	16.1	9.5	11.9	28.2	38.6	94.8	20.6	20.8	1.2	4.2	2.6	30.3
Fe I	6355.029	2.84	-2.36	2.0	...	20.2	11.2	...	30.3	43.0	97.9	22.1	20.1	6.0
Fe I	6380.742	4.19	-1.39	2.0	5.5	4.4	11.3	16.9	40.7	...	3.6	1.9	11.4
Fe I	6393.601	2.43	-1.58	2.0	62.9	77.8	77.0	72.9	100.1	107.0	163.7	91.4	102.2	41.2	54.8	44.9	109.6
Fe I	6481.869	2.28	-2.98	2.0	8.2	21.7	15.7	16.6	34.8	48.4	102.5	22.9	25.8	3.7	9.2	...	31.8
Fe I	6494.980	2.40	-1.26	2.0	67.6	92.7	92.8	89.2	117.1	115.8	191.9	104.2	116.6	58.3	76.9	64.1	122.0
Fe I	6498.940	0.96	-4.69	2.0	8.5	14.2	19.5	11.4	32.4	42.4	114.8	21.4	32.8	4.3	4.4	2.0	34.9
Fe I	6592.913	2.73	-1.54	2.0	46.2	63.8	55.0	49.2	84.1	89.6	144.9	71.5	77.8	24.9	40.0	33.6	87.3
Fe I	6593.868	2.43	-2.39	2.0	20.4	37.8	29.8	28.2	58.5	68.0	121.7	41.9	48.7	10.3	17.7	13.2	62.0
Fe I	6609.109	2.56	-2.68	2.0	7.7	20.7	11.4	13.7	31.6	43.4	96.0	22.1	22.2	5.4	6.7	...	36.7
Fe I	6750.152	2.42	-2.61	2.0	15.2	29.5	23.0	22.8	48.0	58.9	113.4	36.5	36.6	6.5	13.9	...	51.6
Fe II	4508.289	2.86	-2.32	2.5	74.3	60.6	61.6	61.8	79.2	81.7	103.2	71.6	76.3	41.4	64.5	80.9	95.5
Fe II	4515.339	2.84	-2.48	2.5	67.0	54.5	53.5	54.7	73.8	80.2	...	63.3	67.6	33.0	62.0	72.3	93.0

Table 1—Continued

Element	λ (Å)	E.P.	$\log gf$	$\Delta\gamma_6$	1	2	3	4	5	6	7	8	9	10	11	12	13
Fe II	4522.634	2.84	-2.11	2.5	97.1	79.2	54.6	90.0	102.4	...
Fe II	4576.339	2.84	-2.95	2.5	51.1	37.1	33.5	35.5	50.1	57.9	...	45.1	41.7	15.3	38.6	44.7	67.7
Fe II	4583.837	2.81	-1.92	2.5	100.1	84.3	91.4	85.7	108.3	112.5	170.1	99.4	105.3	69.0	100.5	117.6	...
Fe II	4629.339	2.81	-2.37	2.5	72.5	60.8	63.8	62.3	81.3	85.6	113.7	73.6	76.2	41.7	69.7	81.1	97.6
Fe II	4923.927	2.89	-1.32	2.5	120.3	99.5	111.0	107.2	127.8	130.7	154.6	116.5	129.2	90.0	123.3	150.4	151.0
Fe II	5018.440	2.89	-1.23	2.5	139.2	112.1	122.8	116.5	145.3	148.8	...	129.6	145.5	99.1	137.8	165.3	173.6
Fe II	5197.576	3.23	-2.17	2.5	56.8	51.4	46.5	50.5	...	74.3	96.6	52.3	65.9	89.2
Fe II	5234.630	3.22	-2.21	2.5	62.7	55.2	51.0	51.7	69.1	71.7	95.4	61.8	61.5	30.3	60.9	70.8	89.6
Fe II	5276.002	3.20	-2.04	2.5	74.0	68.8	61.9	63.7	85.3	92.2	...	76.1	73.2	37.1	71.6	77.6	...
Fe II	5316.615	3.15	-2.02	2.5	94.7	86.4	135.8	...
Fe II	5325.560	3.22	-2.91	2.5	15.0	15.4	12.0	13.8	21.1	31.4	38.8	18.9	16.1	5.0	13.8	14.9	31.6
Fe II	6247.562	3.89	-2.33	2.5	22.0	20.1	15.6	17.9	25.2	34.2	43.7	23.5	20.5	5.5	16.4	23.3	37.1
Fe II	6456.391	3.90	-2.08	2.5	32.6	27.6	21.3	22.8	38.3	44.6	53.6	32.5	29.6	8.4	26.8	29.3	52.4
Ni I	4714.408	3.38	0.23	2.5	...	56.5	37.4	46.8	68.0	82.8	119.5	58.0	53.8	17.4	38.4	28.8	68.8
Ni I	4715.757	3.54	-0.34	2.5	...	24.0	7.1	12.8	24.4	42.5	2.1	11.6	4.0	22.3
Ni I	4756.510	3.48	-0.34	2.5	16.2	25.4	12.8	16.8	30.8	44.4	67.4	26.2	23.2	5.1	12.5	9.4	33.5
Ni I	4786.531	3.42	-0.17	2.5	35.4	36.8	20.6	26.5	47.3	62.9	91.1	5.6	20.8	...	46.0
Ni I	4829.016	3.54	-0.33	2.5	17.4	25.9	12.8	18.1	30.4	42.6	66.7	...	20.6	3.3	13.1	8.4	33.1
Ni I	4831.169	3.61	-0.42	2.5	15.6	19.9	10.8	14.6	24.5	36.3	57.3	2.1	12.3	...	26.2
Ni I	4904.407	3.54	-0.17	2.5	19.0	31.6	18.3	24.4	37.5	50.6	...	28.3	28.2	...	18.4	10.1	39.7
Ni I	4937.341	3.61	-0.39	2.5	20.6	20.6	12.1	14.0	23.7	31.0	68.0	17.8	15.0	4.0	8.1	5.2	22.2
Ni I	5035.357	3.64	0.29	2.5	30.7	42.9	26.8	32.9	48.8	60.6	84.9	41.4	40.6	9.7	24.9	19.8	53.1
Ni I	5081.107	3.85	0.30	2.5	27.2	34.5	19.9	28.0	40.0	55.4	78.0	37.0	31.0	7.7	22.4	15.1	46.0
Ni I	5084.089	3.68	0.03	2.5	19.7	33.4	17.3	22.8	37.1	51.5	70.7	30.4	...	6.4	16.9	...	39.4
Ni I	5115.389	3.83	-0.11	2.5	11.6	21.3	10.3	13.9	21.8	34.7	51.3	17.7	...	3.1	9.8	7.6	27.0
Ni I	5146.480	3.71	0.12	2.5	22.5	28.0	14.3	20.3	32.2	47.6	73.4	25.9	24.2	4.6	15.0	8.4	34.5
Ni I	5155.762	3.90	-0.09	2.5	...	19.2	7.6	13.7	21.4	29.1	52.4	15.5	13.4	1.3	9.0	6.4	23.0
Ni I	5587.853	1.94	-2.14	2.5	8.1	15.0	9.3	12.6	27.4	38.5	83.1	20.0	24.6	3.4	5.8	...	25.8
Ni I	5592.259	1.95	-2.57	2.5	9.1	17.3	9.2	10.4	27.2	42.2	92.4	17.9	22.9	4.2	30.0
Ni I	5711.883	1.94	-2.27	2.5	11.2	23.2	12.3	16.6	32.9	48.7	...	21.4	28.6	4.1	11.1	...	38.0
Ni I	6108.107	1.68	-2.45	2.5	...	19.3	...	12.3	38.4	47.3	98.8	4.0	8.6	4.3	35.6
Ni I	6256.351	1.68	-2.48	2.5	24.3	44.3	34.1	34.6	66.3	74.9	132.4	52.0	62.2	12.6	22.3	13.1	35.9
Ni I	6482.796	1.94	-2.63	2.5	1.3	11.2	2.8	4.8	12.5	22.0	61.6	9.0	12.7	...	4.9	...	64.5
Ni I	6643.629	1.68	-2.30	2.5	19.6	39.7	32.3	32.3	64.0	73.9	133.5	48.3	65.8	7.4	20.8	3.7	60.0
Ni I	6767.768	1.83	-2.17	2.5	18.5	33.2	27.8	27.9	53.2	65.3	115.5	41.8	...	8.3	17.2	12.4	55.2

|
 ∞
|

Table 1—Continued

Element	λ (Å)	E.P.	$\log gf$	$\Delta\gamma_6$	1	2	3	4	5	6	7	8	9	10	11	12	13
Zn I	4680.134	4.01	-0.82	1.5	...	14.9	5.6	11.2	...	25.5	...	10.4	32.3	2.9	...	3.1	...
Zn I	4722.153	4.03	-0.34	1.5	...	27.3	19.3	22.6	36.6	45.2	48.8	30.6	45.6	8.8	22.4	16.0	35.5
Zn I	4810.528	4.08	-0.14	1.5	31.3	34.9	24.5	31.0	43.8	53.3	57.4	38.5	51.3	12.3	32.0	18.9	43.8
Y II	4900.120	1.03	-0.13	2.5	...	30.5	29.0	30.7	57.8	62.6	14.3	31.1	28.3	...
Y II	5087.416	1.08	-0.31	2.5	61.8	22.0	19.1	21.5	44.6	50.7	72.8	36.1	25.2	9.4	16.9	17.5	31.6
Ba II	4554.029	0.00	0.17	3.0	268.0	136.7	129.9	145.4	188.7	186.6	262.1	168.2	168.4	130.6	161.3	169.0	187.5
Ba II	4934.076	0.00	-0.15	3.0	232.7	146.6	130.7	151.0	193.2	195.7	122.0	172.9	172.9	130.5	161.1	167.5	199.4
Ba II	5853.668	0.60	-1.00	3.0	119.2	42.9	27.0	45.7	75.5	76.0	...	61.3	44.8	21.8	40.1	42.8	72.4
Ba II	6141.713	0.70	-0.08	3.0	102.5	65.1

Table 2. Atomic data and measured equivalent widths (continue)

Element	λ (Å)	E.P.	$\log gf$	$\Delta\gamma_6$	14	15	16	17	18	19	20	21	22	23	24	25	26
Na I	5682.650	2.10	-0.82	2.0	2.0	21.4	...	9.0	9.3	4.8	5.6	10.4	20.9	5.1
Na I	5688.219	2.10	-0.37	2.0	2.8	33.9	...	16.5	23.5	...	9.0	19.3	36.4	8.4
Na I	5889.951	0.00	0.12	2.0	145.2	...	134.0	69.2	47.5
Na I	5895.924	0.00	-0.18	2.0	133.2	...	144.3	52.2	31.2	38.1
Na I	6154.227	2.10	-1.66	2.0	...	4.6	...	7.6	4.6	...
Na I	6160.751	2.10	-1.35	2.0	...	6.3	...	1.6	2.2	...	1.4	4.6	1.3
Mg I	4571.099	0.00	-5.59	2.5	50.1	104.7	34.8	90.5	30.8	19.4	68.0	81.3	45.4	23.7
Mg I	4702.996	4.34	-0.55	2.5	79.8	131.1	48.0	196.0	107.1	88.9	...	181.0	17.1	16.8	20.2	126.4	94.1
Mg I	4730.026	4.34	-2.37	2.5	...	20.3	...	13.2	9.4	5.7	7.3	11.0	13.4	3.1
Si I	5772.148	5.08	-1.75	1.3	...	15.6	1.3	4.0	7.8	6.3	...	6.0	5.8	2.2
Si I	5948.545	5.08	-1.23	1.3	7.6	34.3	4.5	12.8	17.6	11.6	7.1	18.4	21.2	12.8
Si I	6155.141	5.62	-0.84	1.3	5.8	25.1	1.3	9.6	13.3	8.2	3.9	11.1	15.2	7.8
Si II	6347.100	8.12	0.32	2.5	...	10.6	16.0	12.7	6.6
Ca I	4526.934	2.71	-0.49	1.8	13.6	43.6	2.4	44.8	24.1	17.3	27.3	37.8	...	1.5	1.2	30.2	17.5
Ca I	4578.551	2.52	-0.63	1.8	12.2	47.5	...	47.4	26.1	20.1	37.8	45.1	1.7	33.1	17.0
Ca I	4685.268	2.93	-0.88	1.8	4.0	21.3	...	13.8	11.4	8.9	11.7	12.5	12.8	6.8
Ca I	5261.707	2.52	-0.65	1.8	17.2	57.4	7.0	7.1	30.3	24.6	43.0	51.6	1.2	1.7	...	38.1	22.0
Ca I	5262.241	2.52	-0.60	1.8	31.1	100.7	...	60.6	50.5	...	60.2	66.4	1.4	52.7	32.9
Ca I	5512.980	2.93	-0.37	1.8	71.3	44.2
Ca I	5581.968	2.52	-0.63	1.8	18.6	59.4	8.1	60.0	37.0	26.9	...	52.7	1.6	7.4	4.5	37.4	23.6
Ca I	5588.755	2.53	0.28	1.8	56.8	101.5	31.1	125.3	78.5	68.6	10.9	...	14.6	85.0	64.1
Ca I	5590.117	2.52	-0.64	1.8	18.8	57.4	7.0	57.2	29.6	22.8	41.8	46.6	38.2	21.0
Ca I	5594.466	2.52	0.02	1.8	43.9	92.6	20.0	104.8	65.3	58.4	85.0	10.1	74.3	53.6
Ca I	5598.480	2.52	-0.22	1.8	34.6	88.9	17.4	71.9	78.6	4.3	65.1	46.7
Ca I	5601.277	2.53	-0.69	1.8	19.4	61.8	...	61.8	33.1	27.7	...	54.1	3.1	3.7	...	41.4	24.1
Ca I	5857.451	2.93	0.24	1.8	31.1	79.4	11.9	95.2	54.3	43.0	66.7	80.1	4.6	...	5.6	63.0	34.6
Ca I	6122.217	1.89	-0.32	1.8	66.0	118.7	37.4	4.0	83.0	74.2	...	149.8	12.6	14.0	17.3	94.7	60.9
Ca I	6162.173	1.90	-0.09	1.8	76.7	131.8	45.1	218.2	93.0	76.4	...	169.3	20.4	19.5	24.5	109.5	76.4
Ca I	6163.755	2.52	-1.29	1.8	4.8	32.6	...	25.3	11.1	5.9	11.7	20.1	13.9	6.3
Ca I	6166.440	2.52	-1.14	1.8	7.6	52.5	...	31.0	14.3	14.4	19.9	29.3	1.6	...	1.3	20.0	8.1
Ca I	6169.042	2.52	-0.80	1.8	13.1	68.2	3.8	56.2	24.8	19.9	36.6	51.3	30.5	18.3
Ca I	6169.562	2.53	-0.37	1.8	20.5	65.2	7.9	79.6	36.6	32.8	59.0	73.7	3.1	1.0	...	49.8	26.4
Ca I	6449.810	2.52	-0.50	1.8	20.2	23.7	12.0	68.5	40.1	...	50.3	60.2	1.5	...	4.0	43.4	25.0
Ca I	6462.569	2.52	0.29	1.8	60.6	153.8	34.6	20.8	82.6	16.6	11.3	91.1	64.6
Ca I	6471.661	2.53	-0.64	1.8	17.4	57.5	4.8	56.6	26.9	...	42.8	48.5	33.8	19.7

Table 2—Continued

Element	λ (Å)	E.P.	$\log gf$	$\Delta\gamma_6$	14	15	16	17	18	19	20	21	22	23	24	25	26
Ca I	6493.781	2.52	0.02	1.8	38.8	87.9	12.9	95.0	57.8	...	70.0	76.1	...	3.8	3.6	63.6	42.2
Ca I	6499.650	2.52	-0.82	1.8	14.7	58.8	4.7	49.4	24.4	...	33.8	43.2	30.6	16.5
Ca I	6717.686	2.71	-0.57	1.8	15.7	59.9	2.6	60.0	26.8	...	40.0	50.7	1.0	1.4	...	39.0	20.1
Sc II	4246.837	0.32	0.24	2.5	100.4	146.5	88.8	...	103.9	104.2	12.1	39.2	...	101.6	...
Sc II	4314.095	0.62	-0.10	2.5	74.0	112.8	...	63.1	82.4	63.1	72.7	52.4
Sc II	4320.732	0.61	-0.25	2.5	61.6	100.6	60.2	60.2	71.7	62.2	67.1	67.1	...	9.1	...	64.6	48.8
Sc II	4324.996	0.60	-0.44	2.5	69.7	...	48.9	...	67.9	55.5	80.9	80.9	69.0	52.5
Sc II	4354.598	0.61	-1.58	2.5	19.4	67.9	12.7	34.2	14.4	8.6	24.6	24.6	7.1
Sc II	4374.457	0.62	-0.42	2.5	59.1	110.0	49.1	62.0	64.7	55.2	57.8	57.8	61.2	42.9
Sc II	4400.399	0.61	-0.54	2.5	51.3	97.1	34.4	52.6	58.0	49.0	50.3	50.3	...	8.0	...	55.0	38.5
Sc II	4415.563	0.60	-0.67	2.5	50.3	93.1	36.1	71.5	54.6	43.1	52.5	52.5	...	4.5	...	48.2	...
Sc II	4670.417	1.36	-0.58	2.5	16.6	57.7	5.8	13.3	20.5	15.0	11.3	11.3	...	2.4	...	17.0	7.9
Sc II	5031.021	1.36	-0.40	2.5	21.3	65.1	11.5	18.0	29.9	...	23.9	23.9	...	1.5	12.0
Ti I	4512.733	0.84	-0.42	2.5	12.3	52.5	5.0	52.5	15.6	8.7	37.4	41.2	1.3	17.7	...
Ti I	4518.023	0.83	-0.27	2.5	16.5	60.7	6.5	60.6	20.5	12.9	43.4	47.6	...	1.2	1.3	23.9	...
Ti I	4527.305	0.81	-0.47	2.5	15.1	64.0	6.2	56.9	16.6	11.2	38.1	42.9	1.6	21.8	16.0
Ti I	4533.239	0.85	0.53	2.5	48.4	88.7	31.9	103.0	54.5	47.8	4.2	...	7.3	57.2	39.3
Ti I	4534.778	0.84	0.34	2.5	40.4	80.0	25.0	...	46.9	...	79.7	67.8	1.0	...	4.9	48.2	30.8
Ti I	4535.570	0.83	0.12	2.5	33.8	42.5	29.3	2.5	39.0	...
Ti I	4544.688	0.82	-0.52	2.5	13.4	66.0	...	70.2	21.5	10.5	41.7	46.3	25.9	13.0
Ti I	4552.456	0.84	-0.34	2.5	12.7	79.0	24.5	18.4	1.0	...	1.4	31.3	...
Ti I	4555.485	0.85	-0.43	2.5	12.9	50.8	6.5	48.7	16.2	13.3	36.8	40.1	...	1.0	...	16.0	6.5
Ti I	4617.254	1.75	0.45	2.5	9.7	39.5	2.1	39.9	15.0	...	28.0	31.4	17.2	8.2
Ti I	4656.468	0.00	-1.29	2.5	14.5	58.7	7.9	58.0	13.7	8.8	42.3	44.2	17.5	9.5
Ti I	4681.908	0.05	-1.01	2.5	19.6	68.8	11.4	66.4	21.2	13.8	52.4	53.2	24.6	12.4
Ti I	4840.874	0.90	-0.45	2.5	9.7	47.4	3.9	48.3	13.9	8.9	35.4	35.4	15.6	8.5
Ti I	4885.082	1.89	0.41	2.5	6.4	33.0	1.1	33.9	13.1	8.8	20.1	30.3	12.6	7.8
Ti I	4913.616	1.87	0.22	2.5	5.8	27.3	...	27.3	7.8	...	16.0	19.6	7.7	2.5
Ti I	4981.732	0.85	0.56	2.5	52.6	96.6	33.3	111.1	61.4	46.7	88.7	83.7	5.0	6.5	6.6	60.1	42.8
Ti I	4991.067	0.84	0.44	2.5	48.9	...	28.4	...	52.8	43.8	75.0	83.7	3.5	...	6.7	58.2	40.8
Ti I	4999.504	0.82	0.31	2.5	41.4	91.1	24.2	101.8	47.5	37.9	85.7	76.5	4.4	5.3	3.9	51.9	35.1
Ti I	5016.162	0.85	-0.52	2.5	...	50.0	6.2	47.5	15.2	13.0	32.5	32.3	17.5	9.1
Ti I	5020.028	0.84	-0.36	2.5	17.0	60.6	6.2	58.3	21.8	15.4	44.5	43.6	21.3	13.7
Ti I	5022.871	0.83	-0.38	2.5	14.4	58.9	8.2	62.7	18.5	13.2	43.1	45.2	...	1.5	2.5	18.9	9.9
Ti I	5035.907	1.46	0.26	2.5	17.8	69.1	7.6	70.3	29.0	16.8	52.8	58.0	30.4	14.0

Table 2—Continued

Element	λ (Å)	E.P.	$\log gf$	$\Delta\gamma_6$	14	15	16	17	18	19	20	21	22	23	24	25	26
Ti I	5036.468	1.44	0.19	2.5	12.1	49.7	3.2	64.8	19.5	6.3	43.9	42.8	17.9	9.8
Ti I	5038.399	1.43	0.07	2.5	9.4	...	2.2	49.5	15.6	8.5	38.8	35.9	1.6	1.3	1.1	15.7	5.6
Ti I	5039.959	0.02	-1.13	2.5	21.3	68.8	9.4	68.7	20.1	11.9	54.2	51.8	25.6	11.1
Ti I	5064.654	0.05	-0.86	2.5	26.5	74.2	16.1	75.3	24.4	14.5	57.5	56.0	1.4	1.4	...	29.4	15.7
Ti I	5192.969	0.02	-0.95	2.5	26.5	80.5	12.4	66.0	24.6	...	67.6	30.7	...
Ti I	5210.386	0.05	-0.83	2.5	32.0	82.2	29.2	19.0	2.1	35.7	17.6
Ti I	5679.937	2.47	-0.57	2.5	...	1.6	2.3
Ti I	5953.162	1.89	-0.27	2.5	3.2	14.3	...	14.9	1.8	3.2	8.0	9.8	5.0	...
Ti I	5965.828	1.89	-0.35	2.5	2.2	11.0	...	13.2	6.3	7.3	3.1	...
Ti I	5978.543	1.87	-0.44	2.5	1.8	11.4	...	9.0	1.9	2.3	5.7	7.0	1.3	1.4	...
Ti I	6258.104	1.44	-0.36	2.5	4.4	29.3	...	33.2	11.7	...	18.4	20.6	...	1.2	...	5.6	3.9
Ti I	6258.709	1.44	-0.30	2.5	4.6	34.9	1.9	38.7	15.9	...	25.6	25.6	9.3	4.7
Ti I	6261.101	1.43	-0.42	2.5	5.1	24.8	...	27.0	5.1	...	17.4	15.3	1.4	13.9	2.3
Ti II	4501.272	1.12	-0.75	2.5	91.3	129.2	...	87.1	103.5	93.1	79.5	84.9	14.4	...	37.2	89.9	81.6
Ti II	4563.761	1.22	-0.96	2.5	83.4	122.2	80.3	80.8	96.1	89.8	75.0	82.9	8.9	23.1	28.8	87.9	76.4
Ti II	4571.968	1.57	-0.53	2.5	87.3	129.8	78.4	92.9	103.9	95.2	81.8	90.5	12.4	34.3	37.1	95.5	81.4
Ti II	4589.958	1.24	-1.79	2.5	48.2	87.1	36.1	38.3	59.1	47.6	30.4	40.7	...	4.8	5.3	50.6	34.2
Ti II	4657.203	1.24	-2.23	2.5	19.2	58.9	12.6	15.5	25.1	18.4	10.5	17.8	20.3	11.2
Ti II	4779.985	2.05	-1.37	2.5	22.5	61.2	10.7	19.0	35.0	25.4	14.4	22.7	27.7	14.4
Ti II	4805.085	2.06	-1.10	2.5	34.7	79.5	23.2	33.1	52.7	39.5	23.6	35.4	6.3	44.9	30.5
Ti II	5129.152	1.89	-1.39	2.5	27.9	73.3	17.8	29.8	43.2	32.1	20.8	31.4	36.9	22.4
Ti II	5154.070	1.57	-1.92	2.5	26.5	70.2	17.9	31.7	37.9	26.6	20.7	27.2	...	1.0	...	31.8	18.7
Ti II	5188.680	1.58	-1.21	2.5	46.9	...	78.2	8.5
Ti II	5336.781	1.58	-1.66	2.5	32.4	72.8	21.0	...	43.2	39.2	...
Ti II	5418.770	1.58	-2.11	2.5	13.6	50.2	10.1	10.9	21.2	14.4	7.2	13.0	1.0	16.6	10.1
Cr I	4496.842	0.94	-1.15	2.5	22.7	76.7	36.6	...	59.3	58.9	35.5	...
Cr I	4540.734	3.10	0.03	2.5	...	19.2	...	22.6	7.3	9.6	10.9	17.0	5.8	...
Cr I	4545.945	0.94	-1.37	2.5	14.0	61.2	4.8	65.1	19.0	13.8	48.5	41.1	25.6	15.1
Cr I	4591.389	0.97	-1.74	2.5	7.7	48.6	5.0	...	31.1	30.9	1.4
Cr I	4600.741	1.00	-1.26	2.5	15.1	61.9	6.4	66.6	21.4	18.5	50.3	50.8	27.5	18.0
Cr I	4616.120	0.98	-1.19	2.5	18.6	65.4	7.8	70.4	24.0	17.9	55.8	55.0	32.0	18.3
Cr I	4626.174	0.97	-1.32	2.5	15.2	59.9	8.7	63.9	17.1	15.3	51.0	47.8	25.4	15.5
Cr I	4646.148	1.03	-0.70	2.5	34.2	79.7	16.9	89.1	42.6	37.4	72.1	70.7	...	2.1	...	46.0	35.7
Cr I	4651.282	0.98	-1.46	2.5	11.9	54.9	3.8	58.5	16.0	10.9	43.1	41.7	...	0.7	...	20.1	11.8
Cr I	4652.152	1.00	-1.03	2.5	24.8	72.2	9.9	79.1	33.1	23.6	61.4	61.2	1.4	...	1.3	36.8	24.0

Table 2—Continued

Element	λ (Å)	E.P.	$\log gf$	$\Delta\gamma_6$	14	15	16	17	18	19	20	21	22	23	24	25	26
Cr I	4718.426	3.20	0.09	2.5	3.4	24.2	...	24.4	8.3	7.7	12.1	15.4	1.8	10.4	6.5
Cr I	5206.038	0.94	0.02	2.5	73.4	124.4	54.0	...	82.0	73.8	...	138.0	10.4	1.0	15.9	88.6	75.8
Cr I	5208.419	0.94	0.16	2.5	64.1	...	93.5	18.4	...	15.0
Cr I	5247.566	0.96	-1.64	2.5	8.8	51.4	2.5	61.0	13.4	...	36.8	36.2	18.2	...
Cr I	5345.801	1.00	-0.98	2.5	26.5	82.2	14.1	98.7	35.8	28.2	73.6	70.7	1.0	40.6	29.5
Cr I	5348.312	1.00	-1.29	2.5	15.2	65.5	6.1	79.7	24.6	19.1	53.9	55.3	27.5	18.1
Cr I	5409.772	1.03	-0.71	2.5	37.1	93.5	20.2	120.2	47.7	38.1	89.4	84.4	...	2.6	2.4	52.8	38.2
Cr I	6330.093	0.94	-2.92	2.5	0.9	8.6	...	10.5	5.6	6.0	2.7
Cr II	4558.650	4.07	-0.66	2.5	20.3	56.1	...	20.3	43.7	42.0	13.3	2.7	2.7	38.5	29.5
Cr II	4588.199	4.07	-0.63	2.5	14.6	46.5	7.0	14.5	37.0	29.8	8.9	18.3	...	3.4	2.4	30.2	22.6
Cr II	4634.070	4.07	-1.24	2.5	8.0	33.1	3.5	10.1	21.2	9.3	...	1.0	...	20.7	15.7
Cr II	4848.235	3.86	-1.14	2.5	10.5	39.4	4.9	9.4	24.7	19.5	7.6	11.6	1.1	22.7	12.5
Cr II	5237.329	4.07	-1.16	2.5	5.9	28.3	3.1	9.0	18.2	13.2	5.5	7.6	1.1	15.3	9.4
Mn I	4754.040	2.28	-0.09	2.5	14.4	70.2	5.1	...	28.6	17.4	33.5	...
Mn I	4823.496	2.32	0.14	1.5	20.5	73.0	7.7	88.0	38.0	23.5	64.3	64.3	41.1	25.2
Fe I	4489.739	0.12	-3.93	2.0	50.2	93.6	38.9	87.1	35.3	29.1	75.1	68.3	1.4	1.2	1.0	45.8	35.8
Fe I	4494.563	2.20	-1.14	2.0	69.5	109.4	52.9	160.4	72.0	69.3	123.0	11.6	80.8	72.3
Fe I	4528.614	2.17	-0.88	2.0	84.0	...	70.8	...	91.7	18.4	...	18.6	97.8	93.0
Fe I	4531.148	1.48	-2.13	2.0	60.0	102.8	48.6	...	57.9	55.7	95.3	87.0	5.1	...	6.3	66.9	58.3
Fe I	4556.126	3.60	-0.79	2.0	20.9	64.8	6.8	66.3	33.7	31.5	48.7	54.6	0.9	40.0	27.9
Fe I	4592.651	1.56	-2.46	2.0	46.4	...	29.0	...	47.9	42.5	75.3	...	1.5	52.3	44.4
Fe I	4602.000	1.61	-3.14	2.0	13.2	56.4	5.0	48.2	11.3	...	38.0	36.6	3.5	19.9	11.0
Fe I	4602.941	1.48	-2.21	2.0	59.7	98.3	...	109.7	56.5	52.9	92.9	88.3	2.4	1.4	...	65.0	53.2
Fe I	4619.287	3.60	-1.12	2.0	11.8	49.1	4.9	46.6	20.8	20.3	29.4	35.8	1.3	...	1.0	27.4	16.8
Fe I	4625.044	3.24	-1.34	2.0	14.4	57.4	7.1	59.8	22.4	18.5	...	43.3	1.4	...	1.9	29.1	18.7
Fe I	4630.120	2.28	-2.59	2.0	...	52.1	5.8	43.0	11.3	10.8	29.6	32.6	16.3	12.6
Fe I	4637.503	3.28	-1.39	2.0	12.2	53.8	6.1	53.5	20.2	21.0	33.6	39.5	1.0	25.4	17.5
Fe I	4638.010	3.60	-1.12	2.0	11.0	49.8	...	48.3	21.3	18.5	25.6	39.7	25.0	18.0
Fe I	4647.434	2.95	-1.33	2.0	23.5	69.3	10.2	60.4	33.4	30.0	...	51.5	1.9	...	1.7	42.0	28.4
Fe I	4669.171	3.65	-1.31	2.0	7.4	39.0	...	33.0	12.2	...	18.5	29.3	16.2	10.5
Fe I	4678.846	3.60	-0.75	2.0	23.4	64.9	10.3	68.8	35.7	33.0	50.6	...	2.1	...	1.8	44.8	...
Fe I	4691.411	2.99	-1.49	2.0	19.2	78.6	8.4	73.8	29.0	22.6	50.3	59.6	35.1	21.7
Fe I	4710.283	3.02	-1.61	2.0	14.8	64.3	23.1	20.8	43.4	51.9	31.1	17.4
Fe I	4728.546	3.65	-1.17	2.0	8.9	45.1	...	40.2	16.2	13.4	26.1	29.9	...	1.0	...	22.9	13.0
Fe I	4733.591	1.48	-2.99	2.0	23.7	74.2	13.9	64.9	23.1	20.0	37.8	52.9	31.8	21.7

Table 2—Continued

Element	λ (Å)	E.P.	$\log gf$	$\Delta\gamma_6$	14	15	16	17	18	19	20	21	22	23	24	25	26
Fe I	4736.773	3.21	-0.75	2.0	40.2	85.8	22.9	112.4	51.0	47.1	82.0	82.5	1.9	...	1.6	63.4	47.4
Fe I	4741.529	2.83	-1.88	2.0	10.0	46.6	2.8	39.6	13.3	...	26.5	29.6	21.4	12.5
Fe I	4871.318	2.87	-0.39	2.0	72.0	117.8	52.9	...	77.9	72.2	144.1	133.2	10.5	...	13.5	90.2	78.0
Fe I	4872.137	2.88	-0.58	2.0	61.9	...	43.1	...	66.1	64.4	119.5	113.1	6.3	79.1	67.8
Fe I	4882.144	3.42	-1.64	2.0	7.4	38.2	1.9	33.1	10.7	9.2	20.0	23.8	1.0	16.2	10.0
Fe I	4890.755	2.88	-0.41	2.0	69.3	120.3	49.1	...	78.4	74.8	145.7	138.7	9.4	...	13.9	90.6	74.5
Fe I	4891.492	2.85	-0.13	2.0	82.7	132.6	62.4	...	92.3	87.4	...	181.1	17.4	...	22.4	106.7	90.8
Fe I	4918.994	2.87	-0.36	2.0	72.4	120.5	52.2	207.9	85.7	79.4	160.1	147.0	11.2	14.3	15.1	95.8	76.0
Fe I	4920.503	2.83	0.06	2.0	93.8	...	74.8	347.3	109.2	102.2	...	225.3	26.8	...	28.9	132.4	112.7
Fe I	4924.770	2.28	-2.23	2.0	20.9	71.2	14.4	66.0	24.6	18.8	48.8	...	1.5	31.8	23.0
Fe I	4938.814	2.88	-1.08	2.0	37.5	79.9	21.3	106.1	46.9	44.0	69.7	77.3	6.4	1.0	2.1	55.7	35.7
Fe I	4939.687	0.86	-3.31	2.0	41.6	89.0	29.0	88.1	33.1	...	65.6	68.4	3.0	1.1	...	45.2	30.1
Fe I	4946.385	3.37	-1.17	2.0	13.9	59.9	5.4	64.5	24.3	20.5	38.2	47.1	1.8	33.0	22.8
Fe I	4985.253	3.93	-0.56	2.0	16.2	56.8	...	59.2	29.8	24.5	40.1	45.8	1.4	...	1.6	38.0	26.7
Fe I	4985.547	2.86	-1.33	2.0	25.6	71.8	13.4	79.8	33.7	27.1	56.6	45.9	1.2	45.0	28.3
Fe I	4994.130	0.91	-2.97	2.0	51.3	95.8	39.0	94.7	42.9	...	77.3	75.8	3.8	56.7	...
Fe I	5001.862	3.88	0.01	2.0	33.5	76.7	17.9	100.3	50.1	46.2	74.0	77.8	6.9	6.4	3.3	59.6	46.0
Fe I	5006.119	2.83	-0.64	2.0	62.7	108.6	41.5	160.7	72.0	65.0	121.7	120.0	6.3	9.6	9.1	85.1	68.4
Fe I	5012.068	0.86	-2.62	2.0	77.0	125.0	66.8	143.8	72.1	66.7	100.6	104.6	7.3	8.0	7.2	81.5	69.2
Fe I	5022.236	3.98	-0.53	2.0	16.0	57.9	5.9	64.8	28.8	23.9	44.8	52.1	37.6	25.7
Fe I	5028.127	3.57	-1.12	2.0	9.5	45.4	2.9	43.1	15.7	16.1	25.4	32.7	...	1.0	...	24.5	13.3
Fe I	5044.212	2.85	-2.06	2.0	7.6	42.7	2.6	42.8	11.1	10.3	25.2	28.7	1.0	...	1.0	13.9	9.8
Fe I	5049.819	2.28	-1.35	2.0	58.3	102.7	39.5	...	60.5	55.4	100.9	93.9	5.3	5.0	6.6	69.4	59.7
Fe I	5051.635	0.91	-2.76	2.0	66.6	112.4	55.6	117.2	60.5	51.9	91.0	87.2	...	5.8	3.0	67.2	54.9
Fe I	5068.766	2.94	-1.13	2.0	36.3	81.7	21.0	97.7	46.2	40.2	75.6	75.4	1.6	54.6	...
Fe I	5079.224	2.20	-2.09	2.0	31.1	79.6	14.9	83.8	33.1	28.8	66.1	64.3	1.3	1.1	...	43.4	30.1
Fe I	5079.740	0.99	-3.23	2.0	41.2	...	27.4	82.0	34.5	29.9	67.2	68.6	1.8	1.0	...	44.9	31.4
Fe I	5083.339	0.96	-2.84	2.0	55.6	98.1	44.1	97.6	48.7	41.7	79.3	75.8	1.3	59.7	46.9
Fe I	5098.697	2.17	-2.03	2.0	37.9	...	21.4	...	51.6	47.0	70.0	...	1.9	1.0	...	53.4	43.9
Fe I	5110.413	0.00	-3.76	2.0	74.3	125.0	67.8	131.5	62.2	34.5	99.9	94.1	5.2	...	4.4	74.2	57.8
Fe I	5123.720	1.01	-3.06	2.0	48.1	101.5	35.2	100.2	41.0	34.7	78.1	75.0	1.0	...	1.7	53.6	40.3
Fe I	5150.840	0.99	-3.02	2.0	44.9	94.1	30.6	87.8	37.0	30.0	...	64.5	49.2	35.5
Fe I	5151.911	1.01	-3.32	2.0	34.7	85.7	21.9	...	26.9	20.6	62.5	58.1	27.9
Fe I	5192.344	3.00	-0.42	2.0	62.1	109.7	39.7	141.9	70.8	7.4	5.7	9.7	79.0	...
Fe I	5194.942	1.56	-2.06	2.0	63.0	104.8	49.8	101.8	62.3	57.9	5.9	...	67.7	...

Table 2—Continued

Element	λ (Å)	E.P.	$\log gf$	$\Delta\gamma_6$	14	15	16	17	18	19	20	21	22	23	24	25	26
Fe I	5198.711	2.22	-2.11	2.0	26.1	72.6	16.6	77.3	29.4	28.2	...	54.5	4.5	38.0	23.8
Fe I	5202.336	2.18	-1.85	2.0	46.6	106.8	23.6	116.8	53.1	43.8	...	95.1	1.1	...	1.0	67.0	49.8
Fe I	5215.182	3.27	-0.87	2.0	25.3	71.0	13.3	91.5	37.7	33.1	62.0	67.6	...	2.4	...	48.3	34.2
Fe I	5216.274	1.61	-2.11	2.0	57.8	99.2	44.1	105.3	55.2	50.6	86.0	81.7	3.3	...	2.5	65.2	52.6
Fe I	5217.390	3.21	-1.11	2.0	22.2	69.1	11.5	82.1	30.6	26.0	57.0	62.0	42.7	28.5
Fe I	5225.525	0.11	-4.77	2.0	17.3	68.9	10.4	57.8	10.0	8.7	40.2	37.3	15.3	7.8
Fe I	5227.190	1.56	-1.23	2.0	103.9	152.3	93.5	...	103.1	98.2	...	149.9	27.9	24.1	20.5	109.6	98.1
Fe I	5232.940	2.94	-0.10	2.0	82.2	130.7	62.6	257.9	91.4	84.1	190.2	164.9	15.7	22.8	20.1	108.9	92.9
Fe I	5242.491	3.63	-0.90	2.0	12.9	52.9	6.1	49.1	22.0	16.9	31.4	34.5	28.6	18.9
Fe I	5250.210	0.12	-4.92	2.0	13.3	61.8	5.9	52.2	6.2	5.4	36.8	60.5	...	1.0	...	12.2	...
Fe I	5250.646	2.20	-2.11	2.0	29.6	79.4	14.2	77.2	31.4	26.2	57.3	...	2.4	43.3	...
Fe I	5263.305	3.27	-0.92	2.0	27.3	75.3	14.5	...	37.4	35.1	73.4	75.3	1.4	1.7	1.3	49.6	34.9
Fe I	5269.537	0.86	-1.32	2.0	130.7	203.0	125.3	...	120.6	117.9	62.2	55.1	53.4	134.2	122.6
Fe I	5307.361	1.61	-2.95	2.0	19.8	69.0	12.8	61.6	17.4	15.0	44.5	47.4	...	1.6	...	25.4	17.3
Fe I	5328.039	0.92	-1.47	2.0	120.4	...	117.2	...	115.3	106.0	...	105.4	52.4	45.0	44.1	130.8	112.2
Fe I	5328.532	1.56	-1.85	2.0	76.1	...	64.6	...	73.2	66.9	9.1	6.2	79.6	68.6
Fe I	5332.900	1.56	-2.86	2.0	25.6	76.7	16.2	69.9	24.1	18.4	51.0	50.2	34.8	21.2
Fe I	5339.930	3.27	-0.68	2.0	37.7	83.5	...	118.5	49.5	...	86.5	84.4	...	3.6	...	60.1	...
Fe I	5341.024	1.61	-2.01	2.0	70.1	116.7	...	136.9	66.9	60.2	100.4	97.5	4.0	3.7	3.6	76.1	...
Fe I	5373.698	4.47	-0.86	2.0	3.5	20.6	...	17.5	7.8	8.4	5.8	14.2	12.2	9.6
Fe I	5379.573	3.70	-1.50	2.0	4.4	24.1	2.5	21.2	6.1	2.2	1.0	19.0	11.2	...
Fe I	5393.167	3.24	-0.81	2.0	35.3	83.4	17.4	111.6	47.4	42.7	76.5	85.5	2.6	1.0	...	58.0	45.5
Fe I	5405.775	0.99	-1.85	2.0	102.3	146.9	112.0	...	95.8	113.9	189.7	159.4	27.4	...	23.2	101.9	96.3
Fe I	5429.696	0.96	-1.88	2.0	104.8	...	99.5	...	98.2	88.7	161.4	...	26.3	...	22.7	112.8	...
Fe I	5434.524	1.01	-2.12	2.0	89.9	130.7	83.3	...	84.2	16.3
Fe I	5455.609	1.01	-2.09	2.0	94.8	...	101.2	28.6	...	17.0
Fe I	5560.207	4.43	-1.19	2.0	1.3	12.8	...	11.5	4.2	...	6.5	9.0	6.3	4.7
Fe I	5569.618	3.42	-0.51	2.0	35.2	85.9	18.7	119.3	50.2	44.2	85.9	93.9	2.5	...	2.9	61.1	46.2
Fe I	5572.841	3.40	-0.29	2.0	48.4	98.1	28.4	155.7	62.1	...	121.0	111.4	4.4	...	8.7	74.6	61.2
Fe I	5576.090	3.43	-1.00	2.0	21.9	70.1	12.0	84.7	34.0	30.0	59.3	63.8	2.1	44.6	33.0
Fe I	5586.756	3.37	-0.14	2.0	58.6	108.0	37.8	189.9	71.4	61.9	138.8	133.8	6.4	9.8	12.1	84.1	70.5
Fe I	5615.644	3.33	-0.04	2.0	66.2	119.3	41.9	219.5	81.7	74.6	161.9	...	9.3	...	16.0	98.6	83.2
Fe I	5658.816	3.40	-0.84	2.0	26.8	...	10.8	...	39.5	36.4	70.9	74.1	3.1	...	2.7	48.8	37.7
Fe I	5679.025	4.65	-0.92	2.0
Fe I	5717.835	4.29	-1.13	2.0	2.7	20.1	...	16.8	6.8	...	9.8	14.4	9.3	6.3

Table 2—Continued

Element	λ (Å)	E.P.	$\log gf$	$\Delta\gamma_6$	14	15	16	17	18	19	20	21	22	23	24	25	26
Fe I	5775.080	4.22	-1.30	2.0	...	19.2	...	15.0	4.9	6.6	5.7	12.8	6.9	...
Fe I	6012.204	2.22	-4.04	2.0	1.0	6.2	...	4.5	4.3	...	4.1
Fe I	6016.604	3.55	-1.82	2.0	1.6	19.3	...	21.5	5.9	3.2	10.1	11.6	4.2	4.9
Fe I	6027.048	4.08	-1.15	2.0	3.1	25.3	...	21.3	9.2	6.9	11.8	11.9	12.3	7.7
Fe I	6055.992	4.73	-0.46	2.0	5.3	23.5	...	21.5	10.3	6.9	12.8	17.9	12.3	10.6
Fe I	6065.481	2.61	-1.47	2.0	35.3	86.0	19.3	90.1	40.2	37.5	71.2	71.7	1.0	53.7	38.1
Fe I	6078.999	4.65	-1.12	2.0	...	8.3	...	7.8	4.7	4.4	2.7	1.8
Fe I	6082.709	2.22	-3.57	2.0	...	13.8	...	10.5	3.8	6.9
Fe I	6127.904	4.14	-1.40	2.0	...	12.3	1.7	...	8.1	5.4	...
Fe I	6151.618	2.18	-3.30	2.0	4.0	24.9	...	20.0	3.9	...	9.6	11.0	3.3	...
Fe I	6157.725	4.08	-1.26	2.0	3.8	23.4	...	19.5	9.8	...	12.5	13.5	9.9	7.2
Fe I	6173.341	2.22	-2.88	2.0	8.1	42.9	...	37.1	8.9	8.5	25.0	22.8	1.2	4.1
Fe I	6180.203	2.73	-2.62	2.0	...	24.1	1.2	18.0	2.0	...	12.0	13.7	1.2
Fe I	6213.429	2.22	-2.57	2.0	13.3	60.8	...	55.4	16.7	...	33.1	35.9	23.0	...
Fe I	6219.280	2.20	-2.43	2.0	18.5	67.6	9.6	62.0	17.5	42.4	1.3	26.2	16.8
Fe I	6230.723	2.56	-1.28	2.0	53.8	102.5	31.1	124.1	57.5	...	96.6	98.8	4.5	68.6	55.0
Fe I	6240.645	2.22	-3.20	2.0	...	23.0	1.9	...	3.6	11.7	5.8	...
Fe I	6246.318	3.60	-0.88	2.0	19.5	64.9	...	79.2	30.4	...	51.9	56.9	1.1	1.4	...	40.4	27.8
Fe I	6252.555	2.40	-1.73	2.0	41.1	90.2	22.8	94.8	47.6	20.7	70.5	72.4	1.8	4.6	2.3	57.4	40.3
Fe I	6254.257	2.28	-2.44	2.0	18.9	73.3	7.8	59.6	27.4	...	43.3	45.9	1.0	32.4	22.9
Fe I	6322.684	2.59	-2.44	2.0	7.4	50.7	3.4	39.4	7.8	...	24.9	28.2	18.2	9.1
Fe I	6335.330	2.20	-2.20	2.0	26.9	76.2	13.8	74.9	25.3	...	56.6	55.5	35.0	21.8
Fe I	6344.148	2.43	-2.90	2.0	4.3	29.7	1.5	24.3	6.0	...	13.9	15.0	...	1.2	1.0	6.3	...
Fe I	6355.029	2.84	-2.36	2.0	...	36.4	1.8	29.0	5.7	...	17.4	18.6	2.6
Fe I	6380.742	4.19	-1.39	2.0	...	13.5	...	11.3	4.6	...	7.2	9.2	4.8	4.6
Fe I	6393.601	2.43	-1.58	2.0	43.7	96.0	29.4	105.4	47.9	...	83.6	83.3	3.4	3.0	2.3	59.7	48.6
Fe I	6481.869	2.28	-2.98	2.0	7.5	36.9	2.3	32.2	10.9	...	17.5	19.7	3.3	13.6	...
Fe I	6494.980	2.40	-1.26	2.0	62.7	110.2	39.9	135.4	64.7	50.0	96.0	99.1	2.2	...	6.1	75.7	60.0
Fe I	6498.940	0.96	-4.69	2.0	...	28.7	1.1	24.0	12.4	14.9	4.0	2.7
Fe I	6592.913	2.73	-1.54	2.0	30.7	80.1	19.9	87.2	34.7	...	66.3	68.8	3.3	...	2.6	48.3	29.8
Fe I	6593.868	2.43	-2.39	2.0	11.5	56.3	7.0	52.1	14.2	...	35.6	39.6	2.7	22.6	10.3
Fe I	6609.109	2.56	-2.68	2.0	4.5	35.0	...	30.4	9.6	...	18.2	19.5	7.7	...
Fe I	6750.152	2.42	-2.61	2.0	9.3	47.7	1.8	42.5	11.6	...	27.6	31.5	1.5	...	1.2	14.9	9.8
Fe II	4508.289	2.86	-2.32	2.5	36.0	74.3	28.5	30.3	55.3	53.6	21.1	35.9	1.9	3.9	7.1	50.7	42.9
Fe II	4515.339	2.84	-2.48	2.5	29.8	68.5	24.0	26.6	47.7	48.5	17.5	28.2	1.8	...	3.9	43.8	37.4

Table 2—Continued

Element	λ (Å)	E.P.	$\log gf$	$\Delta\gamma_6$	14	15	16	17	18	19	20	21	22	23	24	25	26
Fe II	4522.634	2.84	-2.11	2.5	37.6	...	64.1	65.4	36.3	45.5	2.1	...	11.3	...	53.9
Fe II	4576.339	2.84	-2.95	2.5	15.1	51.3	...	13.0	27.5	26.9	10.1	16.2	...	1.0	18.5
Fe II	4583.837	2.81	-1.92	2.5	60.7	98.9	55.5	55.6	79.5	79.0	42.8	56.8	8.0	...	19.7	75.7	68.9
Fe II	4629.339	2.81	-2.37	2.5	37.3	77.0	30.2	38.8	55.0	55.5	28.4	40.3	1.1	...	3.5	54.0	43.9
Fe II	4923.927	2.89	-1.32	2.5	79.8	118.0	78.2	72.4	100.4	96.3	59.8	67.3	15.2	34.7	31.4	90.2	85.7
Fe II	5018.440	2.89	-1.23	2.5	88.8	135.5	83.3	84.6	111.2	106.5	75.0	79.1	17.5	44.3	42.7	99.4	94.2
Fe II	5197.576	3.23	-2.17	2.5	24.7	56.1	19.4	24.7	40.3	22.5	...	3.2	3.1	42.2	33.1
Fe II	5234.630	3.22	-2.21	2.5	30.7	66.9	21.6	25.1	49.0	44.6	16.9	22.5	1.0	4.5	3.8	46.2	36.1
Fe II	5276.002	3.20	-2.04	2.5	37.9	87.0	26.5	51.2	59.1	56.2	30.5	42.5	5.4	57.2	45.7
Fe II	5316.615	3.15	-2.02	2.5	38.9	39.4	70.5	...	30.9	...	1.3	6.4	8.8
Fe II	5325.560	3.22	-2.91	2.5	4.3	24.0	5.1	3.3	11.7	...	1.6	4.6	11.3	7.1
Fe II	6247.562	3.89	-2.33	2.5	9.0	29.1	1.4	6.4	20.5	...	3.7	16.1	...
Fe II	6456.391	3.90	-2.08	2.5	10.8	40.3	4.6	9.1	28.6	1.5	6.3	13.0	1.2	2.4	...	19.9	19.6
Ni I	4714.408	3.38	0.23	2.5	28.8	71.4	12.7	70.7	46.2	37.9	53.7	54.0	48.6	35.8
Ni I	4715.757	3.54	-0.34	2.5	7.9	33.7	...	23.2	15.4	...	13.7	21.6	19.1	...
Ni I	4756.510	3.48	-0.34	2.5	10.2	40.1	...	26.0	17.1	13.0	18.1	25.6	2.0	19.4	11.6
Ni I	4786.531	3.42	-0.17	2.5	11.5	53.9	4.5	40.1	23.3	20.6	30.4	34.5	15.7
Ni I	4829.016	3.54	-0.33	2.5	9.9	38.3	...	27.1	17.1	...	13.9	22.2	17.5	...
Ni I	4831.169	3.61	-0.42	2.5	7.4	32.1	1.5	...	13.0	2.9	11.4	19.8	1.2	16.6	...
Ni I	4904.407	3.54	-0.17	2.5	11.9	46.7	5.6	35.5	20.8	14.3	22.5	23.9	13.9
Ni I	4937.341	3.61	-0.39	2.5	6.7	32.2	...	21.9	13.8	...	13.0	17.8	1.8	13.9	7.2
Ni I	5035.357	3.64	0.29	2.5	19.3	56.8	...	50.7	34.8	22.7	37.2	42.7	36.4	19.9
Ni I	5081.107	3.85	0.30	2.5	15.7	48.9	3.9	45.8	29.6	18.7	30.8	30.9	17.5
Ni I	5084.089	3.68	0.03	2.5	12.6	44.2	7.2	32.8	23.5	14.1	23.1	30.3	26.9	14.4
Ni I	5115.389	3.83	-0.11	2.5	7.8	31.4	1.5	19.9	15.0	6.7	10.4	19.7	13.2	4.1
Ni I	5146.480	3.71	0.12	2.5	10.2	41.8	2.9	45.9	17.9	12.1	29.9	31.4	22.0	13.9
Ni I	5155.762	3.90	-0.09	2.5	6.8	30.2	2.0	28.3	14.3	...	21.4	20.3	15.3	13.0
Ni I	5587.853	1.94	-2.14	2.5	3.9	29.2	...	17.2	8.1	2.2	8.9	15.1	1.5	6.5	...
Ni I	5592.259	1.95	-2.57	2.5	4.5	30.3	...	18.4	10.5	2.2	10.9	...	2.3	8.2	...
Ni I	5711.883	1.94	-2.27	2.5	6.8	38.3	1.8	26.8	11.2	19.1	10.8	7.7
Ni I	6108.107	1.68	-2.45	2.5	5.3	34.8	1.8	21.6	10.9	17.4	6.4	3.4
Ni I	6256.351	1.68	-2.48	2.5	18.1	65.4	9.1	54.5	20.8	3.8	37.1	42.0	1.1	25.7	12.8
Ni I	6482.796	1.94	-2.63	2.5	2.0	14.8	...	8.3	3.6	6.6	3.8	1.0
Ni I	6643.629	1.68	-2.30	2.5	14.4	62.2	...	44.5	12.5	...	28.2	35.7	19.8	6.7
Ni I	6767.768	1.83	-2.17	2.5	12.2	54.0	5.3	36.7	16.0	...	28.3	34.8	14.5	9.7

Table 2—Continued

Element	λ (Å)	E.P.	$\log gf$	$\Delta\gamma_6$	14	15	16	17	18	19	20	21	22	23	24	25	26
Zn I	4680.134	4.01	-0.82	1.5	2.0	25.4	...	6.7	14.7	5.9	2.0
Zn I	4722.153	4.03	-0.34	1.5	9.4	41.0	5.3	14.0	28.3	14.9	14.0	14.0	21.9	10.2
Zn I	4810.528	4.08	-0.14	1.5	14.6	46.7	8.3	19.6	34.7	15.4	11.7	11.7	27.0	13.3
Y II	4900.120	1.03	-0.13	2.5	4.9	51.2	6.0	8.3	15.9	15.3	...	14.3	20.6	...
Y II	5087.416	1.08	-0.31	2.5	...	39.3	3.0	5.2	9.8	7.3	9.9	9.6	17.3	...
Ba II	4554.029	0.00	0.17	3.0	87.5	165.8	72.0	111.1	105.6	115.0	124.3	122.1	...	19.2	14.0	134.2	91.5
Ba II	4934.076	0.00	-0.15	3.0	80.4	176.3	55.3	119.6	106.4	111.9	122.7	121.8	9.6	132.0	87.3
Ba II	5853.668	0.60	-1.00	3.0	7.2	65.2	5.0	15.1	16.6	15.3	21.5	18.6	39.5	8.7
Ba II	6141.713	0.70	-0.08	3.0	60.6	...	56.0	54.5	50.4	36.1

Table 3. Abundance ratios: Na, Mg, Si, and Ca

Star	[NaI/H]	N	[MgI/H]	N	[SiI/H]	N	[SiII/H]	N	[CaI/H]	N
BD+04°2466	-1.76 ± 0.08	2	-1.67 ± 0.08	1	-1.42 ± 0.07	2	-1.47 ± 0.08	21
BD+01°3070	-1.61 ± 0.06	3	-1.20 ± 0.09	3	-1.16 ± 0.09	3	-1.17 ± 0.06	1	-1.28 ± 0.06	19
BD+09°2870	-2.62 ± 0.09	2	-2.26 ± 0.13	2	-2.26 ± 0.10	25
BD+10°2495	-2.04 ± 0.06	2	-1.88 ± 0.08	1	-1.65 ± 0.05	3	-1.76 ± 0.06	23
BD+12°2547	-2.04 ± 0.06	1	-1.53 ± 0.08	1	-1.59 ± 0.09	2	-1.66 ± 0.06	21
BD+29°2356	-1.49 ± 0.09	3	-1.09 ± 0.08	1	-1.10 ± 0.07	3	-1.20 ± 0.04	1	-1.20 ± 0.07	18
BD+30°2611	-1.74 ± 0.08	2	-1.27 ± 0.08	1	-1.17 ± 0.08	3	-1.07 ± 0.05	1	-1.36 ± 0.07	12
HD 33771	-2.10 ± 0.06	2	-1.77 ± 0.08	1	-1.62 ± 0.07	2	-1.76 ± 0.06	19
HD 85773	-3.29 ± 0.08	.	-2.29 ± 0.09	3	-2.34 ± 0.07	17
HD 107752	-3.63 ± 0.05	.	-2.78 ± 0.10	2	-2.62 ± 0.06	15
HD 108577	-2.32 ± 0.05	.	-1.95 ± 0.08	2	-1.97 ± 0.06	20
HD 119516	$-1.66/pm0.07$.	-1.66 ± 0.09	3	-1.60 ± 0.07	19
HD 124358	-2.05 ± 0.06	2	-1.43 ± 0.05	3	-1.62 ± 0.07	19
HD 128279	-2.62 ± 0.09	.	-1.80 ± 0.07	2	-1.77 ± 0.08	2	-1.89 ± 0.07	20
HD 175305	-1.37 ± 0.07	2	-1.01 ± 0.08	1	-1.04 ± 0.07	3	-0.97 ± 0.05	1	-1.12 ± 0.07	19
HD 237846	-3.40 ± 0.05	.	-2.54 ± 0.10	2	-2.64 ± 0.08	14
HD 134439	-1.79 ± 0.06	1	-1.27 ± 0.12	2	-1.30 ± 0.05	3	-1.34 ± 0.05	19
G 112-43	-1.34 ± 0.06	1	-0.96 ± 0.12	1	-1.05 ± 0.06	3	-1.05 ± 0.05	1	-1.03 ± 0.06	23
G 115-58	-1.79 ± 0.05	.	-1.21 ± 0.08	2	-1.25 ± 0.07	2	-1.13 ± 0.07	14
G 15-13	-2.00 ± 0.06	2	-1.42 ± 0.08	1	-1.54 ± 0.07	19
G 166-37	-1.58 ± 0.07	2	-1.11 ± 0.10	2	-1.18 ± 0.07	2	-1.21 ± 0.07	20
G 238-30	-4.09 ± 0.06	.	-2.70 ± 0.08	1	-2.75 ± 0.06	3
G 41-41	-3.55 ± 0.07	2	-2.39 ± 0.08	1	-2.38 ± 0.06	2
G 48-29	-3.32 ± 0.06	2	-2.26 ± 0.08	1	-2.24 ± 0.09	5
G 53-41	-0.97 ± 0.08	2	-1.00 ± 0.08	1	-0.99 ± 0.07	2	-0.89 ± 0.04	1	-1.02 ± 0.06	22
LP 894-3	-1.67 ± 0.06	2	-1.36 ± 0.08	2	-1.22 ± 0.05	1	-1.36 ± 0.06	20

Table 4. Abundance ratios: Sc, Ti, Cr and Mn

star	[ScII/H]	N	[TiI/H]	N	[TiII/H]	N	[CrI/H]	N	[CrII/H]	N	[MnI/H]	N
BD+04°2466	-1.75 ± 0.08	4	-1.55 ± 0.08	33	-1.55 ± 0.08	8	-2.02 ± 0.08	14	-1.80 ± 0.09	5	-2.36 ± 0.04	2
BD+01°3070	-1.29 ± 0.05	7	-1.29 ± 0.06	32	-1.11 ± 0.08	8	-1.66 ± 0.06	14	-1.37 ± 0.09	5	-2.10 ± 0.03	2
BD+09°2870	-2.69 ± 0.05	6	-2.50 ± 0.11	32	-2.44 ± 0.10	9	-3.05 ± 0.05	12	-2.59 ± 0.09	5	-3.34 ± 0.07	2
BD+10°2495	-1.98 ± 0.06	9	-1.93 ± 0.06	32	-1.78 ± 0.08	7	-2.28 ± 0.09	14	-1.91 ± 0.07	5	-2.59 ± 0.03	2
BD+12°2547	-1.69 ± 0.07	3	-1.79 ± 0.06	29	-1.50 ± 0.09	7	-2.09 ± 0.07	15	-1.74 ± 0.09	5	-2.49 ± 0.03	2
BD+29°2356	-1.20 ± 0.07	2	-1.21 ± 0.06	27	-1.00 ± 0.10	6	-1.57 ± 0.07	14	-1.31 ± 0.11	5	-2.12 ± 0.08	2
BD+30°2611	-1.36 ± 0.07	9	-1.13 ± 0.08	2	-1.43 ± 0.10	3	-1.35 ± 0.09	2	-2.06 ± 0.04	2
HD 33771	-1.90 ± 0.08	4	-1.87 ± 0.05	31	-1.68 ± 0.08	8	-2.30 ± 0.05	12	-1.92 ± 0.09	5	-2.60 ± 0.04	2
HD 85773	-2.60 ± 0.06	4	-2.30 ± 0.07	21	-2.25 ± 0.08	7	-2.85 ± 0.07	12	-2.40 ± 0.10	4	-3.02 ± 0.06	2
HD 107752	-3.30 ± 0.08	7	-3.03 ± 0.07	14	-2.98 ± 0.07	11	-3.39 ± 0.07	10	-3.02 ± 0.06	2	-3.71 ± 0.03	1
HD 108577	-2.24 ± 0.07	10	-2.10 ± 0.05	25	-2.06 ± 0.08	8	-2.53 ± 0.07	14	-2.28 ± 0.11	3	-2.68 ± 0.04	2
HD 119516	-1.74 ± 0.07	8	-1.51 ± 0.10	20	-1.55 ± 0.08	8	-1.97 ± 0.08	12	-1.74 ± 0.08	5	-2.23 ± 0.04	2
HD 124358	-1.73 ± 0.07	3	-1.73 ± 0.06	27	-1.54 ± 0.08	5	-2.01 ± 0.06	12	-1.69 ± 0.11	4	-2.21 ± 0.03	1
HD 128279	-2.02 ± 0.07	9	-1.94 ± 0.05	21	-1.80 ± 0.07	11	-2.42 ± 0.05	12	-2.04 ± 0.09	3	-2.66 ± 0.03	2
HD 175305	-1.00 ± 0.10	5	-1.11 ± 0.06	30	-0.90 ± 0.08	8	-1.47 ± 0.07	13	-1.16 ± 0.09	5	-1.94 ± 0.04	2
HD 237846	-3.05 ± 0.09	7	-2.74 ± 0.06	19	-2.73 ± 0.07	11	-3.25 ± 0.06	10	-3.04 ± 0.04	1	-3.49 ± 0.03	2
HD 134439	-1.27 ± 0.09	6	-1.10 ± 0.06	26	-1.01 ± 0.08	8	-1.34 ± 0.07	15	-1.12 ± 0.09	5	-1.86 ± 0.03	1
G 112-43	-1.07 ± 0.05	9	-0.91 ± 0.05	27	-0.86 ± 0.07	2	-1.37 ± 0.05	13	-1.20 ± 0.04	2	-1.58 ± 0.03	2
G 115-58	-1.31 ± 0.07	8	-1.06 ± 0.06	18	-1.01 ± 0.08	10	-1.47 ± 0.05	11	-1.32 ± 0.10	4	-1.78 ± 0.03	2
G 15-13	-1.48 ± 0.08	8	-1.34 ± 0.06	27	-1.25 ± 0.06	9	-1.69 ± 0.06	19	-1.37 ± 0.04	1	-2.03 ± 0.10	2
G 166-37	-1.02 ± 0.10	8	-1.05 ± 0.07	26	-0.93 ± 0.10	10	-1.42 ± 0.06	15	-1.21 ± 0.04	2	-1.84 ± 0.03	1
G 238-30	-3.40 ± 0.20	4	-2.95 ± 0.10	3	-3.20 ± 0.09	3	-3.57 ± 0.09	2
G 41-41	-2.50 ± 0.10	6	-2.25 ± 0.09	3
G 48-29	-2.56 ± 0.08	4	-2.26 ± 0.10	3	-2.89 ± 0.10	2	1
G 53-41	-1.04 ± 0.07	8	-0.96 ± 0.08	29	-0.80 ± 0.08	11	-1.35 ± 0.06	14	-1.03 ± 0.09	5	-1.62 ± 0.03	2
LP 894-3	-1.45 ± 0.09	9	-1.32 ± 0.11	13	-1.19 ± 0.08	10	-1.65 ± 0.05	11	-1.29 ± 0.10	4	-1.95 ± 0.03	1

Table 5. Abundance ratios: Fe, Ni, Zn, Y and Ba

Star	[FeI/H]	N	[FeII/H]	N	[NiI/H]	N	[ZnI/H]	N	[YII/H]	N	[BaII/H]	N
BD+04°2466	-1.92 ± 0.05	80	-1.92 ± 0.09	12	-1.90 ± 0.08	15	-1.96 ± 0.10	3	-1.37 ± 0.05	1	-0.61 ± 0.05	3
BD+01°3070	-1.52 ± 0.05	91	-1.52 ± 0.06	12	-1.63 ± 0.07	22	-1.58 ± 0.03	3	-1.66 ± 0.05	2	-1.59 ± 0.06	3
BD+09°2870	-2.73 ± 0.05	85	-2.73 ± 0.06	12	-2.74 ± 0.07	15	-2.78 ± 0.03	2	-3.21 ± 0.05	2	-3.53 ± 0.06	3
BD+10°2495	-2.10 ± 0.05	89	-2.10 ± 0.06	12	-2.17 ± 0.07	21	-2.11 ± 0.03	3	-2.36 ± 0.05	2	-2.21 ± 0.06	3
BD+12°2547	-1.89 ± 0.05	77	-1.89 ± 0.06	9	-1.83 ± 0.07	22	-1.96 ± 0.03	2	-2.03 ± 0.05	2	-1.99 ± 0.06	3
BD+29°2356	-1.45 ± 0.05	74	-1.46 ± 0.06	10	-1.54 ± 0.08	22	-1.53 ± 0.03	3	-1.5 ± 0.05	2	-1.44 ± 0.06	3
BD+30°2611	-1.40 ± 0.06	55	-1.41 ± 0.08	7	-1.56 ± 0.09	15	-1.73 ± 0.03	2	-1.63 ± 0.05	1	-1.46 ± 0.06	3
HD 33771	-2.06 ± 0.05	85	-2.06 ± 0.06	10	-2.13 ± 0.07	16	-2.14 ± 0.04	3	-2.21 ± 0.05	1	-2.15 ± 0.06	3
HD 85773	-2.58 ± 0.05	60	-2.58 ± 0.05	9	-2.58 ± 0.08	15	-2.14 ± 0.05	3	-3.15 ± 0.05	1	-3.27 ± 0.06	4
HD 107752	-3.16 ± 0.05	84	-3.16 ± 0.05	12	-3.18 ± 0.08	9	-3.11 ± 0.04	3	-3.56 ± 0.06	2	-3.72 ± 0.06	4
HD 108577	-2.37 ± 0.05	87	-2.37 ± 0.07	12	-2.29 ± 0.07	15	-2.27 ± 0.04	2	-2.69 ± 0.08	2	-2.54 ± 0.06	3
HD 119516	-1.82 ± 0.05	82	-1.82 ± 0.07	10	-1.89 ± 0.10	6	-1.96 ± 0.07	3	-1.96 ± 0.05	2	-1.71 ± 0.06	3
HD 124358	-1.77 ± 0.05	68	-1.77 ± 0.06	9	-1.94 ± 0.07	23	-2.05 ± 0.04	6	-2.37 ± 0.05	1	-2.20 ± 0.06	3
HD 128279	-2.24 ± 0.05	85	-2.24 ± 0.06	11	-2.21 ± 0.08	11	-2.27 ± 0.06	3	-2.97 ± 0.07	3
HD 175305	-1.35 ± 0.05	80	-1.35 ± 0.08	11	-1.44 ± 0.07	22	-1.38 ± 0.04	3	-1.35 ± 0.06	2	-1.36 ± 0.06	3
HD 237846	-3.01 ± 0.05	77	-3.01 ± 0.06	12	-3.06 ± 0.12	5	-2.95 ± 0.04	2	-3.52 ± 0.07	2	-4.09 ± 0.10	3
HD 134439	-1.35 ± 0.05	70	-1.35 ± 0.08	11	-1.47 ± 0.08	21	-1.45 ± 0.03	2	-1.65 ± 0.05	1	-1.59 ± 0.06	4
G 112-43	-1.31 ± 0.05	95	-1.31 ± 0.06	13	-1.29 ± 0.05	14	-1.12 ± 0.04	3	-1.4 ± 0.05	2	-1.61 ± 0.06	3
G 115-58	-1.36 ± 0.05	71	-1.36 ± 0.06	9	-1.49 ± 0.10	8	-1.57 ± 0.07	2	-1.44 ± 0.05	2	-1.51 ± 0.10	4
G 15-13	-1.63 ± 0.05	78	-1.63 ± 0.08	11	-1.71 ± 0.08	19	-1.65 ± 0.04	2	-1.66 ± 0.06	2	-1.41 ± 0.09	4
G 166-37	-1.36 ± 0.05	86	-1.36 ± 0.08	12	-1.43 ± 0.08	18	-1.62 ± 0.09	2	-1.27 ± 0.06	2	-1.19 ± 0.07	4
G 238-30	-3.44 ± 0.06	20	-3.44 ± 0.09	3	2
G 41-41	-2.81 ± 0.06	50	-2.82 ± 0.07	6	-3.20 ± 0.06	1
G 48-29	-2.63 ± 0.05	24	-2.64 ± 0.07	7	-3.36 ± 0.08	2
G 53-41	-1.22 ± 0.05	93	-1.22 ± 0.06	12	-1.29 ± 0.07	17	-1.28 ± 0.05	3	-1.12 ± 0.05	2	-0.95 ± 0.06	3
LP 894-3	-1.50 ± 0.05	82	-1.50 ± 0.05	11	-1.59 ± 0.10	10	-1.74 ± 0.03	2	-1.70 ± 0.06	4

Table 6. Abundance relative to Fe : Mg, Si, Ca, Sc and Ti

Star	[Fe/H]	[Na/Fe]	[Mg/Fe]	[Si/Fe]	[Ca/Fe]	[Sc/Fe]	[Ti/Fe]
BD+04°2466	-1.92 ± 0.05	0.16 ± 0.08	0.25 ± 0.08	0.50 ± 0.07	0.45 ± 0.08	0.17 ± 0.08	0.37 ± 0.08
BD+01°3070	-1.52 ± 0.05	-0.09 ± 0.06	0.32 ± 0.09	0.36 ± 0.09	0.24 ± 0.06	0.23 ± 0.05	0.23 ± 0.06
BD+09°2870	-2.73 ± 0.05	0.11 ± 0.09	0.46 ± 0.13	...	0.46 ± 0.10	0.04 ± 0.05	0.23 ± 0.11
BD+10°2495	-2.10 ± 0.05	0.06 ± 0.06	0.22 ± 0.08	0.45 ± 0.05	0.34 ± 0.06	0.12 ± 0.06	0.17 ± 0.06
BD+12°2547	-1.89 ± 0.05	-0.15 ± 0.06	0.36 ± 0.08	0.30 ± 0.09	0.23 ± 0.06	0.2 ± 0.07	0.10 ± 0.06
BD+29°2356	-1.45 ± 0.05	-0.04 ± 0.09	0.36 ± 0.08	0.35 ± 0.07	0.25 ± 0.07	0.25 ± 0.07	0.24 ± 0.06
BD+30°2611	-1.41 ± 0.06	-0.33 ± 0.08	0.14 ± 0.08	0.24 ± 0.08	0.05 ± 0.07	...	0.05 ± 0.07
HD 33771	-2.06 ± 0.05	-0.04 ± 0.06	0.29 ± 0.08	0.42 ± 0.07	0.30 ± 0.06	0.16 ± 0.08	0.19 ± 0.05
HD 85773	-2.58 ± 0.05	-0.71 ± 0.08	0.29 ± 0.09	...	0.24 ± 0.07	-0.02 ± 0.06	0.28 ± 0.07
HD 107752	-3.16 ± 0.05	-0.47 ± 0.05	0.38 ± 0.10	...	0.54 ± 0.06	-0.14 ± 0.08	0.13 ± 0.07
HD 108577	-2.37 ± 0.05	0.05 ± 0.05	0.42 ± 0.08	...	0.40 ± 0.06	0.13 ± 0.07	0.27 ± 0.05
HD 119516	-1.82 ± 0.05	0.16 ± 0.07	0.16 ± 0.09	...	0.22 ± 0.07	0.08 ± 0.07	0.31 ± 0.10
HD 124358	-1.77 ± 0.05	-0.28 ± 0.06	...	0.34 ± 0.05	0.15 ± 0.07	0.04 ± 0.07	0.04 ± 0.06
HD 128279	-2.24 ± 0.05	-0.38 ± 0.09	0.44 ± 0.07	0.47 ± 0.08	0.35 ± 0.07	0.22 ± 0.07	0.30 ± 0.05
HD 175305	-1.35 ± 0.05	-0.02 ± 0.07	0.34 ± 0.08	0.31 ± 0.07	0.23 ± 0.07	0.35 ± 0.10	0.24 ± 0.06
HD 237846	-3.01 ± 0.05	-0.39 ± 0.05	0.47 ± 0.10	...	0.37 ± 0.08	-0.04 ± 0.09	0.27 ± 0.06
HD 134439	-1.35 ± 0.05	-0.44 ± 0.06	0.08 ± 0.12	0.05 ± 0.05	0.01 ± 0.05	0.08 ± 0.09	0.25 ± 0.06
G 112-43	-1.31 ± 0.05	-0.03 ± 0.06	0.35 ± 0.12	0.26 ± 0.06	0.28 ± 0.06	0.24 ± 0.05	0.40 ± 0.05
G 115-58	-1.36 ± 0.05	-0.43 ± 0.05	0.15 ± 0.08	0.11 ± 0.07	0.23 ± 0.07	0.05 ± 0.07	0.30 ± 0.06
G 15-13	-1.63 ± 0.05	-0.37 ± 0.06	0.21 ± 0.08	...	0.09 ± 0.07	0.15 ± 0.08	0.24 ± 0.06
G 166-37	-1.36 ± 0.05	-0.22 ± 0.07	0.25 ± 0.10	0.18 ± 0.07	0.15 ± 0.07	0.34 ± 0.10	0.17 ± 0.07
G 238-30	-3.44 ± 0.06	-0.65 ± 0.06	0.74 ± 0.08	...	0.69 ± 0.06	0.04 ± 0.20	0.49 ± 0.10
G 41-41	-2.84 ± 0.06	-0.71 ± 0.07	0.36 ± 0.08	...	0.39 ± 0.06	0.34 ± 0.10	0.59 ± 0.09
G 48-29	-2.82 ± 0.05	-0.50 ± 0.06	0.56 ± 0.08	...	0.58 ± 0.09	0.26 ± 0.08	0.56 ± 0.10
G 53-41	-1.22 ± 0.05	0.25 ± 0.08	0.22 ± 0.08	0.23 ± 0.07	0.20 ± 0.06	0.18 ± 0.07	0.26 ± 0.08
LP 894-3	-1.50 ± 0.05	-0.17 ± 0.06	0.14 ± 0.08	0.28 ± 0.05	0.14 ± 0.06	0.05 ± 0.09	0.18 ± 0.11

Table 7. Abundance relative to Fe : Cr, Mn, Ni, Zn, Y and Ba

Star	[Fe/H]	[Cr/Fe]	[Mn/Fe]	[Ni/Fe]	[Zn/Fe]	[Y/Fe]	[Ba/Fe]
BD+04°2466	-1.92 ± 0.05	-0.10 ± 0.08	-0.44 ± 0.04	0.02 ± 0.08	-0.04 ± 0.10	0.55 ± 0.05	1.31 ± 0.05
BD+01°3070	-1.52 ± 0.05	-0.14 ± 0.06	-0.58 ± 0.03	-0.11 ± 0.07	-0.06 ± 0.03	-0.14 ± 0.05	-0.07 ± 0.06
BD+09°2870	-2.73 ± 0.05	-0.32 ± 0.05	-0.61 ± 0.07	-0.01 ± 0.07	-0.05 ± 0.03	-0.48 ± 0.05	-0.80 ± 0.06
BD+10°2495	-2.10 ± 0.05	-0.18 ± 0.09	-0.49 ± 0.03	-0.07 ± 0.07	-0.01 ± 0.03	-0.26 ± 0.05	-0.11 ± 0.06
BD+12°2547	-1.89 ± 0.05	-0.20 ± 0.07	-0.60 ± 0.03	-0.06 ± 0.07	-0.07 ± 0.03	-0.14 ± 0.05	-0.10 ± 0.06
BD+29°2356	-1.45 ± 0.05	-0.12 ± 0.07	-0.67 ± 0.08	-0.09 ± 0.08	-0.08 ± 0.03	-0.05 ± 0.05	0.01 ± 0.06
BD+30°2611	-1.41 ± 0.06	-0.02 ± 0.10	-0.65 ± 0.04	-0.15 ± 0.09	-0.32 ± 0.03	-0.22 ± 0.05	-0.05 ± 0.06
HD 33771	-2.06 ± 0.05	-0.24 ± 0.05	-0.54 ± 0.04	-0.07 ± 0.07	-0.08 ± 0.04	-0.15 ± 0.05	-0.09 ± 0.06
HD 85773	-2.58 ± 0.05	-0.27 ± 0.07	-0.44 ± 0.06	0.00 ± 0.08	0.44 ± 0.05	-0.57 ± 0.05	-0.69 ± 0.06
HD 107752	-3.16 ± 0.05	-0.23 ± 0.07	-0.55 ± 0.03	-0.02 ± 0.08	0.05 ± 0.04	-0.40 ± 0.06	-0.56 ± 0.06
HD 108577	-2.37 ± 0.05	-0.15 ± 0.07	-0.31 ± 0.04	0.08 ± 0.07	0.10 ± 0.04	-0.32 ± 0.08	-0.17 ± 0.06
HD 119516	-1.82 ± 0.05	-0.15 ± 0.08	-0.41 ± 0.04	-0.07 ± 0.10	-0.06 ± 0.07	-0.14 ± 0.05	0.11 ± 0.06
HD 124358	-1.77 ± 0.05	-0.24 ± 0.06	-0.44 ± 0.03	-0.17 ± 0.07	-0.28 ± 0.04	-0.60 ± 0.05	-0.43 ± 0.06
HD 128279	-2.24 ± 0.05	-0.18 ± 0.05	-0.42 ± 0.03	0.04 ± 0.08	-0.03 ± 0.06	...	-0.73 ± 0.07
HD 175305	-1.35 ± 0.05	-0.12 ± 0.07	-0.61 ± 0.04	-0.09 ± 0.07	-0.03 ± 0.04	0.00 ± 0.06	-0.01 ± 0.06
HD 237846	-3.01 ± 0.05	-0.24 ± 0.06	-0.48 ± 0.03	-0.04 ± 0.12	0.06 ± 0.04	-0.51 ± 0.07	-1.08 ± 0.10
HD 134439	-1.35 ± 0.05	-0.09 ± 0.07	-0.51 ± 0.03	-0.12 ± 0.08	-0.10 ± 0.03	-0.30 ± 0.05	-0.24 ± 0.06
G 112-43	-1.31 ± 0.05	-0.06 ± 0.05	-0.27 ± 0.03	0.02 ± 0.05	0.19 ± 0.04	-0.09 ± 0.05	-0.30 ± 0.06
G 115-58	-1.36 ± 0.05	-0.11 ± 0.05	-0.42 ± 0.03	-0.13 ± 0.10	-0.21 ± 0.07	-0.08 ± 0.05	-0.15 ± 0.10
G 15-13	-1.63 ± 0.05	-0.06 ± 0.06	-0.40 ± 0.10	-0.08 ± 0.08	-0.02 ± 0.04	-0.03 ± 0.06	0.22 ± 0.09
G 166-37	-1.36 ± 0.05	-0.06 ± 0.06	-0.48 ± 0.03	-0.07 ± 0.08	-0.26 ± 0.09	0.09 ± 0.06	0.16 ± 0.07
G 238-30	-3.44 ± 0.06	-0.13 ± 0.09
G 41-41	-2.84 ± 0.06	-0.36 ± 0.06
G 48-29	-2.82 ± 0.05	-0.07 ± 0.10	-0.54 ± 0.08
G 53-41	-1.22 ± 0.05	-0.13 ± 0.06	-0.41 ± 0.03	-0.07 ± 0.07	-0.06 ± 0.05	0.10 ± 0.05	0.27 ± 0.06
LP 894-3	-1.50 ± 0.05	-0.15 ± 0.05	-0.45 ± 0.03	-0.09 ± 0.10	-0.24 ± 0.03	...	-0.20 ± 0.06

